Ph.D. Program in Civil, Chemical and Environmental Engineering

Curriculum in Chemical, Materials and Process Engineering

Department of Civil, Chemical and Environmental Engineering

Polytechnic School, University of Genoa, Italy

Solid Oxide Fuel Cells: Numerical and Experimental Approaches

Bruno Conti

SOLID OXIDE FUEL CELLS:

NUMERICAL AND EXPERIMENTAL APPROACHES

BY

BRUNO CONTI

Dissertation discussed in partial fulfillment of

the requirements for the Degree of

DOCTOR OF PHILOSOPHY

Civil, Chemical and Environmental Engineering

curriculum in Chemical, Materials and Process Engineering,

Department of Civil, Chemical and Environmental Engineering, University of Genoa, Italy

April 2019

Adviser(s):
Prof. Barbara Bosio – DICCA, University of Genoa
Dr. Stephen John McPhail – ENEA

External Reviewers:
Prof. Marco Baratieri – Faculty of Science and Technology, Free University of Bozen - Bolzano
Dr. Alfonso Martinez-Felipe – School of Engineering, University of Aberdeen

Examination Committee:
Prof. Renzo Di Felice– DICCA, University of Genoa
Prof. Linda Barelli – Department of Engineering, University of Perugia
Prof. Giovanna Ferrari – DIIN, University of Salerno

Ph.D. program in Civil, Chemical and Environmental Engineering

Curriculum in Chemical, Materials and Process Engineering

Cycle XXXI

Acknowledgements

I wish to thank ENEA, for supporting my PhD work.

ABSTRACT

Solid oxide fuel cell (SOFC) is a promising electrochemical technology that can produce electrical and thermal power with outstanding efficiencies. A systematic synergetic approach between experimental measurements and modelling theory has proved to be instrumental to evaluate performance and correct behaviour of a chemical process, like the ones occurring in SOFC. For this purpose, starting from SIMFC **(**SIMulation of Fuel Cells) code set-up by PERT-UNIGE (Process Engineering Research Group) for Molten Carbonate Fuel Cells [1], a new code has been set-up for SOFCs based on local mass, energy, charge and momentum balances. This code takes into account the proper reactions occurring in the SOFC as well as new geometries and kinetics thanks to experiments carried out on single cells and stack in ENEA laboratories of C.R. Casaccia and VTT Fuel Cell Lab in Finland. In particular using an innovative experimental setup it has been possible to study experimentally the influence of a multicomponent mixtures on the performance of SOFC and also validate locally a 2-D model developed starting from SIMFC code. The results obtained are good, showing a good agreement between experimental and numerical results. The obtained results are encouraging further studies which allow the model validation on a greater quantity of data and under a wider range of operating conditions.

ACKNOWLEDGEMENTS

I wish to express my sincere appreciation to those who have contributed to this thesis and supported me during this amazing journey. I would especially like to thank all the co-authors of the scientific paper included in this PhD thesis. I would like to thank all my colleagues at ENEA Casaccia R.C. and express my gratitude to the HOTlab (High-temperature fuel cells Operation and Testing Laboratory) Team, for their positive and constructive attitude as well as their valuable advice. I am grateful to all the researchers at the Technical Research Center of Finland Ltd. (VTT) of Espoo, and above all, I would like to express my sincere gratitude to Dr. Olli Himanen for his ongoing precious support of my research activity and for his kind hospitality. Most importantly, I am very grateful to my PhD thesis advisor, Professor Barbara Bosio, for encouraging and support my research activity as a friend not only as a professor. Undertaking this PhD has been a life-changing experience for me and I really appreciate the patient and unflagging support as well as exemplary guidance that I have received from my co-advisor, Dr. Stephen McPhail, to whom I would like to give my special thanks for encouraging my growth as a research scientist. I have gained much from my friends and family, and I am extremely lucky to know such a bunch of nice and fun people. Especially I would like to thank my mother and my sister Antonella for always supporting me. But mainly I want to dedicate this work to my father that is in the sky, I hope I am becoming the man he wanted. Finally, I want to be graceful to Villa PERT group for beautiful three years I spent in the group. Furthermore, I want to say thanks to scout group Genova 100 that is for me a second house.

INDEX

1. GOAL OF THIS WORK

The general aim of the work is to develop a numerical simulation tool for SOFCS which implements mass, energy, charge and momentum balances. To do so, we use conventional characterization techniques such as polarization curves and electrochemical impedance spectroscopy (EIS), and also an innovative, in-house built, multisampling set-up which allows the contemporaneous measurements of gas compositions and temperatures with a spatial resolution along the anode surface, making it possible to study the evolution of all the reactions occurring at the fuel electrode and investigating the concentration and thermal gradient arising at different operating conditions. By means of these investigating tools, a number of different aspects of the coupling of syngas fuels with IT-SOFC systems were studied, resulting in an in-depth comprehension of the single physicochemical processes and their effect on the overall performances, of the thermal and chemical gradients arising during the operation, Thanks to experimental data collected in ENEA laboratories and VTT Technical Research Centre laboratories, we developed, starting from an in house numerical tool developed for MCFC technology, a new code able to predict performance and spatial distribution of chemical variables along the anode surface and validate it on the basis of experimental data. In Sections 2 of this work, an initial description of the operating principles of SOFCs also with non-conventional fuels, general aspects about the materials and designs related to this technology are briefly resumed. In Chapter 3 an extensive description of SOFC suppliers is provided. There is an effectiveness presentation of the state of the art of this technology around the world. A complete description of modelling approaches is explained in Section 4 with attention to the modelling scales and governing equations. Moreover, there is a detailed explanation of the numerical tool used in the work, the SIMFC code. The experimental campaigns, the testing procedures, the characteristics of the samples, and the experimental apparatus employed are reported in Chapter 5 both in ENEA and in VTT laboratories; within this chapter, the novel multisampling housing developed in-house is described in detail, along with the details of the experimental campaign carried out with it. Also, there are the results of experimental validation of the novel multisampling experimental apparatus. In Chapter 6, that is the core of the work, the numerical tool is validate, with an appropriate experimental campaign, in terms of global and local values. More in detail there is a comparison of experimental and simulated values for the characteristics curve, but the novelty of the work is represented by the possibility of comparing experimental and simulated data in local terms, by means of the experimental test rig showed in chapter 5. Finally, in Chapter 7 there are the conclusion of the work in terms of obtained results and possibility to update the issued involved in some aspects.

2. INTRODUCTION

Fuel cells are electrochemical devices that convert chemical energy in fuels into electrical energy directly, promising power generation with high efficiency and low environmental impact. Because the intermediate steps of producing heat and mechanical work typical of most conventional power generation methods are avoided, fuel cells are not limited by thermodynamic limitations of heat engines such as the Carnot efficiency. In addition, because combustion is avoided, fuel cells produce power with minimal pollutant. However, unlike batteries the reductant and oxidant in fuel cells must be continuously replenished to allow continuous operation. Fuel cells bear significant resemblance to electrolyzes. In fact, some fuel cells operate in reverse as electrolyzes, yielding a reversible fuel cell that can be used for energy storage. Though fuel cells could, in principle, process a wide variety of fuels and oxidants, of most interest today are those fuel cells that use common fuels (or their derivatives) or hydrogen as a reductant, and ambient air as the oxidant. Most fuel cell power systems comprise several components:

- Unit cells, in which the electrochemical reactions take place;
- Stacks, in which individual cells are modularly combined by electrically connecting the cells to form units with the desired output capacity;
- Balance of plant which comprises components that provide feed stream conditioning (including a fuel processor if needed), thermal management, and electric power conditioning among other ancillary and interface functions.

In the following, an overview of SOFC technology is given followed by a brief review of key potential applications of fuel cells in worldwide market.

2.1. Operating principles of Solid Oxide Fuel Cells

A schematic picture of the principal reactions in solid oxide fuel cell is depicted in Figure 2.1. Fuel is fed to the anode (negative electrode) and oxygen or air to the cathode (positive electrode). The fuel (e.g. H_2) flows through the porous structure of the anode and reaches the interface with the electrolyte. In the region known as triple phase boundary (TPB), where the gas, the electronic conducting phase (metal catalyst) and the ionic conducting phase meet, hydrogen is oxidized at the catalytic active sites to water (H_2O) by the oxygen ions (O^{2-}) coming from the electrolyte layer, releasing 2 electrons (e^-) to the external circuit. The electrons are then transferred to the cathode side, where they reduce the oxygen present in the air. Thanks to peculiar properties of the cathode materials, the O^{2-} ions pass through the cathode layer and reach the electrolyte layer which, being an ionic conductor, move the O^{2-} ions to the TPB region, where they are ready for the oxidation of the incoming fuel.

If hydrogen is used as a fuel, the cell reactions can be written as follows:

Cathode: $\frac{1}{2}O_2 + 2e^- \rightarrow O^{2-}$ (2.1)

Anode: $H_2 + O^{2-} \rightarrow H_2O + 2e^-$ (2.2)

Total: $H_2 + \frac{1}{2}O_2 \rightarrow H_2O$ (2.3)

SOFCs works at high temperatures (800–1000 ºC). The operating temperature gives the possibility to operate the cell directly on hydrocarbon fuels without the need for a separate complex to reform the hydrocarbon fuel into hydrogen and carbon dioxide. The direct internal reforming offers a significantly higher system efficiency for the cell, recuperating waste heat from the stack into the fuel supply and reducing its complexity by means of the elimination of external reformer and of associated heating arrangements. More detailed information on SOFC technology can be found in [2–4].

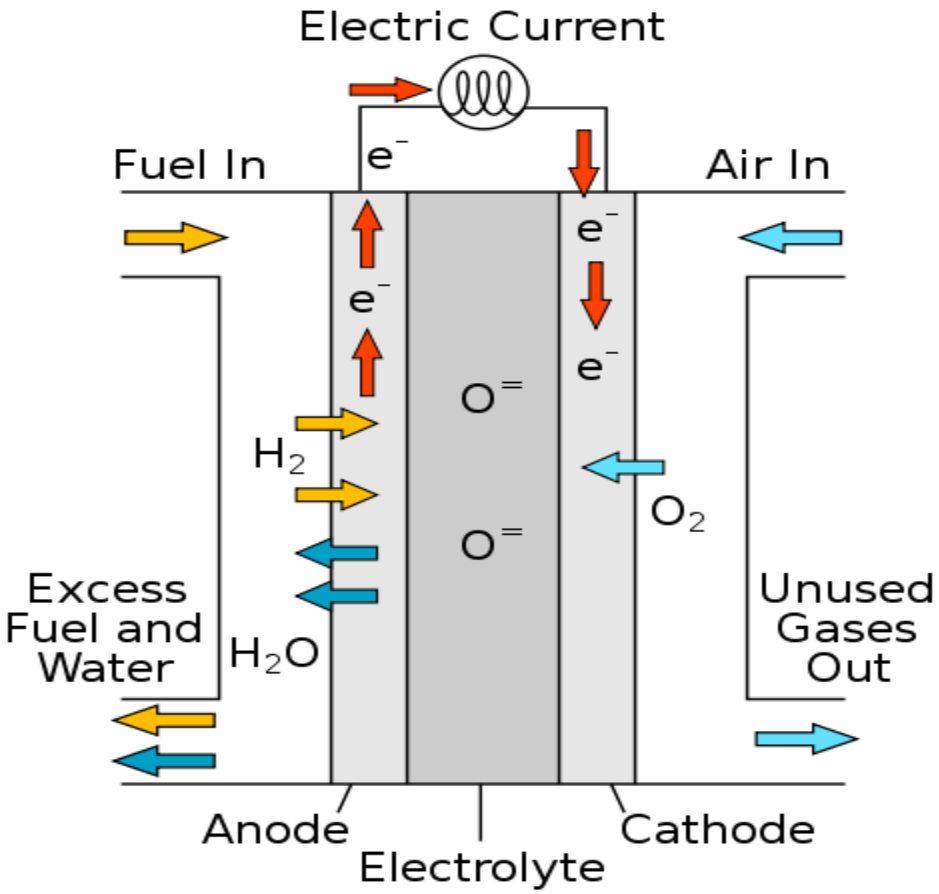

Figure 2.1. Schematic representation of a solid oxide fuel cell operating mechanism, considering the oxidation reaction of H_2.

2.2. Fuel flexibility

Hydrogen is the preferred fuel for SOFCs systems, as it guarantees high power and thermal output, safe operation for cell components and water as the only exhaust gas; it is also planned in the future to be generated from renewable sources, thereby becoming an attractive energy vector for the spread of green technologies. Nevertheless, to the present day, hydrogen is produced almost totally from hydrocarbons, and there is a very low penetration of hydrogen distribution infrastructures or storage facilities; this clearly hinders to some extent the possibility of hydrogen-fed SOFCs to become competitive systems for heat and power generation on the market. However, as explained also in the previous Sections, fuel flexibility is one of the most attractive proprieties of SOFCs, thereby being able to produce electricity and heat starting from more conventional carbon-based fuels, due to their high operating temperatures, high catalytic activity and low susceptibility compared to low-temperature fuel cells. Several different fuels can be successfully employed with SOFCs: natural gas, syngas produced from gasification of coal and biomasses, biogas coming from anaerobic digestion of organic wastes, and even liquid fuels such as diesel [5,6]. Since one of the aims of this work is to shed light on the different processes occurring when IT-SOFCs are fed with syngas mixtures, in the following section a brief discussion about the feeding of SOFC with syngas is reported, highlighting those aspects that will be instrumental for the discussion of the experimental results obtained within this work.

2.2.1. Non- conventional fuel: syngas

With the term syngas a gas mixture is generally intended in which the principal components are H_2 and CO. There are several ways to produce a syngas; however, the most interesting sources of syngas for the application in SOFC systems are the gasification of biomass and the conversion of natural gas by means of the reforming reaction. From these two sources, the produced syngas is generally a mixture of H_2, H_2O, CO, CO_2, CH_4 and N_2. A typical syngas composition resulting from a biomass gasifier is reported in Table 2.1. below [6]:

Table 2.1. Mean composition of a syngas

syngas					
H_2 (%)	H_2O (%)	CO (%)	CO_2 (%)	CH_4 (%)	N_2 (%)
10-50	0-30	10-45	10-30	1-20	0-50

The gasification process is a thermochemical process that uses air, oxygen or steam as gasification agents that convert the biomass (or coal) in a gas rich in hydrogen and carbon monoxide.

Natural gas can be converted into a syngas by means of the steam reforming reaction. In the case of SOFC systems, this fuel conversion can proceed directly at the SOFC anode, thanks to the catalytic proprieties of dispersed Ni particles, or in an upstream reformer. The former process is called Direct Internal Reforming (DIR) while the latter is known as Indirect Internal Reforming (IIR). Depending on the applications, either the DIR or the IIR conversion can be applied; nevertheless, IIR is generally preferred due to the significant thermal and concentration gradients that arise when methane is reformed directly at the anode, which can compromise the longevity of the entire system. For methane, the main reactions occurring in this conversion to syngas are the steam reforming reaction (equation 2.4), and the subsequent water gas shift (equation 2.5) and dry steam reforming (equation 2.6), that may occur once the steam reforming products start to appear in the gas mixture.

$$CH_4 + H_2O \leftrightarrows CO + 3H_2 \qquad \Delta H^0_{298} = 206\ \text{kJ mol}^{-1} \tag{2.4}$$

$$CO + H_2O \leftrightarrows CO_2 + H_2 \qquad \Delta H^0_{298} = -46\ \text{kJ mol}^{-1} \tag{2.5}$$

$$CH_4 + CO_2 \leftrightarrows 2CO + 2H_2 \qquad \Delta H^0_{298} = 247\ \text{kJ mol}^{-1} \tag{2.6}$$

The endothermic steam reforming reaction is thermodynamically favoured at high temperatures and low pressures and, along with the water gas shift reaction, they are generally carried out at temperatures above 700 °C and with Nickel based catalysts.

2.2.2. Operation of SOFC with syngas

When an SOFC cell is fed with a syngas, several different reactions, both of chemical and electrochemical nature, occur. Figure 2.2. below summarize all the possible reactions than can develop in a SOFC fed with syngas.

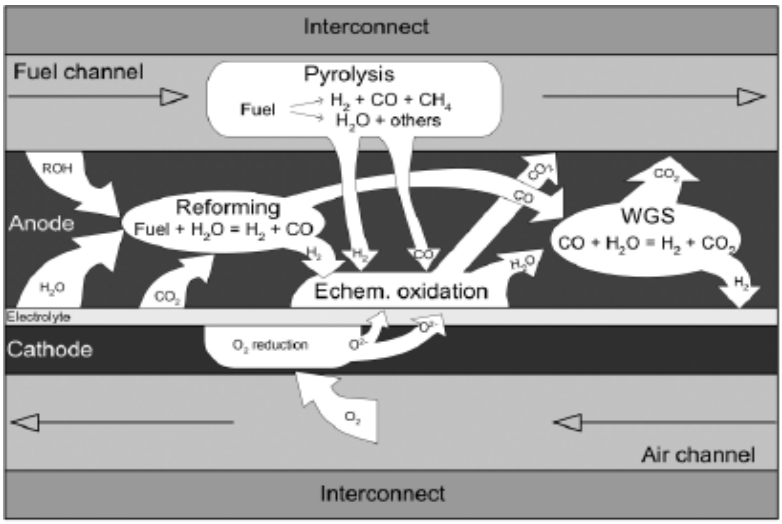

Figure 2.2. Schematic representation of the possible reactions within an SOFC fed with syngas.

Along with the electrochemical oxidation of H_2 (Equation 2.1) and the steam reforming and water gas shift reactions (Equations 2.4 and 2.5) other mechanisms are theoretically possible, depending on the conditions of temperature, gas compositions, cell materials, and operating point at which the SOFC works. Carbon monoxide and methane can be electrochemically oxidized (equations 2.6 and 2.7 respectively) and equilibria like the methane cracking (Equation 2.8) and the Boudouard reaction may be present, forming carbon deposits:

$$CO + O^{2-} \rightarrow CO_2 \tag{2.6}$$

$$CH_4 + 4O^{2-} \rightarrow CO_2 + 2H_2O + 8e^- \tag{2.7}$$

$$CH_4 \leftrightarrows C + 2H_2 \tag{2.8}$$

$$2CO \leftrightarrows CO_2 + C \tag{2.9}$$

The operation of SOFCs with syngas has been widely studied in literature, but a clear comprehension of the occurrence of all these reactions and their pathway is still missing, especially due to the lack of analysis tools able to provide information directly *in-operando*. As previously mentioned, the study of these reactions by means of innovative tools of analysis will be one of the objectives of this work.

2.3. Historical background

SOFCs are a cutting-edge technology for converting the chemical energy in fuels, the most common being H_2, directly to electrical power and heat by means of an electrochemical reaction. SOFC technology has many advantages over conventional power trains, such as combustion engines, because they allow to avoid the intermediate steps of combustion-thermal energy- mechanical energy- electrical energy.

Among the advantages some of these are:

- High efficiency, including at small scale;
- Fuel flexibility;
- Insignificant NO_x, SO_x and particulate emissions, reduced CO_2 emissions;
- Silent and vibration-free operation.

SOFCs have come a long way to become practical power generation devices since the initial discovery of a ceramic material consisting of 85 % ZrO_2 and 15 % Y_2O_3, the so-called ‘‘Nernst Mass’’, by Walther Nernst in late 1890s that laid the foundation for the electrolyte material for these cells [7]. During the 1970s and 1980s, support for the development of SOFCs came from large generating equipment manufacturers such as Westinghouse, ABB, and GEC. Unfortunately, the costs of SOFCs have remained high because of their high operation temperature of 850-1000 °C. By the mid-1990s to the present, for other type of applications such as micro-CHP and APUs there is a trend to move to lower temperatures of operation, into the so-called intermediate temperature (IT) range of 500-750°C, as defined by Steele [8]. The reduction of temperature provided the internal resistance of the cell and the electrode kinetics were adequate and that internal reforming could be carried out if possible [3]. Anode-supported planar Intermediate Temperature Solid Oxide Fuel Cells (IT-SOFCs) have become quite popular because of performance and cost considerations. Today, IT-SOFCs in many different designs and containing different cell materials are being explored and produced for power generation in small (few Watts) to large (several hundred kWs) sizes in residential, commercial, and central power station applications. Although still small, most demonstrations of SOFC power systems to date have been made of the 1–5 kW sized residential combined heat and power (CHP) units. The biggest drawback to the large-scale commercialization of IT-SOFC power systems remains their relatively high cost relative to other power generation technologies.

2.4. Components

IT-SOFCs are, at the state of art, multilayered structures of anode, electrolyte and cathode. Depending on the materials, typology and design of the cell, the operating conditions, their durability and their resistance to fuel contaminants may significantly vary. Furthermore, when single cells are connected in series to form a stack of the desired power output, other fundamental components are needed: the interconnects layer, or bipolar plates, and, in the case of planar cells, the sealant layers. In the following sections, a brief description is provided of the most important types and proprieties of the materials employed for the state-of art IT-SOFC cells and stack, along with the different typologies of cells.

2.4.1. Electrolyte

Generally, an electrolyte for IT-SOFCs has to be ionically conductive, but electronically insulating. It should be chemically stable under a large oxygen partial pressure gradient from highly reducing to oxidizing conditions at high temperatures. The structure has to be gas tight i.e. not porous. It should be possible to produce very thin layers of the material in order to reduce ohmic losses. The thermal expansion of the material should match the thermal expansion of adjacent components of the cell. Moreover, of course, the material should be inexpensive. Typical electrolyte materials for IT-SOFCs are oxides with low valence element substitutions, sometimes named acceptor dopants, which create oxygen vacancies through charge compensation. The most conventional material for SOFC electrolytes us the 8YSZ (8YSZ: 8% Yttria-Stabilized Zirconia), which possesses a good conductivity of 0.5 S cm^{-1}, measured at T=800 °C; acceptor doped CeO_2 and perovskite structure oxides have also been investigated as electrolyte materials. A plot of ionic conductivity as a function of temperature for common IT-SOFC electrolyte materials is shown in Figure 2.3.

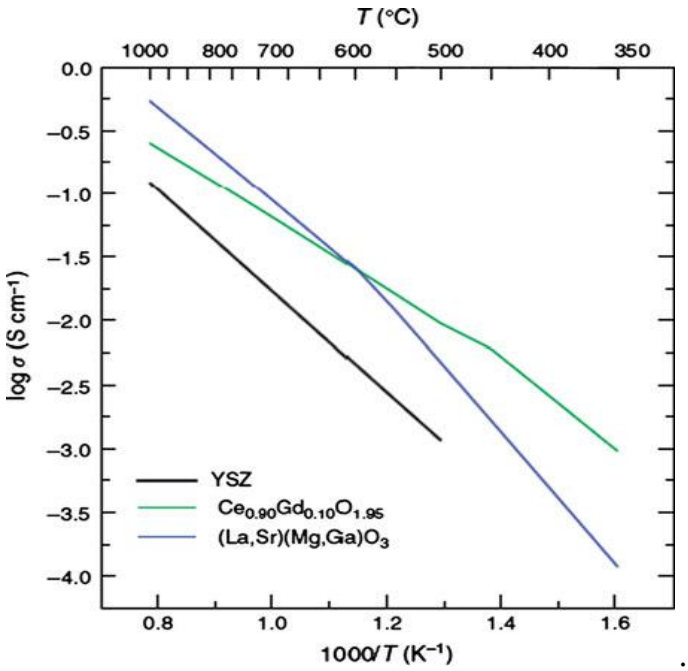

Figure 2.3. Conductivity as a function of temperature for YSZ, gadolinium-doped CeO2, and (La,Sr)(Mg,Ga)O3 (LSMG) [3].

Although YSZ shows the lowest ionic conductivity in Figure 2.3 it remains as the only material that has been demonstrated to provide long-term stability under cell operation conditions.

In order to use YSZ in the IT regime, a typical approach to minimize ohmic loss is to decrease the thickness of the YSZ electrolyte. Another approach to reduce ohmic loss is to improve the ionic conductivity of a ZrO_2-based electrolyte. Sc-doped zirconia shows higher conductivity than yttrium-doped ZrO_2; however, the cost and known aging of Sc-doped ZrO_2 present challenges in using this material for commercial IT-SOFCs. Doped CeO_2 materials are candidates for the electrolyte for cell operation at temperatures below about 600 °C as discussed by Steele [9] and utilized by Ceres Power Inc. (UK), due to their higher oxide ion conductivity. The principal challenge with doped CeO_2 is the onset of electronic conduction in reducing conditions at temperatures above about 650 °C due to the reduction of Ce^{4+} to Ce^{3+} to compensate the formation of oxygen vacancies. Further reduction of Ce^{4+} results in lattice expansion and often creates microcracking in the electrolyte. Cell temperatures below about 600 °C seem necessary for successful use of doped CeO_2 in SOFCs for long-term operation. The use of (La, Sr) (Mg, Ga) O_3 (LSMG) is attractive because it has reasonable oxide ion conductivity and is compatible with a variety of cathodes, in particular the highly active ones; The challenges for LSMG are the uncertain costs of Ga sources and its chemical and mechanical stability.

2.4.2. Anode

IT-SOFC anode is generally a cermet structure i.e. a mixture of Nickel and a ceramic supporter, like YSZ [2]. Nickel is a good electro-catalyst when hydrogen is used as fuel and it has chemical stability with the electrolyte. Also, it presents good performance at all temperature ranges and it is competitive from an economic point of view. the most diffused typologies of SOFC cells, the planar anode supported cells (AS-SOFCs), the Ni-YSZ is prepared in two different morphologies: the first, thicker one (up to several hundred μm) is the anode substrate, which acts as a support for the whole cell, and possesses a high porosity in order to minimize the mass transport losses. The second structure is a thinner layer (c.a. 10-20 μm), the so-called Anode Functional Layer (AFL), which consist of smaller sintered YSZ particles in which the fine Ni catalytic particles are dispersed, in order to extend to the maximum, the active surface of the three-phase boundary region, at the interface with the electrolyte, in order to minimize the activation polarization losses. This structure results in stable, good performing and low-cost anodes. Unfortunately, Ni-YSZ anodes are not adapt when we use non-conventional fuels because of carbon deposition that poison the anode. For this reason, in the recent years Ni-Gadolinia Doped Ceria (GDC), Samaria Doped Ceria (SDC) or Yttria Doped Ceria (YDC) have been studied for application as anode materials in IT-SOFCs. Nevertheless, one of the problems is still represents from lattice expansion due to Ce^{4+} / Ce^{3+} reduction with the consequent instability of CeO_2 based anode [10,11].

2.4.3. Cathode

Similar to the anode, the cathode is a porous structure that must allow rapid mass transport of reactant and product gases. Strontium-doped lanthanum manganite $(La_{0.84}Sr_{0.16})$ MnO_3, a *p*-type semiconductor is most commonly used for the cathode material. Although adequate for most SOFCs, other materials may be used, particularly attractive being *p*-type conducting perovskite structures that exhibit mixed ionic and electronic conductivity (MIEC). This is especially important for lower-temperature operation since the polarization of the cathode increases significantly as the SOFC temperature is lowered. It is in cells operating at around 650 °C that the advantages of using mixed conducting oxides become apparent. As well as the perovskites, lanthanum strontium ferrite (LSF), lanthanum strontium cobaltite (LSC), and *n*-type semiconductors are better electrocatalysts than the state-of-the-art lanthanum strontium manganite, because they are mixed conductors.

2.4.4. Interconnects

The interconnects in SOFC stacks is the component which electrically connects the single cells and in planar systems it additionally separates the gas compartments. Metals can be used as interconnect, but these tend to be expensive `Inconel` type stainless steels, particularly for stacks that need to operate at 800 to 1000 °C. Conventional steels also have a mismatch in thermal expansion coefficient

with the YSZ electrolyte. To overcome this, Siemens and others have tried to develop new alloys, such as the Cr-5Fe-1Y_2O_3 Siemens/Plansee alloy. This type of alloy can give raise to Cr evaporation and poisoning of cathode materials. An advantage for IT-SOFCs is that cheaper materials may be used, such as austenitic steels, which do not contain chromium. Metal interconnects also tend to form oxide coatings, which can limit their electrical conductivity and act as a barrier to mass transport. Alternatively, for tubular configurations, ceramic materials, such as lanthanum chromite can be used.

2.4.5. Sealants

A key issue with SOFCs is the method of sealing the ceramic components to obtain gas tightness, particularly with planar SOFCs. The usual approach has been to use glasses that have transition temperatures close to the operating temperature of the cell. These materials soften as the cells are heated up and form a seal all around the cell. There are two classes of seals: rigid and compressive. Glass or glass ceramics have demonstrated to be chemically stable in both oxidizing and reducing environments[12]. However, due to the addition of barium or calcium silicates to fulfil the requirements of thermal expansion coefficient, diffusion and segregation of species may occur during long term operation at the interface with the cell[13].Besides glass-ceramics, compressive seals have also been investigated. They are generally metallic gaskets or mica-based materials [14].

2.5. Designs

In this section it will be provided a brief description of the two typical configurations of SOFC technology that are used in different applications.

2.5.1. Planar design

Planar IT-SOFCs are generally square-shaped with dimensions that range between 10 x 10 cm^2 and 20 x 20 cm^2, in order to avoid fractures during manufacturing due to the high temperature and pressure gradients, and with a mean thickness of around one mm (or even less).

Depending of the supporting layer, upon which the other layers are deposited, there are four typologies of planar IT-SOFCs: Electrolyte Supported (ES-IT-SOFCs), Anode Supported (AS-IT-SOFCs), Cathode Supported (CS-IT-SOFCs) cells and Metal Supported (MS-IT-SOFCs)[15–17]. In the planar design, a series of cell components are configured as thin, flat plates, then electrically connected to build up desirable electrochemical performance. Each of these designs can also have a number of interesting variants; for example, the planar SOFC may be in the form of a circular disk fed with fuel from the central axis, or it may be in the form of a square or rectangular plate fed from the edges. Advantages of planar configuration are lower cost and higher power output density respect to tubular one. A big drawback is the necessity of sealants between the component of the cell. Usually, the interconnect is ribbed on both sides to allow cross-flow, co-flow, or counter-flow configurations. Anode supported type is the most widespread, allowing to reduce the thickness of the electrolyte layer below 10 μm, and thus dramatically reducing the overall internal resistance of the cell; moreover, the anode support results more mechanically stable and has better manufacturing proprieties than the cathode materials. In Figure 2.4 it is shown a representation of planar design.

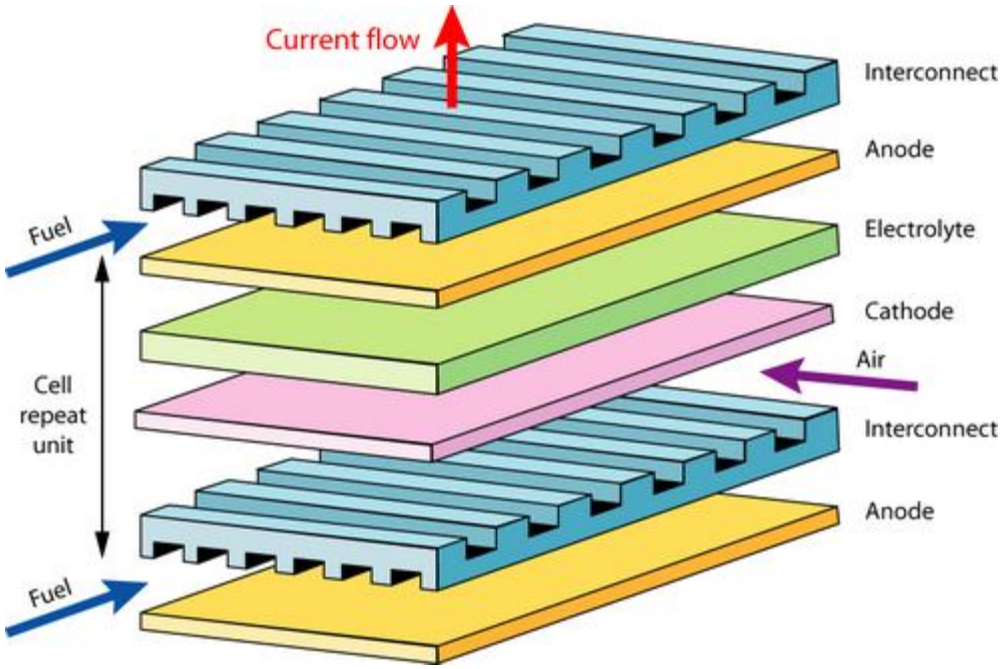

Figure 2.4. Schematic representation of SOFC planar design [18].

2.5.2. Tubular design

Tubular SOFCs are cylindrically shaped with a length comprised between 1.5 – 2 m for most of their applications. This geometry comprises three cylindrical and concentric layers of anode, electrolyte and cathode materials, that generate a rigid tube with only one opened extremity. Depending on the external layer, the fuel (or air) is fed by a coaxial tube, while the air (or fuel) flows over the external part of the cell. One great advantage of the tubular design of SOFC is that high-temperature gas-tight seals are eliminated. They also allow faster start-up and shut down processes. Two main disadvantages are instead, low power output density and high cost production. in Figure 2.5. there is a schematic representation of a SOFC with tubular arrangement.

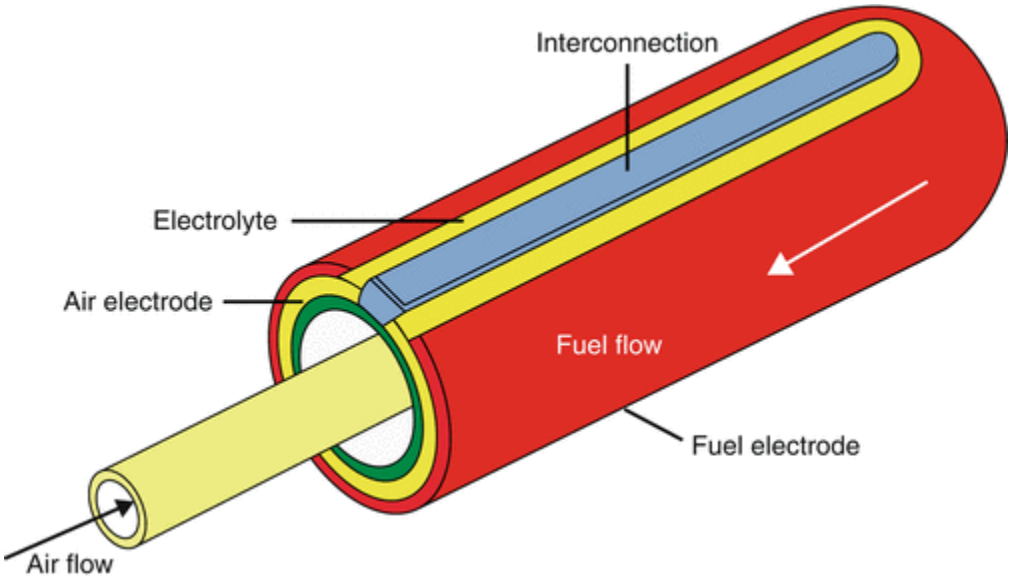

Figure 2.5. Tubular solid oxide fuel cell design [3]

3. OVERVIEW OF WORLD WIDE SOFC DEVELOPERS

In this section it will show an exhaustive overview of industrial SOFCs developers around all the world.

3.1. Application areas

Since Solid Oxide Fuel Cell (SOFC) systems can be built to any scale between several watts up to several hundreds of kilowatts, they can serve a large variety of applications, maintaining their properties of fuel flexibility and high electrical efficiency. The most promising areas for their immediate utilization are:

- Mobile, military and strategic (<1 kW);
- Auxiliary Power Units (APU) and back-up power (1–250 kW);
- Stationary small-scale combined heat and power (m-CHP) (1–5 kW);
- Stationary medium-large scale (0.1–10 MW).

For each of these fields of application, there are already pioneering industrial developers attempting to enter the market, gaining valuable experience and expertise in terms of practical know-how and end-user requirements. This front-line activity is highly necessary to make up the lag between the SOFC and the conventional technologies utilized in these areas, especially in terms of robustness, costs and familiarity with consumers. That is why for each of the application areas mentioned, a brief overview will be given of the current suppliers of end-user-ready systems.

3.1.1. Mobile, military and strategic

One of today's major concerns in the energy field is to fulfil the harsh requirements for mobile applications (<1 kW), especially in the field of military defence and strategic reconnaissance. Above all reduced weight and volume with high power densities, as well as robustness, are the requested characteristics. In Figure 3.1. there is a picture of this type of device.

Figure 3.1. The iRobot PackBot UGV AM is a reconnaissance unmanned system, capable of 12 hours autonomy covering about 40 miles of terrain. This System is hybridized with a standard battery for 2.5 hours (8 miles) extra autonomy [19].

The portable electronics market represents a niche market for SOFC micro-systems. State of the art Li-ion and Ni-ion rechargeable batteries and the Polimeric Electrolyte Fuel Cells (PEFCs) have significantly lower energy densities than the SOFCs. More powerful hand-held electronic devices such as mobile phones or laptops could be used uninterruptedly for weeks fuelling the micro-unit with a small fuel cartridge.

Fuel consumption in military defence applications represents an enormous economic cost to defence departments, and thus to the taxpayers. Currently, power generator sets (*gensets*) are the largest consumers of fuel on the battlefield, making the transport of fuel to be an army's Achilles' heel. SOFC systems not only offer up to 85% fuel savings when compared to traditional diesel electricity generators but can run on a variety of fuels. The silent operation of the fuel cell technology is an inherent advantage for strategic operations and the generation of water as a by-product makes the unit even more valuable as it could be a source of clean water supply for soldiers.

In the civilian field there is a vast number of telecommunication systems located in isolated regions, far away from the natural gas grid or electricity network, which are powered by traditional inefficient stand-alone gensets. SOFC technology fits like a glove for supplying clean, reliable and efficient energy to the telecommunications' network. Another industry that could certainly take advantage of these characteristics is the gas & oil industry. Apart from providing more efficient power off-shore, SOFC systems can be used for cathodic protection of gas pipelines to prevent corrosion, substituting the devices used today, which have an extremely low efficiency.

The most important industries providing these devices are:

- Ultra Electronics AMI;
- Protonex;
- Adelan;
- Plansee.

3.1.2. Auxiliary Power Units (APU) (1–250 kW)

SOFCs can also be employed in auxiliary power units (APU) for on-board generation of electricity on vehicles of any kind. The main scope for application is that of electricity supply while a vehicle is at a standstill, ranging from caravans stationed overnight to aircraft parked at an airport gate. An SOFC-based APU also improves electricity generation efficiency during the vehicles' journeys and can supply back-up power during emergencies.

Many large vehicles run on diesel today, and SOFCs offers the advantage of being able to operate on diesel reformate without the necessity of further gas processing steps that would be required to purify the reformate to hydrogen. It is the ideal APU unit from a size of 500 Wel (watts electric power) up to several tens of kWel for road vehicles or even several hundreds of kWel as required by aircraft and marine vessels. In Figure 3.2. a Delphi APU on board of a truck is depicted.

Figure 3.2. A demonstration model of the Delphi APU on-board of a commercial truck [19].

The efficiency of electricity generation on board of vehicles, using a conventional generator coupled to the engine, is in the range of 10 to 15% today. The system net efficiency of an SOFC APU could

reach above 30%, which would more than double the power yield from the same amount of fuel. Additionally, on-site emission of diesel fumes, noise, and other pollutants would be reduced to near-zero. Utilization of the heat produced by the SOFC for heating or cooling (via absorption coolers, for instance) on the vehicles would further increase the overall efficiency. In Figure 3.3. it is shown the comparison between a conventional engine- based power train and a fuel cell- based power train.

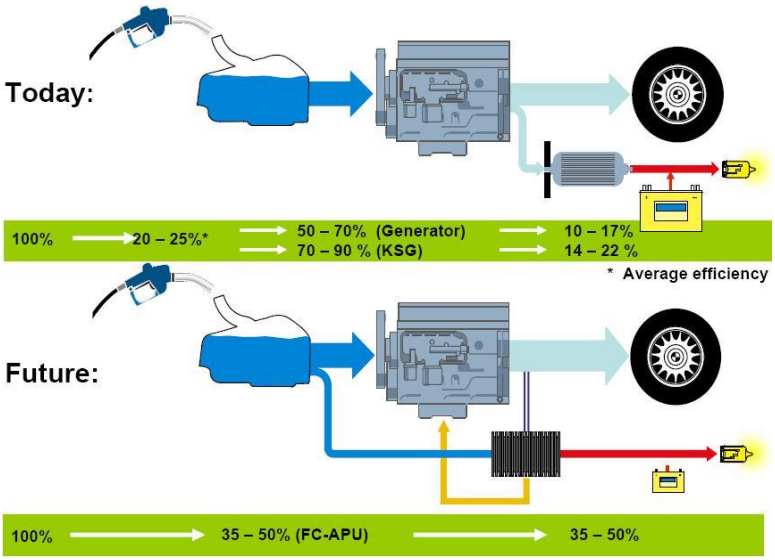

Figure 3.3. Comparison of overall electric efficiency between a conventional engine-based power train (fuel-engine-generator-load) and a SOFC-based APU (fuel-SOFC-load) [20].

The most important industries providing these devices are:

- Delphi;
- Protonex;
- MSRI;
- Ultra Electronics AMI;
- New Enerday.

3.1.3. Stationary small-scale combined heat and power

Stationary small-scale power plants (1–5 kW) are usually referred to as micro-CHP, which stands for residential-scale combined heat and power. The great potential of this application lays in the fact that both power and heat for a household can be generated on the premises, from a single primary energy carrier, such as natural gas or LPG. This obviates transportation losses and greatly enhances the utilization of these fuels, reducing wastes. Each end-user thus becomes a producer as well, creating the opportunity to sell electricity when supply exceeds the household's demand. This concept is known as distributed, or decentralized, generation and is explained in the following figure.

As can be seen, considerable amounts of primary energy input can be saved by producing power on the spot and utilizing the excess heat for heating purposes, rather than relying on centralized production of power and separate heat generation. In Figure 3.4. an example of comparison between centralised and decentralised supply of electricity and heat is provided.

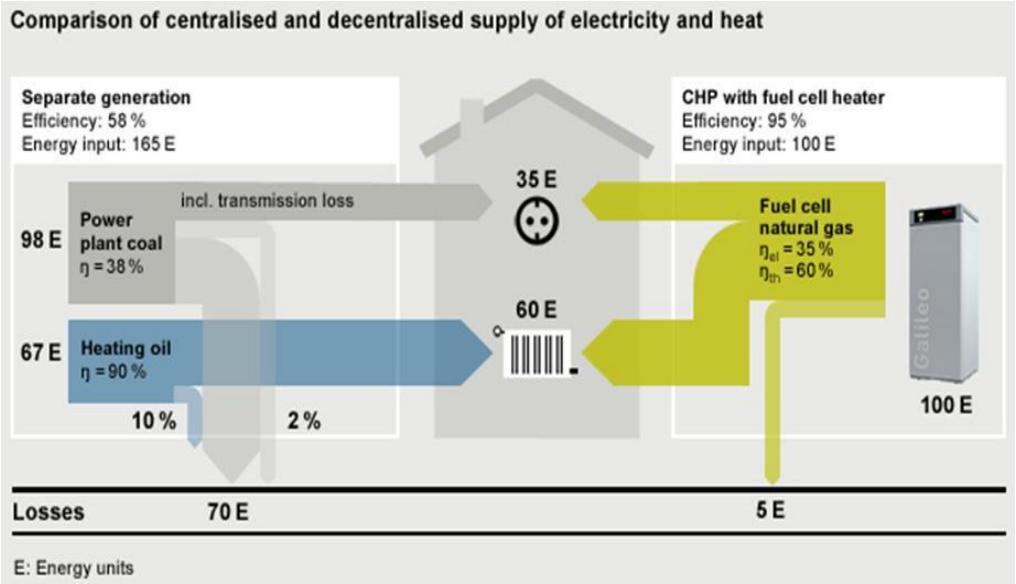

Figure 3.4. Comparison of overall primary energy consumption between centralized supply or on-the-spot micro-CHP, for given household power and heat requirements [21].

Two main modalities can be distinguished of micro-CHP systems: those that obtain the fuel from the grid (e.g. natural gas) and those that work isolated from the grid (off-grid or stand-alone) thus having to store the fuel.

Thanks to the widespread availability of natural gas through the distribution grid, the grid-connected application has the potential to become very widespread, and the potential market – aiming at the replacement of old household boilers could be of several hundreds of thousands of systems per year in Europe alone.

The most important industries providing these devices are:

- Acumentrics;
- Atrex Energy;
- Ceres Power;
- Ceramic Fuel Cells
- Ceramatec;
- Nexceris;

- Elcogen;
- Hexis;
- Kyocera;
- SOLIDpower;
- Staxera-Sunfire;
- Topsøe Fuel Cells;
- Bosh thermotechnology;
- ErlingKlinger;
- mPower gmbh;
- G-Cell;
- H2epowersystems Inc.;
- Huatsing Jingkun New Energy Technology Co. Ltd;
- MiCo.

3.1.4. Stationary medium-large scale

Electricity can be transported over long distances with little power loss, but heat cannot be piped efficiently far from the point of generation. In order to make use of the generated heat, power plants should therefore be smaller, dispersed and located nearby the end-users. However, conventional power plants cannot be down-scaled without efficiency loss, and also the negative impact of a combustion-based plant is generally not desirable in the vicinity of the end-user basin. Medium and large SOFC-based generation systems (in the range of hundreds and thousands of kilowatts) do not have these drawbacks and can efficiently combine heat and power delivery at "neighbourhood scale", as well as to other centres that can benefit from having their own, independent power and heat supply.

Medium-scale SOFC generation can also fit the needs of the automotive industry for clean and efficient powering, either by integrating the unit inside the vehicle (see the section on Auxiliary Power Units), or by externally recharging battery electric vehicles (BEV). The transportation sector represents the fastest-growing sector in terms of energy consumption, with a vast majority of greenhouse gas emissions being produced by road-based transport. Battery-recharging stations installed strategically in areas isolated from the electricity grid could contribute to improve the infrastructure and promote the use of electric vehicles, thereby reducing local CO_2 emissions and overall fuel consumption.

Though smaller systems limit the liability of SOFC products in the early stages of market introduction, and are therefore favoured by industry today, large-scale SOFC plants certainly represent the next step in providing clean affordable energy to society at large. At multi-megawatt scale, traditional powering technologies can be integrated into fuel cell-based power plants to achieve

even higher electrical efficiencies, for example by incorporating a bottoming cycle with gas and/or steam turbines working either under atmospheric or pressurized conditions. As depicted in Figure 3.5., integrated gasification fuel cell power plants (IGFC) become economically feasible with large-sizes, as the efficiency of turbines increases with their size.

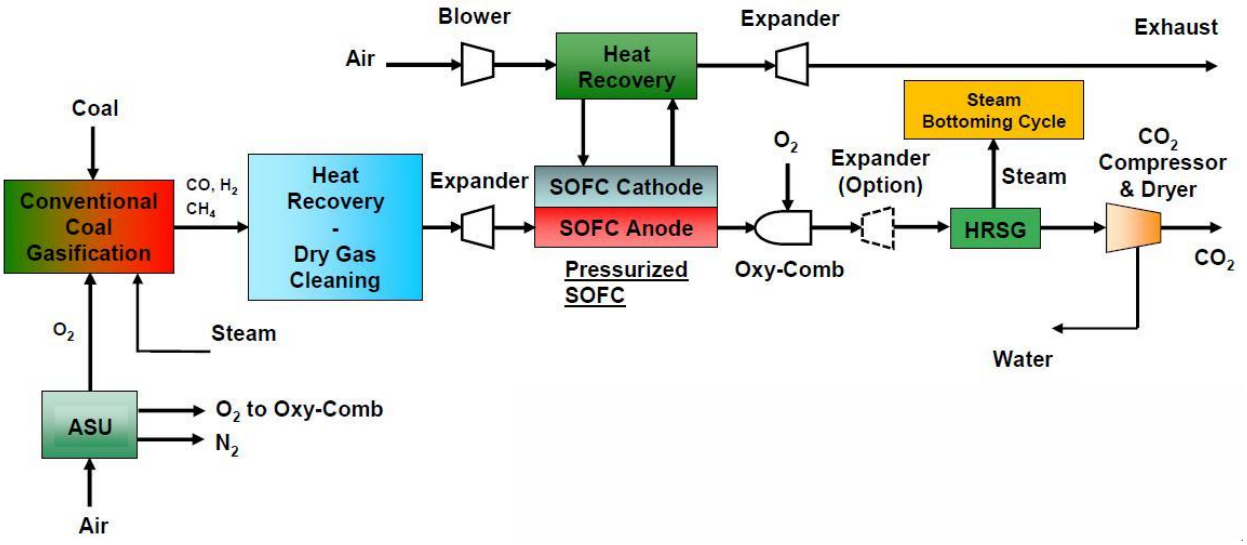

Figure 3.5. SECA Coal-Based Systems Pressurized IGFC (conventional coal gasification, low water use, 99% carbon capture, 50% efficiency) [22].

The most important industries providing these devices are:

- Bloom Energy;
- Fuel Cell Energy;
- Delphi;
- Convion;
- Mitsubishi Heavy Industries;
- LG Fuel Cell Systems
- Versa Power Systems;
- ZegPower;
- Posco energy.

3.2. North America

3.2.1. Atrex Energy

It began as the advanced Research and Development Division of Acumentrics Corporation, a manufacturer of highly reliable power products. These include rugged, uninterruptible power supplies for use in harsh environments. Founded in 1994, Acumentrics created the R&D division in 1999 to help develop both a compact energy storage device based on a rapidly spinning flywheel and a unique fuel cell unlike any others at the time. With the growing market success of the remote power products, in 2015 Atrex Energy was formed as an independent, stand-alone company. The goal of Atrex Energy is to continue to expand the SOFC portfolio as well as develop and commercialize new power and energy products. Since 2000 Atrex Energy has spent over $100 million on the research and development of a commercially viable Remote Power Generator utilizing SOFC. Atrex Energy has made substantial progress in improving the technology over this timeframe:

- Increasing the output per fuel cell tube 120-fold
- Developing SOFC designs with peak output over 10 kW; the first working SOFC generated a mere 20 watts of power
- Tripling power density
- Developing 15 patented innovations.

A key design feature of the Atrex Energy SOFC design is the actual tubular shape of the fuel cell. The patented tubular design eliminates one of the biggest issues facing fuel cell technology – catastrophic damage due to temperature gradients. Temperature gradients occur during the normal thermal cycling that takes place during start-up, shut down and load changes. This cycling, over the lifetime of the unit, introduces stresses that could eventually manifest into cracks and ultimately failure. The small radius geometry of Atrex Energy's tubes, their inherent strength, the strong seal at one end and the operation under low pressure combine to minimize temperature gradients. This allows the tubes to easily tolerate thermal cycling. In addition, Atrex Energy's tubular design is much more tolerant to the stresses from internal reforming. So, the need for costly external reformers common with planar fuel cell systems is eliminated. In fuel cells using planar ceramic plates there is an inherent weakness in the plates. They are fragile and hard to seal. Once assembled in stacks they require air and fuel to be supplied under high pressure. As a result, the plates can be prone to breaking under thermal stress. Internal reforming of fuel is also destructive to planar or membrane fuel cells due to the temperature gradients resulting from the reforming process. This makes external reforming

a necessity even for simple fuels, adding cost and complexity to the operation. It is also less efficient at reforming the fuel than the internal method used in Atrex Energy's SOFC design as well represented in Figure 3.6.

Figure 3.6. The Atrex Energy SOFC tubular design.

The Atrex Energy Remote Power Generator System, in Figure 3.7, has been designed to provide users with the most flexibility possible to meet a wide range of customer needs. Atrex Energy can work with users to configure the power generator to optimize the performance for each application. Some of the key attributes that can be configured:

- Power Output: Four different models handling loads of 100 watts up to 4500 watts;
- Voltage range: Output voltage from 2 VDC up to 60 VDC;
- Fuel Flexibility: Propane or Natural Gas;
- Electrical modes: three electrical operating mode options – constant current, constant voltage or battery charge;
- System data interface to a customer-provided SCADA system;
- Remote Current Interrupt (RCI) capabilities with customer-provided Remote Monitoring Unit (RMU);
- 12VDC or 24VDC Auxiliary Output option.

Figure 3.7. The Atrex Energy RP250

3.2.2. Bloom Energy

It was founded in 2001 with the name Ion America and based in California (USA). The company changed its name to Bloom Energy (BE) few years later, following major investments.

Bloom Energy develops and commercializes large reliable SOFC systems with high efficiencies. At the core of their products are stacks of planar electrolyte-supported fuel cells manufactured with noble metals sprayed on ceramic supports that require no special inks. Part of the technology adopted was al-ready developed through their work as a partner in NASA's Mars Program.

In cooperation with the University of Tennessee (USA), BE produced a 5 kW_{el} stack which was tested in field trials starting in 2006 in places with diverse climatology, including California, Alaska and Tennessee. In the period ranging from November 2006 to December 2009, in cooperation with the U.S. Department of Energy (DoE), R&D activities were directed towards a 25 kW_{el} grid-connected system for co-production of electricity and hydrogen. The field-tested units worked for more than 5000 hours and the availability of the plants was over 97%. The company has continued increasing the size of their systems during these last years, producing the servers: ES-5000, ES-5400 and ES-5700, generating 100, 105 and 210 kW_{el} respectively.

The heart of these servers is built up with 1kW_{el} stacks, labelled as 'Bloom Boxes', which are composed of 40 cells of 25W_{el} each, fuelled with natural gas or biogas and achieving over 50% net electrical efficiency.

Several renowned multinationals have chosen to install Bloom Energy's servers to power their headquarters, the vast majority of these are in California. As an example, Google, Coca-Cola, Ebay, Walmart and Bank of America are amongst their clients. Each Energy Server can be connected, remotely managed and monitored by Bloom Energy, this way minimizing possible failures. The system can be fuelled by natural gas or biogas, in grid-connected or stand-alone configuration, ensuring continuous supply of energy, with high electrical efficiency even at part loads.

The Uninterruptible Power Module (UPM), depicted in Figure 3.8., allows Bloom Energy Servers to supply constant, stable power to protected loads during grid outages or grid flicker events. It is a modular addition to the Bloom Energy Server platform that enables delivery of high quality, grid-independent power for business and operational continuity.

Figure 3.8. UPM-570 Uninterruptible Power Module with a nameplate power output of 160 kW [23].

3.2.3. Ceramatec

It is an advanced ceramics material technologies research and development company that provides solutions to difficult scientific challenges facing companies, governments and research institutions worldwide. A CoorsTek company established in Utah (U.S.A.), Ceramatec is a key competency center of its global research and development organization, focused primarily on applications in the energy and environment sectors. Ceramatec has pioneered research and development in a variety of technologies based on ceramic solid-state ionics and electrochemical systems such as oxygen sensors, oxygen production, chemical production, and solid oxide fuel cells. CoorsTek is the partner of choice for technology & manufacturing companies worldwide, whose success requires the unique, high-performance properties of products manufactured from engineered ceramics & advanced materials. They deliver outstanding value through:

- Operational excellence
- Broad research, development, and manufacturing capabilities
- Unsurpassed expertise in materials engineering
- Highly collaborative, responsive, and reliable relationships.

Examples of Ceramatec’ s single cells and stacks can be found in Figure 3.9.

Figure 3.9. Ceramatec's anode supported single cells and stack [24].

Ceramatec is exploring several different solutions in the area of renewable energy storage. It has more than two decades of experience in developing and testing Solid Oxide Fuel Cell systems. kW size stacks have been tested using a variety of fuels such as natural gas, reformed JP-8, etc. Electrolyte materials investigated include oxygen ion conducting stabilized zirconia, doped ceria, and doped lanthanum gallate and proton conducting doped barium cerate.

3.2.4. Delphi

It is a leader in electronics for automotive technologies. The company has created solid oxide fuel cell units for over a decade, focusing their R&D towards powering vehicles, stationary power generation and military applications.

As a result of its fuel flexibility, the Delphi SOFC can be engineered to operate with many types of fuels including natural gas, diesel, bio-diesel, propane, gasoline, coal-derived fuel and military logistics fuel. It will also be able to use tomorrow's next generation fuels. Delphi began work on solid oxide fuel cells in 1998 and has been a leader in the technology ever since. Delphi is the only member of the U.S. Fuel Cell Council that has developed and demonstrated a practical, operational SOFC auxiliary power unit (APU) for heavy duty commercial trucks. Delphi has partnered with private industry and leading academic institutions in the development of solid oxide fuel cell technology and has received funding from the U. S. Department of Energy and the U. S. Department of Defense for fuel cell development. A single Delphi Gen 4 SOFC Stack (see Figure 3.10) can provide 9 kW of electrical power and it features a modular design, ideal for integration into large power plants.

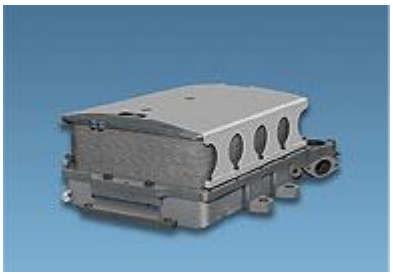

Figure 3.10. Delphi SOFC stack [25].

Delphi develops rectangular robust anode-supported cells. Generation-4 is their latest product in which the anode, cathode and electrolyte are based on nickel oxide yttria-stabilized zirconia, yttria-stabilized zirconia (YSZ) and Strontium-Cobalt-Lanthanum-Ferrite (LSCF) with Ceria-based interlayer respectively. Generation-4 stacks have 403 cm^2 of active area, providing high quality and reliable power (110 VAC and/or 12 VDC), with electrical efficiencies ranging from 40 to 50%. This stack is less expensive than Generation-3 thanks to improved interconnects and coatings and the pack's increased power (5 kW). The system can be run on several fuels including natural gas, diesel, bio-diesel, propane, gasoline and coal-syngas.

In cooperation with Volvo Trucks North America (VTNA) Delphi has developed a backup system suitable for heavy duty trucks and recreational vehicles. This APU allows shut-off of the main engine during long-term parking and full use of the cabin services, saving up to 85% of the fuel currently required for a main diesel engine running idle. It is the only member of the United States Fuel Cell Council that has developed and demonstrated in practice an SOFC power unit for heavy commercial vehicles.

3.2.5. Fuel Cell Energy

It is a world-leading developer of molten carbonate fuel cell (MCFC) systems, it absorbed Canadian Versa Power progressively from 2004 taking over and furthering their SOFC technology. In this way Fuel Cell Energy (FCE) brought their knowledge of fuel cell system deployment, especially related to multi-megawatt power plants for urban heat and power supply, to value in the smaller power scales targeted by SOFC. SOFC development facilities are divided between Calgary (CAN) and Danbury (CT). In Figure 3.11 it is shown an example of FCE stack building block.

Figure 3.11. Baseline FCE/Versa SOFC stack building block: Cell size 25 25 cm2, 120 cells, 68% fuel utilization, 25-70% in-stack reforming, around 16 kW gross DC electrical power [26].

FCE have incorporated the SOFC components into fuel cell stacks as part of FCE's project under the U.S. Department of Energy Solid State Energy Conversion Alliance (SECA) program. The SECA program has a long-term objective to introduce low-emission, high- efficiency SOFC based systems operating on coal gas in the size range of hundreds of megawatts. Other members of FCE's Coal-Based program team include the Gas Technology Institute (GTI), Pacific Northwest National Laboratory (PNNL), WorleyParsons Group, Inc., SatCon Power Systems, Inc., and Nexant, Inc.

The high efficiency and fuel flexibility of SOFC technology also makes it attractive for select portable power applications as FCE contracts with the U.S. Navy and a sub-contract to a U.S. Defense Advanced Research Projects Agency (DARPA) program illustrate. The U.S. Navy is evaluating the use of SOFC power for propulsion and ship power of unmanned submarine applications as the virtual lack of emissions, high efficiency, and quiet operating nature are well suited for stealthy operations. DARPA is evaluating SOFC based systems for unmanned airborne applications. The DARPA airborne system is an example of SOFC technology deployed for energy storage. The complete system incorporates both SOFC and solar power generation. During the day, the solar power generation is used to power the aircraft and excess solar power generation is converted to hydrogen by the fuel cells as they operate in electrolysis mode. At night, the fuel cells run in fuel cell mode, converting the stored hydrogen to power. SOFC based energy storage systems (see Figure 3.12) have the potential to provide unprecedented round-trip energy efficiency as the storage application of the technology is further developed.

Figure 3.12. Prototype large-scale SOFC combined heat and power module to be developed with [27].

In terms of stationary heat and power generation, FCE has been awarded $10M by the DOE for the design, fabrication, and testing of a 400 kW prototype system comprised of two thermally self-sustaining atmospheric-pressure 200 kW Solid Oxide Fuel Cell (SOFC) power generators to be installed and operated at a prominent site. This work will demonstrate SOFC stack reliability and endurance and utilize FCE's SOFC system design philosophy based on factory-assembled stack building blocks, which may be used to fabricate larger multi-stack modules for both sub-megawatt (MW) and multi-MW systems applications. Ultimately, thirty-two baseline 120-cell SOFC stack blocks will be fabricated and integrated into four 100 kW modular power blocks (MPBs) for the 400 kW prototype system. The system design will include novel balance of plant (BOP) components and operational/control strategies to improve SOFC stack endurance and reliability. The project is due to conclude towards the end of 2017.

3.2.6. LG Fuel Cell Systems (LGFCS)

It is part of the Korean multinational company LG. It acquired US Rolls Royce Fuel Cell Systems (RRFCS) in June 2012, investing $ 45 million for the acquisition of 51% of RRFCS stock. According to the agreement, RRFCS now takes the name LGFCS. RRFCS was created in 1992 in the United Kingdom for the development of SOFC MW-size cogeneration systems. In 2007, RRFCS had acquired SOFCo-EFS, a US company engaged in the development of SOFC systems and fuel processing. The enterprise has offices in the UK, US and Singapore, and has actively participated in European and North-American public fundamental research programs, amongst which are the Large-SOFC project financed by the European commission and the SECA Coal Based Systems and Coal Based SOFC Model Development Programme.

In 2008 they commenced the development of a hybrid pressurized SOFC-μGT system, where 250 kW_{el} modules would be operated simultaneously obtaining power plants with nominal power higher than 1 MW_{el}. The ultimate goal of this project is to develop the suitable SOFC technology for use in integrated coal gasification plants with sizes greater than 100 MW, achieving an overall efficiency (considering the gasification of coal and CO_2 separation) higher than 50%.

LGFCS uses flat tubular cells in a segmented configuration where anode, electrolyte and cathode are repeated transversely and longitudinally on a porous ceramic support which, in operation, is crossed by the fuel while the oxidant laps the cathodic surfaces from the outer side, inside of a collector. In Figure 3.13, there is an exhaustive explanation of fabrication of LG SOFC units.

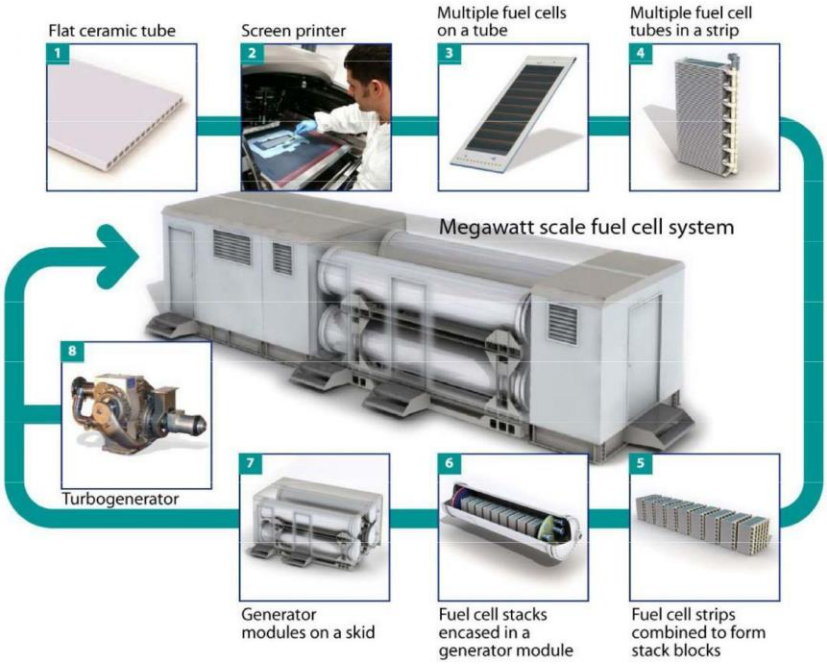

Figure 3.13. From component to final product: integration of RR-SOFC in the bundle, making up stacks, electrochemical modules and thermal units as base for multi-MW installations [27].

3.2.7. Materials and Systems Research, Inc. (MSRI)

It was founded in 1990 by Dr. Dinesh K. Shetty and Dr. Anil V. Virkar. Since that time MSRI has expanded into a 10,000 square foot state-of-the-art research, testing, and production facility. MSRI's facilities include over 15 high-temperature furnaces, three ovens, a surface grinder, two tape casting machines, an isostatic press, a laminating press, and six fuel cell testing systems. MSRI is a world leader in materials research and development. Its expertise includes the following areas:

- Solid Oxide Fuel Cell (SOFC) Technology — Low emission, high efficiency electrochemical power generation;
- Hydrogen Production Electrolyzer Technology — Small scale hydrogen production;
- β"-alumina — Used in batteries and nuclear reactors;
- Rechargeable Battery Technology — For high temperature applications;
- Sensor Technology - Multi-species gas sensors;
- Functionally Graded Si-C Technology — Will withstand a torque of 6,800 in. lbs.

MSRI has developed anode-supported fuel cells with very high-power density amount of power measured in watts per square centimeter of surface area by optimizing the microstructure of composite electrodes. MSRI has demonstrated 1-3 kW class SOFC power modules under various projects. Currently MSRI is developing a 3 kW air-independent SOFC stack for U.S. Navy's Unmanned Undersea Vehicles (UUV). Figure 3.14 shows a 33-cell stack capable of delivering 1 kW of power at 800 °C. The dimensions of the stack are 5.5" x 5.5" x 4.7" (W x L x H).

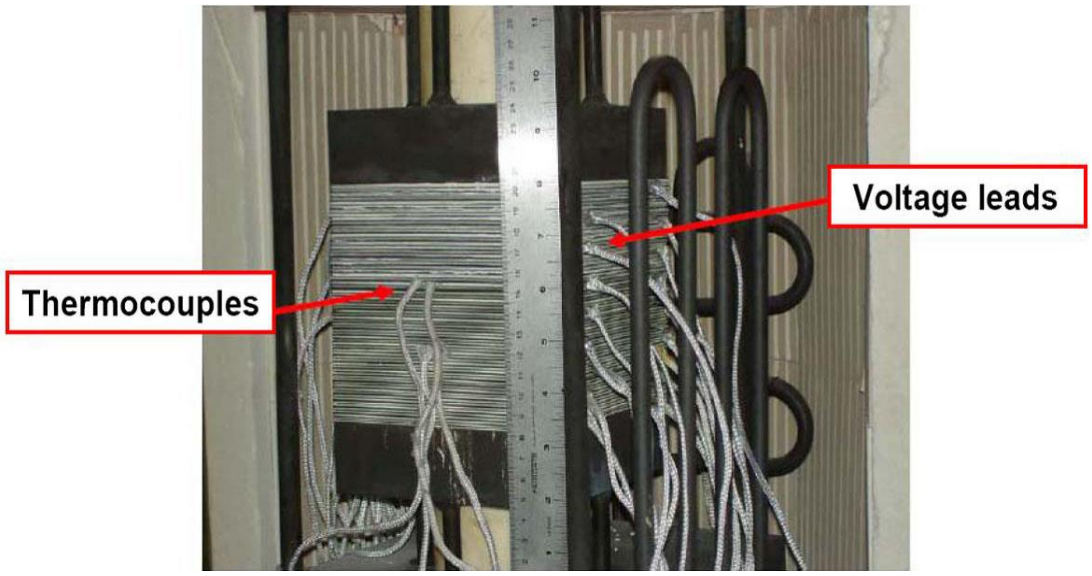

Figure 3.14. 1 kW 33-cell stack working at 800 °C [28].

Anode-supported tubular design showed in Figure 3.15 can be subjected to numerous thermal cycles and can be rapidly heated (e.g., within a couple of minutes) without cracking. No hot seal is needed.

Figure 3.15. 36-tube bundle for a 300 W portable power unit [28] .

3.2.8. Protonex

It was founded in 2000 with the aim of developing and marketing PEFC units. In 2007 it acquired Mesoscopic Devices LLC, a company involved in the research and development of SOFC technology, fuel reforming, and desulphurization systems, which expanded its commercial interests to SOFC technology.

In the past, Mesoscopic Devices had built ‘MesoGen-75’ and ‘MesoGen-250’ portable systems, at 75 W and 250 W respectively, with funding from the Department of Defence and the U.S. Navy. These units were able to provide suitable power levels for radios, sensors, and small batteries; both versions could be fuelled by propane or kerosene. MesoGen-250 models were also designed to operate as a field battery charger, and as auxiliary and emergency units on military vehicles.

Protonex develops SOFC systems based on tubular-cell technology, compact and suitable to better guarantee the robustness required for portable and mobile applications. The SOFC products currently exhibited is the P200i (see Figure 3.16).

Figure 3.16. Protonex P200i (20-200W) uses readily available commercial propane; made possible with an integrated sulfur filter [29].

Based on Protonex's industry-leading Solid Oxide Fuel Cell (SOFC) technology, the P200i powers remote sensors, signaling, and communications systems in blistering heat and arctic cold, for months or years without human contact. Easily coupled with solar panels to minimize fuel usage, the P200i withstands the elements for far more cycles and operation hours than other SOFC systems, and uses inexpensive, easy-to-obtain propane for fuel. The P200i supports all common lead-acid and lithium battery chemistries, and has full hybridization support built-in, making integration fast and easy.

3.2.9. Ultra USSI

It was established in 1993 in Ann Arbor. It is a successful international defence, security, transport and energy company. In 2011 Ultra Electronics Holdings acquired Adaptive Materials, an industrial developer of small SOFC systems using microtubular technology. Adaptive Materials was the first company to develop portable SOFC systems demonstrating their applicability in the field, since 2001 in collaboration with the U.S. Department of Defence. The company has developed, demonstrated and delivered successfully since then portable, affordable and fuel flexible SOFC systems, most of them to military customers and partners.

Ultra-USSI has a portfolio of compact, quiet and eco-friendly SOFC-based generation sets fed with propane to be utilized in the military, civilian and industrial sectors. The D300 (300W) model is suitable for applications as power support of on-field military power demand. The P250i (250 W) is suitable for remote power supplies (boats or campers, to power GPS systems, radios, refrigerators) and emergency back-up power, and can also be fuelled with natural gas.

USSI delivered 45 units of the D300 adapted for unmanned air vehicles (UAV) for use by the U.S military in unmanned aerial systems. The D245XR (245 W) unit provides long duration flights of more than eight hours in small unmanned aerial vehicles, being much more suitable than conventional batteries.

All of the devices provide 12-24 DC Voltage power supply (to integrate with batteries, solar charge controllers, DC-DC converters, fused external communications, computers, modems, and other customer electronics), targeting robustness and light-weight, compromising on efficiency which stands at 20%. Examples of Ultra USSI products are shown in Figure 3.17.

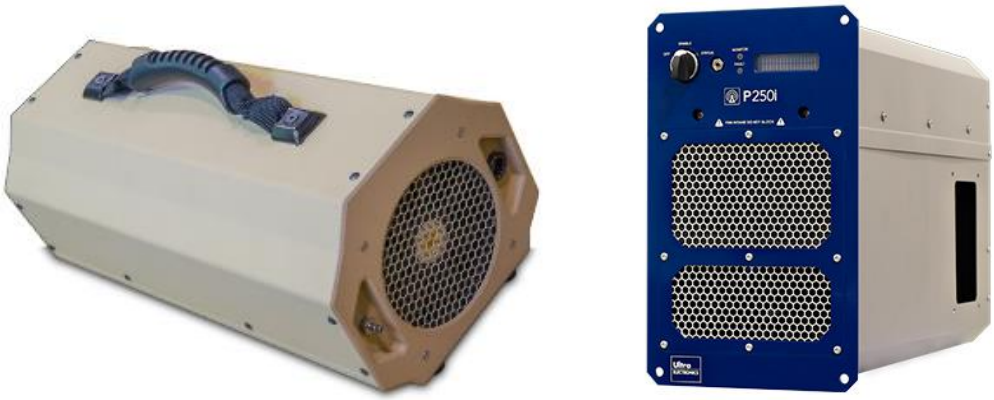

Figure 3.17. USSI D350 (245 W, 6"H x 16"L x 8"W, 5.1 kg, 134g/h propane) and P250 (250 W, 13"H x 17"L x 7"W, 10.7 kg, propane or natural gas-fuelled) [30].

3.2.10. Nexceris

It was founded in 1994. It is an American developer of advanced ceramics and electrochemical devices. Its commercial products are: SOFC materials and components, SOFC interconnect coatings and their products in the pipeline are SOFC stacks, based on their patented FlexCell components (see Figure 3.18).

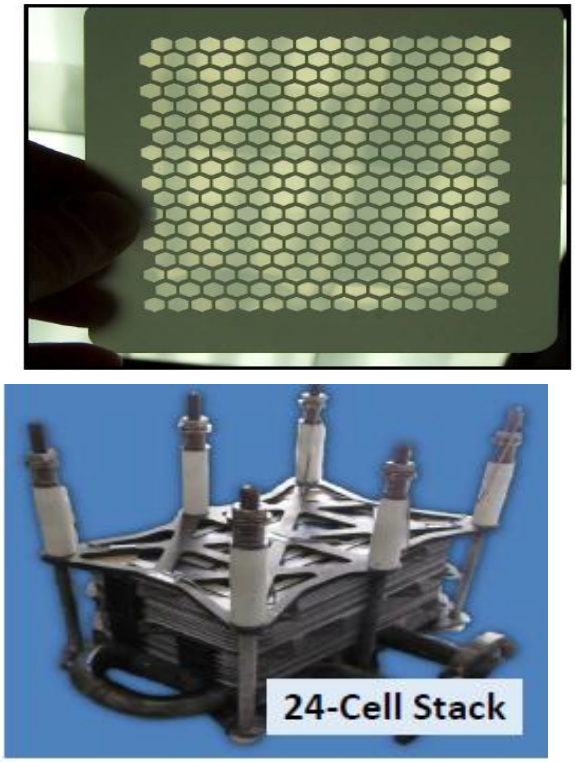

Figure 3.18. FlexCell (U.S. Patent No. 8,192,888) and Nexceris's 1 kW stack

The FlexCell has distinct characteristics:

- Thin electrolyte membrane for high performance;
- Small repeat units for high gravimetric power density;
- Dense electrolyte perimeter, enabling gasketed sealing;
- Thin electrode to reduce gas diffusion limitations;
- Sulfur tolerant anodes.

These cells are integrated into SOFC stacks with the following features:

- Thin-foil interconnects: Crofer 22 APU with cathode-face coatings;
- Seals: Ceramic/glass composites;
- Shims: Alloys or inorganic materials;
- Cathode current collectors: Silver mesh and coated metal alloy meshes;
- Anode current collectors: nickel foam, coatings to preserve sulfur tolerance.

3.3. Europe

3.3.1. Adelan

It is a cleantech development company established in 1996 in United Kingdom, by Professor Kevin Kendall FRS and Dr. Michaela Kendall.The Adelan team has the skills and capabilities to design, develop and implement micro-power solutions for a range of applications. Delivery of portable and mobile power solutions is Adelan's key strength. Adelan has more than three decades experience in SOFC material performance and degradation analysis, microtubular SOFC (m-SOFC) system design, and fuel cell demonstration. m-SOFC technology is developed and optimised by Adelan, with an aim to commercialise this technology in bespoke applications. Adelan technical skills are in the intellectual property related to m-SOFC systems, materials processing, SOFC testing and using various fuels, including hydrocarbons. Adelan produced many demonstrators over the years, including a m-CHP unit in 1997 and 2000. Adelan fuel cells (see Figure 3.19) are used in applications where power and heat are needed, typically in vehicles, buildings and remote areas. The energy is stored as liquid propane/butane or in methane as Natural Gas (NG) or Liquid Natural Gas (LNG). Electrical power is up to 250 W and heat is up to 1 kW. Start-up time is good for solid oxide fuel cells, around 10–20 minutes, 3000 hours of operation and 100 cycles at this performance level can be readily achieved. The benefits include light weight compared to batteries and low maintenance costs. Using 100 g/hr of propane gives 1000 hours of operation with a 100 kg propane store. Key market is the rapidly expanding decentralised power market.

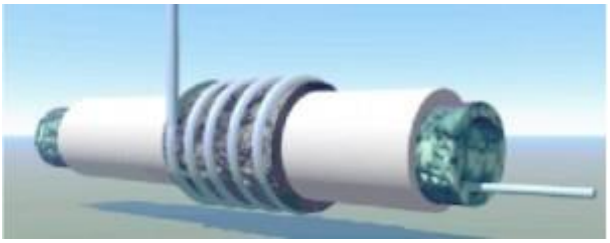

Figure 3.19. Adelan Microtubular SOFC [31].

3.3.2. Bosch Thermotechnology

It was founded in 1886 and is located in Germany. It produces mainly fuel cell 'energy centres' for single- and two-family houses. The Bosch Thermotechnology division is responsible for all activities involving heating technology and hot-water solutions. The division has a number of major international and regional thermotechnology brands and supplies people with state-of-the-art

technologies worldwide. They use for their products flat-tubular stack technology from the Japanese AISIN group (see entry in Asia section). Their main ‘energy center’ product is CERAPOWER (see Figure 3.20): the system is based on the Aisin 700 W system and is currently tested in the frame of the European m-CHP demonstration project *ene.field*.

Table 3.1. Characteristics of Bosch Cerapower [32].

ENERGY CENTRE	
Dimensions, WxHxD [mm]	1220x80x600
Weight [kg]	220
FUEL CELL	
Power output [W]	700
Thermal output [W]	700
Electrical efficiency [%]	45
Overall efficiency [%]	90

Figure 3.20. BOSCH’s Cerapower energy center [32].

3.3.3. Ceres Power

It is located in the United Kingdom and was founded in May 2001 to commercialize the unique core materials technology developed at Imperial College during the 1990s. Today, Ceres Power develops micro-CHP SOFC systems for the residential sector and for energy security applications, basing their operations and technology centre in Crawley and fuel cell mass manufacturing facility in Horsham,

Sussex. Ceres Power has built and developed relationships with key industry partners such as British Gas, Calor Gas and Bord Gáis.

The patented Ceres fuel cells (see Figure 3.21) are metal-supported (stainless-steel), allowing rapid start-up times and a great number of on/off cycles with little degradation. Their operating temperature range is 500-600ºC, significantly lower than the cells designed with conventional materials which typically operate at around 800 °C. This is possible thanks to the metal support (allowing the use of extremely thin and active catalytic components) and by using a new generation of ceramic material known as CGO (Cerium Gadolinium Oxide) instead of the industry standard YSZ (Yttria-Stabilised Zirconia).

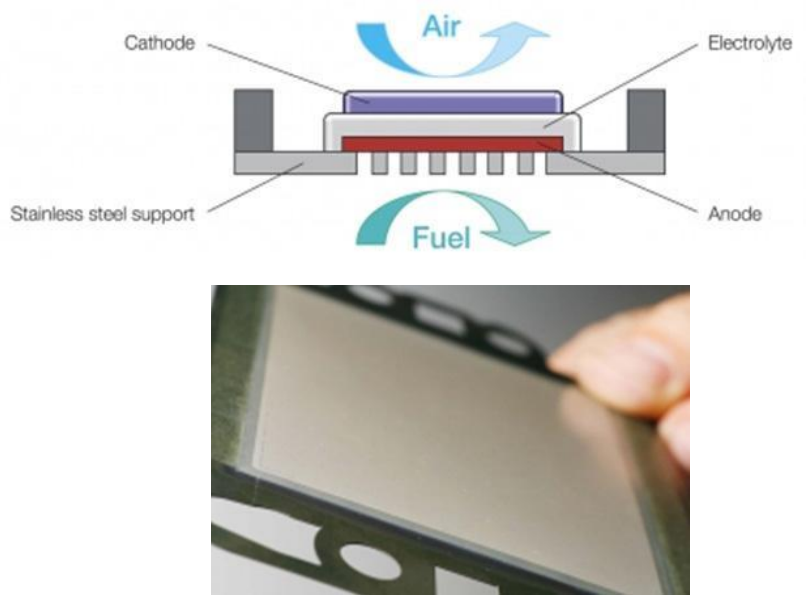

Figure 3.21. Detail of Ceres Power's single, metal-supported fuel cell, allowing extremely thin active layers and low temperature operation [33].

The company's first pre-commercial product is an integrated wall-mounted residential fuel cell combined heat and power (CHP) product (See 3.22). The compact product is designed to replace a conventional boiler, using the same natural gas, water and electrical connections and with similar installation and maintenance requirements. These m-CHP units have showed degradation rates of approximately 1% per 1000 hours of operation. According to Ceres, the micro-CHP product has the potential to meet the overall commercial performance requirements supporting mass market deployment from 2018. Under a new agreement, Ceres' partners British Gas (UK) and Itho-Daalderop (Netherlands) are to purchase 174 micro-CHP units for sale, installation and trial in UK and Dutch homes from 2014. Select customers will have the opportunity to purchase a Ceres micro-CHP unit with full service and maintenance package provided by British Gas in the UK and by Itho-Daalderop in the Netherlands. Feedback from these trials will be used by Ceres to refine the product

and validate performance and operability prior to mass volume launch in 2018. The trials will be part of the *ene.field* project, a large-scale demonstration of a thousand fuel cell micro-CHP products across Europe.

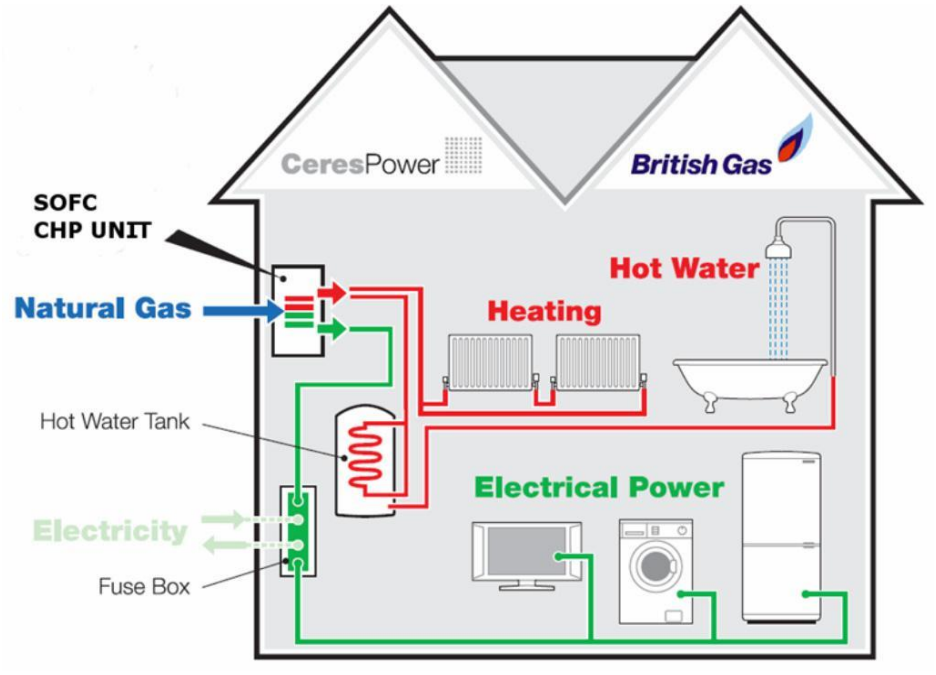

Figure 3.22. Ceres Power fuel cell integration concept in residential environment [33].

3.3.4. Convion Ltd.

It was established in 2012 and in January 2013 the company took over Wärtsilä's fuel cell program and continued development and commercialization of products based on solid oxide fuel cell technology as an independent company. Convion Ltd. is a leading fuel cell system developer committed to commercializing solid oxide fuel cell (SOFC) systems in power range of 50-300kW for distributed power generation fuelled by natural gas or biogas. Convion shareholders include VNT Management and Wärtsilä. Convion aims to provide a complete power generation solution based on SOFC technology. Convion fuel cell stack is depicted in Figure 3.23.

Figure 3.23. Convion's C50 product: a 50 kWe CHP generator with 53% electrical efficiency [34].

The main figures of the Convion C50 fuel cell unit are shown in the table below.

Table 3.2. Characteristics of Convion C50 [34].

Performance	Targets
Net power output	58 kW (3x400-440V AC 50/60 Hz)
Energy efficiency (LHV)	
Electrical (net,AC)	> 53%
Total (exhaust 40 °C)	>80%
Heat recovery	
Exhaust gas flow	650 kg/h
Exhaust gas temperature	222 °C
Emissions	
NO_x	< 2 ppm
Particulates (PM10)	<0.09 mg/kWh
CO_2 (NG, nominal load)	354 kg/MWh
CO_2 (with heat recovery)	234kg/MWh
Fuels	Natural gas, City gas, Biogas
Dimensions (LxWxH)	
Power unit	3.5 x 1.9 x 2.3 m
Auxiliary equipment	2.4 x 0.6 x 2.2 m
Noise level	< 70 dB (A) at 1 m
Installation	Indoor/outdoor
Ambient temperature	-20 -+ 40 °C

Each Convion C50 module is a fully integrated and autonomously operable power unit. Installations of multiple parallel modules can form an on-site power plant of power output of several hundreds of kilowatts, securing critical loads and providing continuous power and heat generation as a back-bone generator of a local microgrid.

3.3.5. Elcogen

It is located in Estonia and Finland and was established in 2001 in Estonia. Elcogen is a privately-owned company which focuses on commercializing anode-supported SOFC cells and stack to open markets. Its cell technology is optimized for 600–700°C operating temperature with state-of-the art cell performance proved both in fuel cell and electrolysis operation modes. The lifetime expectation of well over 20,000 hours for the unit cells combined with the low-cost manufacturing methods already implemented in cell production enhances the cost effectiveness of stack and system structures. Elcogen has been developing its cell and stack technologies closely with the Estonian and Finnish research institutes KBFI and VTT Technical Research Centre of Finland. It offers fuel cell stacks of 1 kW_{el} utilizing Elcogen unit cells. Elcogen SOFC stacks operate at temperatures between 600 and 700°C. They are based on a new generation of design focused on high efficiency, long lifetime, low cost materials and efficient, cost-effective mass manufacturing. The design is modular to enable its use in applications ranging from hundreds of watts to hundreds of kilowatts. The design is supported by long SOFC stack research as well as practical system knowledge from real-life applications. Two types of Elcogen stack are shown in Figure 3.24.

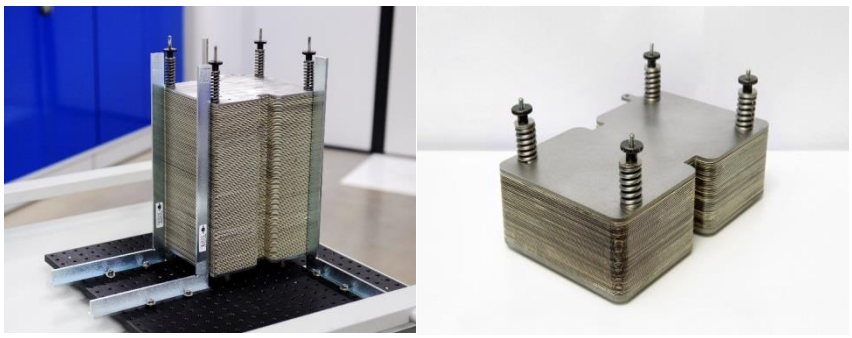

Figure 3.24. Left: E3000, 3kW stack; right: E1000, 1kW stack [35] .

The performance specifications of Elcogen stack E3000 and E1000 are presented in the table below.

Table 3.3 Characteristics of Elcogen stacks [35].

	E3000	**E1000**
Rated power [W]	3000	1000
Number of unit cells [pcs]	39	119
Maximum voltage (OCV, H_2) [V]	47	141
Minimum voltage [V]	27	81
Nominal current [A]	30	30
Maximum current [A]	40	40
Air utilization	0.12-0.3	0.12-0.3
Maximum fuel utilization	0.7	0.7
Maximum degree of internal reforming	0.65	0.65
Maximum temperature[°C]	720	720
Maximum inlet temperature for air [°C]	580	580
Maximum temperature difference [°C]	100	100
Maximum working pressure [mbar]	50	50

Elcogen SOFC unit cells (see Figure 3.25) are designed to operate at lower temperatures (600–700°C) to facilitate use of cost-effective metals in stacks. The Elcogen manufacturing process enables the production of various forms of cell, circular or rectangular up to a maximum of 20 x 20 cm for a cell. The anode-supported cell technology offers excellent efficiency and durability even at these lowered temperatures. Unit cells can be produced in different thicknesses, shapes or sizes and together with strict quality control specific customer requirements will be met.

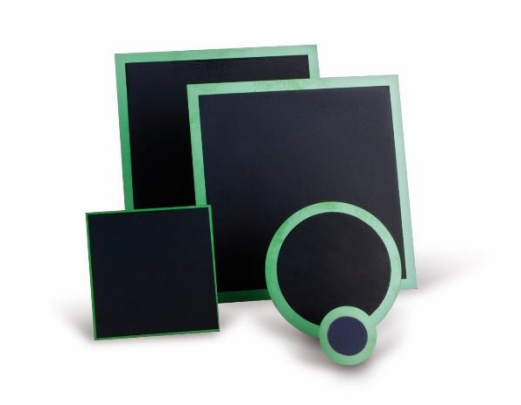

Figure 3.25. Elcogen's fuel cells. Cell show 5.5% degradation after 1000 h at 60% fuel utilization and 650 °C operating temperature with a reformate mixture of 15% CH_4, 26% CO_2, 29% H_2, 30% H_2O [35].

3.3.6. ElringKlinger AG

It is a family-owned company founded in 1879, located in Germany. ElringKlinger AG has worldwide activities in the development and the supply of cylinder head gaskets as well as several other flat gaskets, housing modules and thermal shielding modules for engines, gear boxes and exhaust systems. ErlingKlinger is the only independent gasket manufacturer with global activities and supplies almost every European and American vehicle manufacturer as well as numerous Asian car and truck companies. With more than 6990 employees at 41 locations in Europe, America, Africa and Asia the ElringKlinger group generated a turnover of 1175 million € in the year 2013. ElringKlinger has been developing processes and producing components for planar SOFC fuel cell stacks since the year 2000. ElringKlinger started to produce SOFC stacks in the year 2004. Today a pilot line for stack assembly is established in the headquarters in Dettingen an der Erms. The stack concept is based on the use of anode substrate cells. ElringKlinger manufactures interconnectors (see Figure 3.26) for SOFCs with the help of high-precision, volume-production-capable tools and by applying closely intermeshed production processes.

Figure 3.26. ElringKlinger interconnector for SOFC [36].

Solid oxide fuel cells (SOFCs) are categorized as high-temperature fuel cells and can therefore be run on standard fuels such as natural gas or diesel. Wherever hydrocarbon-based fuels are available, this fuel cell technology can be deployed effectively in all those areas of application in which low consumption, noise and emission levels are an essential requirement. ElringKlinger supplies lightweight SOFC stacks as a central component for these applications; they can be easily integrated into customer systems (electrical output: 0.2–5 kW) (see Figure 3.27).

Figure 3.27. ElringKlinger SOFC stack with power output 0.5 kW [36].

3.3.7. Haldor Topsøe AS

It was founded by Mr. Haldor Topsøe April 10, 1940. Haldor Topsøe delivers a wide range of catalysts and process technology that is essential for producing clean fuels from crude oil and waste, removing harmful emissions from power plants and vehicle exhaust, and raising the efficiency of industrial processes.

In 2004 Topsøe Fuel Cell (TOFC) was established as a subsidiary owned by the Haldor Topsøe AS and focused on the development of residential micro-CHP and auxiliary power units with SOFC planar anode-supported technology. Cell manufacture was established in a 1400 m^2 building based on semi-automated, modular and scalable processes. The facility output capacity exceeds 5 MW per year. In 2014, TOFC was closed and the activities transferred back to the mother company. As part of this closure, the development of its SOFC technology was put on hold and focus was instead set on the development of selected applications in solid oxide electrolysis cell development (SOEC).

It has introduced a SOEC system for the production of CO from CO_2 called eCOs plant. Further activities comprise upgrading of biogas to natural gas quality using SOEC, as it is pointed out in Figure 3.28.

Figure 3.28. Haldor Topsøe stacks for solid oxide electrolysis[37]

3.3.8. Kerafol GmbH

It was founded in 1985 in Germany. The company Kerafol® – Keramische Folien GmbH is the specialist for ceramic foils and a major manufacturer of technical ceramics. At their production site in Eschenbach in der Oberpfalz (Bavaria), products for thermal management, porous ceramic filter materials for fuel cells, ceramic substrates and ceramic foils are fabricated. These are used in a wide variety of applications, such as microelectronics, thermal management, filtration, sensor technology, SOFC fuel cells and LTCC technology. Since 1990, Kerafol® is involved in the field of the SOFC technology. In addition to the key components, being electrolyte substrates and electrolyte supported cells, Kerafol® also produces glass sealing tapes for stacks. Kerafol® offers both electrolyte substrates and electrolyte supported cells. In the electrolyte supported cell the electrolyte is the bearing component. The electrolyte separates the anode and cathode spatially from each other and usually consists of zirconia. At operation temperatures between 750 °C to 950 °C zirconia is a good oxygen ion conductor when doped with various metal oxides. Important factors for producing electrolyte tape and the choice of the doping metal oxide are the oxygen ion conductivity, the mechanical stability, the long-term stability, gas tightness, and planarity. Kerafol® offers partially stabilized variations with high mechanical stability, fully stabilized zirconia with higher ionic conductivity, and a mixed version, which combines both properties. Example of this cells are shown in Figure 3.29.

Figure 3.29. Various type of electrolyte substrates (left) and electrolyte-supported cells (right) [38].

Kerafols' electrolyte supported cells have a high planarity and are optimized for use in SOFC-stacks. Highly efficient electrodes with low polarization resistances have been developed. The robustness of the cells has been proven by several long-term tests, by thermal cycles, and by oxidation/reduction tests. Kerafol also developed the cell type KeraCell III, which is based on a LSCF oxygen electrode.

3.3.9. Hexis/Viesmann

It was created in 1997 as a venture division of Swiss engineering and manufacturing firm Sulzer and became independent in 2006. One year later they created the subsidiary company in Germany, Hexis. In 2016, Hexis was taken over 100% by Viesmann, the multinational boiler manufacturing company. The working principles of Hexis' cells are depicted in Figure 3.30.

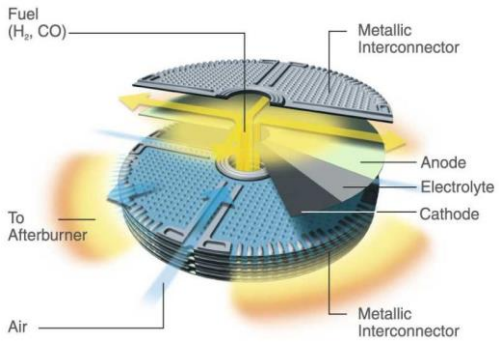

Figure 3.30. Working principles of a Hexis fuel cell [21].

Hexis develops SOFC-based CHP units for stationary applications with electrical power requirements below 10 kW. The company develops planar SOFC technology, where the cells have a circular design. The fuel enters the anode part of the cell through the centre of the disc, flowing radially outwards. The preheated air follows the same path on the cathode side.

Their commercial product is ‘Galileo 1000N’, which uses a stack module made up of approximately 60 cells and can be fed either with natural gas or bio-methane, as the system integrates a catalytic partial oxidation (CPOX) reactor. The nominal electrical power output is 1 kW (AC), and the thermal power output is 2 kW, with an electrical efficiency of up to 35% and maximum overall efficiency of 95% (LHV). Galileo 1000N (see Figure 3.31) also incorporates a 20 kW auxiliary burner to complete the supply of thermal on-demand requirements of a house or small apartment building. The commercial unit, geared towards end-consumers, is available since 2013.

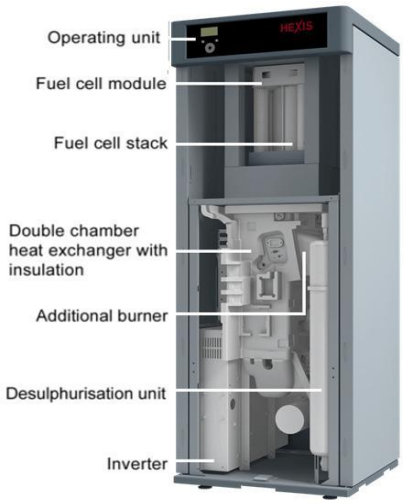

Figure 3.31. The Hexis Galileo 1000N m-CHP model [21].

3.3.10. MPower GmbH

It is a Dresden-based company formed in 2015 to commercialise the SOFC stacks developed by Fraunhofer IKTS & Plansee (see entry in Europe section). mPower has a world-wide license to manufacture, market and service the stacks for commercial applications. mPower GmbH is a startup of h2e Power Systems Inc. (see entry in Asia section) which is developing a complete 1kW, 2kW, 5kW & 10kW fuel cell power generators for stationary power applications. Using h2e's wide network and domain expertise in the food value chain, mPower is developing hotbox and stack solutions that will help build fuel cell systems for the food value chain all over the world. mPower GmbH is focused on providing extended lifetime (currently 20.000 h demonstrated), ease of integrating the stacks within the system and to bring down the costs to a level that will enable fuel cell systems to become commercially viable. Stacks with cumulative power output of more than 300 kW have been sold to commercial customers and the company is gearing up to develop solutions for various industry verticals in USA, Europe & India.

MK35x stacks are already being used in commercial stationary fuel cell systems for decentralised power generation with multi-fuel compatibility. The stacks are known for their robustness, reliability & efficiency. mPower currently manufactures fuel cell stacks of different size for various stationary

applications with the typical characteristics shown in the table 3.4 below.

Table 3.4. Characteristics of commercial MK35x stacks mPower's [39].

Available Power Output Range in W	250 to 1200
Weight in kg	3.3 to 13.6
Operating Temperature in °C	780 to 860
System Compatibility	Compatible to partial oxidation, steam and auto-thermal reformers
Internal Reforming of CH_4 in %	up to 32
Fuel utilization in %	up to 85

The company works closely together with Fraunhofer IKTS to design HotBox solutions, with which it can offer along with the stacks and stack modules for systems in the power range from 1 kW to 50 kW. An example of mPower stack is represented in Figure 3.32.

Figure 3.32. mPower stacks [39].

3.3.11. New enerday GmbH

Originates in the former fuel cell development department of Webasto AG in Neubrandenburg, it was founded in 2010 as an independent company to continue the development of innovative SOFC-based fuel cell systems with a special focus on highly compact systems with ratings of up to 1000 watts. New Enerday is a company of the ElringKlinger Group. The principal product of New Enerday is presented in the Figure 3.33 below.

Figure 3.33. Fuel Cell System EN 300/500 with electric power 150-500 W, voltage 24-28 V DC, electric efficiency (net) 30–35% [40].

3.3.12. Plansee SE

It was founded in 1921 and it is located in Austria. The Plansee Group is entirely focused on producing, processing and marketing the refractory metals molybdenum and tungsten. Plansee High Performance Materials is the world's leading manufacturer of products made of molybdenum, tungsten, tantalum, niobium and chromium – from powder production through powder-metallurgical processes to the customer-specific processing and recycling of these materials. The materials are used by customers in advanced industries and are key to today's and tomorrow's high-tech products. Important growth drivers include consumer electronics, coating technology, medical engineering and the semiconductor industry. The automotive sector, the aerospace industry, mechanical engineering and the construction sector also turn to the Plansee Group for expertise and materials solutions. Plansee supplies chromium-based interconnects for SOFC fuel cells. These provide the electrical and thermal connection between the fuel cell's anode and cathode and distribute fuel gas and air in the system. Using their powder metallurgical production process, they can manufacture near-net shape interconnects (See Figure 3.34).

Figure 3.34. Plansee CFY interconnector for SOFC [41].

With a mix of 95% chromium and 5% iron, Plansee's CFY can adjust the interconnect's coefficient of thermal expansion to match that of the electrolyte in the fuel cell. The electrochemical reaction in the fuel cell produces a lot of heat. The temperature can rise as high as 850°C. At the same time, the surfaces of the interconnects are exposed on one side to the oxygen present in the air, while the opposite side has to withstand high hydrogen concentrations. For this type of interconnects, that's not a problem. With a chromium content of 95%, their properties and geometry are unaffected. Another Plansee product are their metal-supported cells for mobile applications. These cells supply low-emission electrical power to trucks, mobile homes and yachts quietly and efficiently. With their short start-up time, low weight and long service life which can tolerate a large number of on-off cycles, SOFC fuel cells (see Figure 3.35) are able to meet the exacting requirements involved in mobile applications. Plansee uses a powder metallurgical process involving an Fe-26% Cr alloy to manufacture both the porous support for the electrochemically active cell and the interconnects themselves.

Figure 3.35. Plansee metal-supported cell for mobile applications [41].

3.3.13. SOLIDpower SpA

SOLIDpower, SOFCpower SpA before January 2015, is an Italian high-tech company based in Mezzolombardo, Trentino founded in 2006, by carving out the SOFC activities started in 2002 within the Eurocoating – Turbocoating Group, a privately-held group active in the fields of coatings and processes for gas turbines, machinery and biotechnology. In early 2007, SOLIDpower acquired 100% of HTceramix SA, a spin-off of the Swiss Federal Institute of Technology in Lausanne (EPFL). In 2015 it acquired in Heinsberg, Germany, the business and employees of Ceramic Fuel Cells GmbH (CFC) after the Australian parent company, Ceramic Fuel Cells Ltd, ceased activities.

SOLIDpower specializes in development, manufacturing and commercialisation of SOFC technology and systems for stationary applications including micro-cogeneration and remote power, SOFC testing and engineering services, SOFC system integration and high-temperature electrochemical membrane reactors. Over 750 SOLIDpower micro-CHP systems have already been

sold globally and contracts with utilities for further micro-CHP deployment are in place. An example of SOLIDpower's single cell is depicted in Figure 3.36.

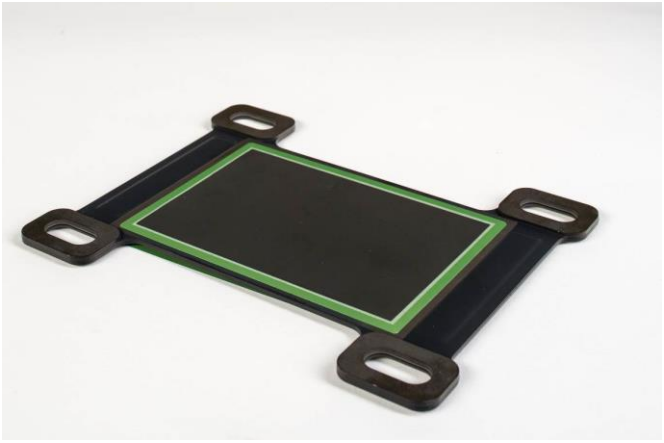

Figure 3.36. SOLIDpower's single planar cell unit for stacking [42].

SOLIDpower commercializes two highly efficient products for distributed cogeneration, both using natural gas from the grid:

- BlueGEN, which is the most efficient small-scale generator in the world, generates continuous 1.5kW$_e$ electric power at 60% efficiency (plus 0.6kW$_{th}$ for 85% overall efficiency). With an annual production of 13.000 kWh of electricity, it is appropriate for small commercial applications and is commercially available in various European markets.

- EnGEN 2500, a CE-certified m-CHP system with a nominal electrical output of 2,5 kW and 50% electric efficiency, which targets multi-family houses and commercial applications, even though larger generation units in MW-size can be realized by combining several modules. The wide range of modulation [30-100%] guarantees operation according to the user's actual electricity and heating needs. Furthermore, it can be combined with other power/heat generators from renewable sources (wind, solar) or heat pumps, as well as electric storage or UPS systems. Heat created in the generation process also provides up to 200 litres of hot water each day, which takes the overall efficiency to 90%. This can save up to 4 tonnes of CO_2 emissions per year.

The integration of SOLIDpower's single cells in BlueGen and EnGen systems is explained in Figure 3.37.

Figure 3.37. Integration of individual SOLIDpower cells in the 1 kWe BlueGEN (centre), and the 2.5 kWe EnGEN 2500 (right) [42].

3.3.14. Sunfire-Staxera

It is a joint venture between Webasto AG and H.C. Starck GmbH and is located in Dresden, Germany. Energy-related German company Sunfire and SOFC developer Staxera merged in 2011 as equal partners creating a brand-new company, although the Staxera brand has been retained. Sunfire is a manufacturer and developer of clean and efficient solutions for decentralized power generation and energy storage. Sunfire's high-temperature fuel cells (SOFC) efficiently generate electrical power and heat according to the principle of cogeneration (CHP). They allow on-demand generation for residential and industrial applications as well as off-grid power supply in remote areas. Sunfire uses the Staxera stack technology, based on the cells shown in the Figure 3.38 below.

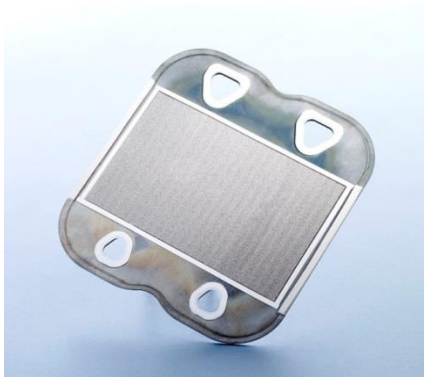

Figure 3.38. Sunfire single ESC cell design [43].

Staxera-sunfire has commercialized products up to 4.5 kW, based on their Mk200 stack. The robust, cost-optimized design of the Staxera Mk200 stack makes use of ferritic bipolar plates and electrolyte-supported cells (ESC). Low pressure loss and specially optimized fuel gas distribution mean that the Staxera Mk200 stack can be used to realize top-quality systems with low parasitic losses and therefore high levels of efficiency. The stack is designed to operate in combination with a wide range of fuel gases (e.g. as part of catalytic partial oxidation (CPOX) or steam reforming (SR) systems) and is characterized by excellent reliability in terms of both thermal and redox cycles. Stack size (i.e. the number of levels or cells) can be tailored to client requirements. The stack directly heated by anodic and cathodic gases. The gases are preheated to 400 °C. The thermal energy generated by chemical reactions within the stack further increases the temperature, up to the operating point of 850°C. In Figure 3.39 there is a description of a Staxera-Sunfire' cell.

Figure 3.39. Staxera-Sunfire's 116 x 168 x 182 mm3 cell stack, Fuel utilization 75 %, rated power output 600 W, operating voltage 19.5 V, weight < 14 kg. Performance at specified fuel compositions: 1: H2/N2 40%/60%, process efficiency (reformer and stack, LHV) 40% power output at operating Voltage 650 W; 2: steam reformate (S/C=2) power output at operating Voltage 550 W, process efficiency (reformer and stack, LHV) 48% [43].

3.3.15. Zegpower

It was established in 2008 as a Joint Venture between the two Norwegian research institutes Institute for Energy Technology (IFE, Kjeller) and Christian Michelsen Research AS (CMR; Bergen). Its Cooperation Partners are: Statoil Financing and technology development, Norges Forskningsråd (Financing of R&D projects) , Innovasjon Norge (Financing of business development and technology development, Miljøteknologiordningen), Gassnova (Financing of technology development and demonstration), IFE (Hydrogen production); Reactor technology and CO_2 sorbents, Hynor Lillestrøm AS (Test facilities), Kjeller Innovasjon (Company establishment), Bergen Teknologioverføring (Company establishment). The objective is to design, build and verify the patented ZEG® technology for commercial power plants of increasing size and complexity. Main deliverables are concepts and detailed designs of ZEG® plants for selected applications of different sizes, and complete small-scale plants. This technology is characterized by:

- High overall efficiency (more than 75%), including ~ 100% CO_2 capture and compression of CO_2 to 110 bar;
- All types of carbon-based fuels can be used; natural gas, biogas, gasified biomass, coal, tar or oil;
- Product compositions can be varied (within design limits) depending on market demand and customer need of electricity, hydrogen and heat;
- Possibility of standalone production;
- Applications and scale from small scale distributed plants based on biogas to industrial scale power plants based on natural gas.

ZEG-technology is a hybrid technology for highly efficient co-production of electric power and hydrogen from hydrocarbon fuels with integrated CO_2 capture. High total efficiency is achieved through thermal integration of high temperature fuel cells (SOFC – Solid Oxide Fuel Cells) and a reactor system for hydrogen production (SER – Sorption Enhanced Reforming). The principle of ZEG technology is depicted in Figure 3.40.

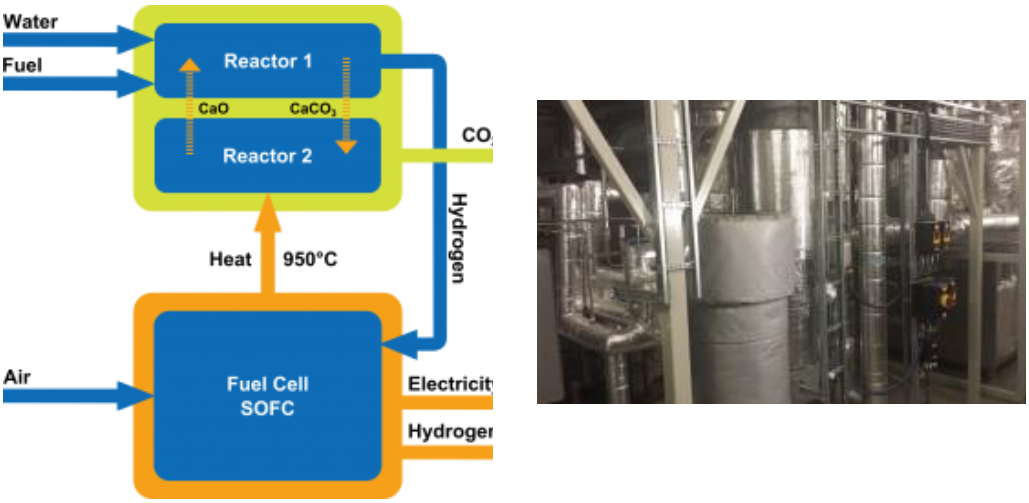

Figure 3.40. The principle of ZEG technology (left) and the 50 kW BioZEG plant at Hynor Lillestrøm, Akershus Energy Park [44].

The SOFC stacks produce electricity and high temperature waste heat. The waste heat is used to produce hydrogen in a modified reforming reaction where a solid (CaO – calcium oxide) is added, that captures CO_2 as an integrated part of the process. The CO_2 is delivered pressurized from the plant ready for industrial use or storage. The ZEG-technology enables conversion of hydrocarbons into energy with a very high efficiency, from 70 to more than 80%, depending on the plant size and design. In-site production of hydrogen from biomass will, when used for transportation, in addition to reducing CO_2 emissions, also reduce the need for transport of hydrogen to a refuelling station. CO_2 capture is an integrated part of the ZEG-technology, and it is advantageous for the total energy yield that the CO_2 is captured. If bio CO_2 is emitted this is seen as climate-neutral, and if CO_2 is used or sequestered (BioCCS) this will represent a positive climate contribution. Work is ongoing to identify industrial applications and customers that require both hydrogen and electric power and with integrated systems where carbon capture and sequestration (CCS) can be a part of a larger process plant.

3.4. Asia

3.4.1. Aisin Seiki

It was established in 1965 with head office in in Aichi, Japan. It comprises 181 consolidated subsidiaries, 66 of which in Japan and 115 overseas, and its businesses span the manufacture and sales of automotive parts (drivetrain, body, brake and chassis, engine, information technology-related), lifestyle- and energy-related products (mCHP, gas heat pump, sewing machines, beds, etc.), and wellness-related products. In terms of SOFC technology, they produce an innovative concept of flat sheet and tube cell which operate at between 700 and 750°C. Japan has a major deployment campaign of micro-CHP systems ongoing, named 'ENE-FARM', based on both PEFC (polymer electrolyte fuel cell) and SOFC technology. Already well over 140,000 ENE-FARMS have been installed since 2009. Currently AISIN is the only company supplying stacks to the systems based on SOFC, though competitors TOTO and NGK will introduce their stacks to the ENE-FARM programme soon. In close collaboration with Osaka Gas, Kyocera and Chofu, AISIN's 'ENE-Farm Type S', for residential fuel cell CHP fed with utility natural gas, was launched in 2014, achieving a power generation efficiency of 46.5% (LHV), and an overall efficiency of 90% (LHV). The SOFC system includes a heating unit, to optimally utilize the high-temperature heat exhausted during power generation, which fills a small storage tank of 90 litres with hot water, as well as a high-efficiency latent heat recovery type unit for the back-up boiler. The micro-CHP system is environmentally and economically optimized and avoids annual CO_2 emissions by approximately 1.9 tons while also reducing annual energy costs by about $ 909 compared to ordinary gas-powered hot-water supply and heating units. Within the co-development agreement, Kyocera produces the stack, Aisin the generation units with the cell stack incorporated into it, Chofu the hot-water supply and heating unit using exhausted heat. In Figure 3.41 there is a representation of an Ene Farm type S m-CHP system. Osaka Gas commenced sales of the system in 2014 (only to the Japanese market) and the standard price of the system has reduced considerably since then (see Table 3.5).

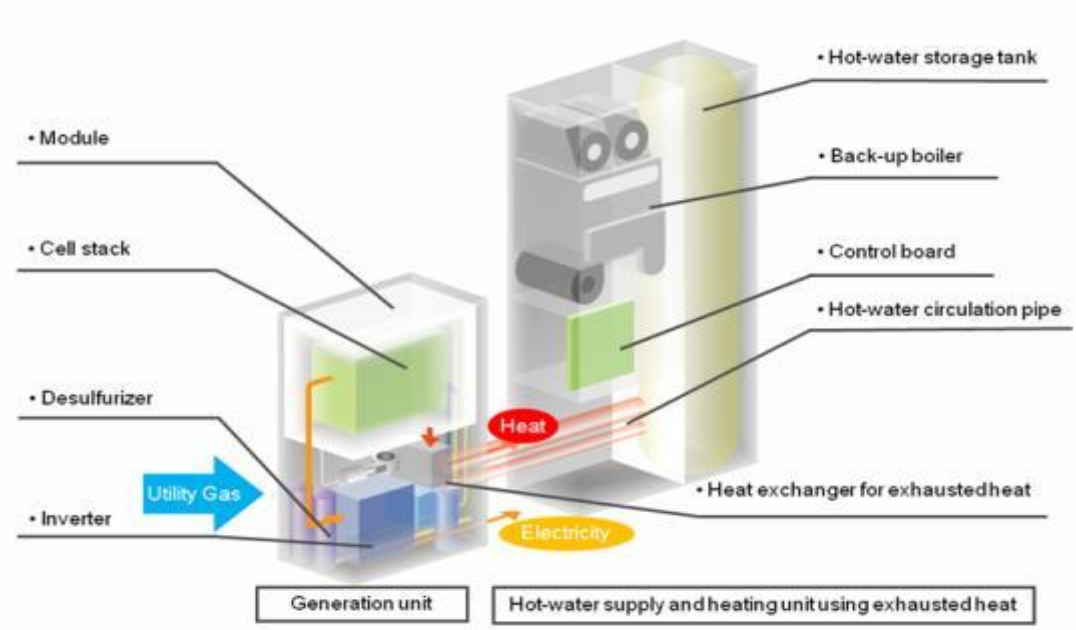

Figure 3.41. Schematic of an Ene Farm type S m-CHP system [45].

Table 3.5. Characteristics of ENE-FARM residential fuel cell CHP system.

ENE-FARM RESIDENTIAL FUEL CELL CHP

Selling date: April 27, 2012		
Basic Function	Rated power output	700 W
	Power output range	5 ~ 700 W
	Power generation efficiency	46.5% (LHV)
	Overall efficiency	90% (LHV)
	Operation temperature range	-10 ~ 43 °C
	Start-up time	120 ~ 180 min
	Operation time	24 hrs continuous
	Hot-water tank capacity	90 litres
	Hot-Water Temperature	~ 70 °C
	Installation	outdoor
	Voltage	100 V (50/60Hz)
Dimensions	Power Generating Unit	600 W × 935 H × 335 D (mm)
	Hot-Water Supply and Heating Unit using Exhausted Heat	740 W × 1,760 H × 310 D (mm)
Weight	Power Generating Unit	96 kg
	Hot-Water storage Unit	94kg (188kg in operation)
Installation Space		Approx. 1.9 m^2 (Approx. 1.6 m^2 with side exhaust gas cover)
Standard Price (incl. taxes and excl. installation cost)		¥2,322.000

3.4.2. Chaozhou Three-Circle Co., Ltd. (CCTC)

It was established in 1970 in Chaozhou, China. CCTC develops material, manufactures products and equipment, and carries out research and development as well. The application of its hi-tech ceramic products has extended to telecommunication, electronics, machinery, environmental protection, new energy biology and fashion etc. Previously including Ceramic Fuel Cell Limited (CFCL), CCTC branches include electrical, electronic, optical, medical, and structural ceramic manufacturer. Its principal products are anode supported SOFC cells, SOFC electrolyte membranes and Stack (see Figures 3.42 and 3.43).

Figure 3.42. CCTC anode supported SOFC cells (left), SOFC electrolyte membranes (right) [46].

Figure 3.43. C1 stack, 1 kW power stack efficiency degradation < 0,2%/khrs at BlueGen system Stack DC electrical efficiency > 65% at BlueGen system.

3.4.3. G-cell Technology Co., LTD

It was founded in 2013. It is established in Hefei Anhui, China. The company mission relies on the relevant technology of SOFC to provide energy efficient, environmental protection solutions and applications. It produces distributed power stations and standby power supply and application of SOFC in environmental protection and emission reduction, through for example Experimental SOFC stacks and 1 kW power station. In this company Air Brazing technology is used to improve the sealing ability between the SOFC cell and metal support, and to achieve the SOFC stack by combination of series and parallel connections. In Figures 3.44 and 3.45 there are a representation of G-cell SOFC cells and stacks.

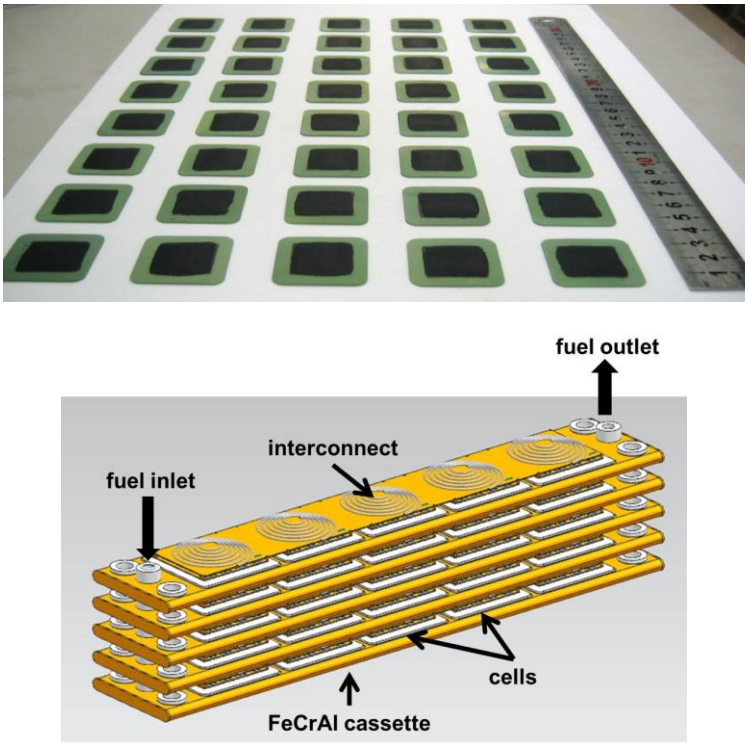

Figure 3.44. G-cell Technology SOFC cells and stack [47].

Figure 3.45. The G-cell C1 stack provides 24V, power output 1kW [47].

3.4.4. H2e Power Systems Inc.

It is located in Pune, India, and New York, U.S.A., was founded in 2012. H2e power systems is a part of the Mayur consortium. The company is internationally well connected and has contacts with several production plants and trading companies in the fields of residential construction, energy engineering, agriculture and waste management. h2e Power Systems aims at producing fuel cell systems in India and establishing integrated efficient energy supply solutions in order to allow for a cost-efficient, reliable and environmentally friendly power supply.

Fraunhofer IKTS and h2e Power Systems Inc. (part of India's Mayur Group) have set up a joint venture for the development and distribution of cost-efficient fuel cell devices. The know-how and technology transfer are initiated in order to facilitate local device production and commercialization in India by h2e Power Systems Inc. from 2016. In 2015, India's first ever solid oxide fuel cell system, (two prototype systems) developed by Fraunhofer IKTS was commissioned by h2e Power Systems Inc. During operation with natural gas, the prototype reached the intended key performance indicators with an electrical power production between 300 and 1000 W(el) and an electrical net efficiency around 35 to 40%.

h2e's product range is aimed at various market segments:

- Commercial: h2e can provide 1–10 kWe fuel cell generators for small commercials, hospitals, office buildings, schools/colleges, telecom towers & small/medium enterprises & small industries;
- Residential: h2e can provide 0.5–5 kWe fuel cell generators for apartments, Villas, high end homes, small, medium & rural households;

- Agricultural: h2e can provide 1–3 kWe fuel cell generators for food processing, cold storages, green house and farms.

An example of H2e generator is represented in Figure 3.46.

Figure 3.46 Artist's impression of a h2e Power Generator.

3.4.5. Huatsing Jingkun New Energy Technology Co., Ltd

It was created by an academician of the Chinese Academy of Engineering Peng Suping, chief scientist of the National 973 Project, Professor Han Minfang, and others, in February 2010. Huatsing New Energy is a high-tech enterprise integrating scientific research, new technology development, and high-tech production. It has independent intellectual property rights, whose main businesses include high-efficiency clean new energy technologies, new materials technology products, environmental protection products and engineering, and the design, manufacturing and services of related equipment. The specific products include SOFC core components and key materials, SOFC power generation systems, fuel cell test systems, engineering materials products, thermal equipment, environmental protection engineering and related services. In Figures 3.47 and 3.48 there is a representation of Huatsing New Energy SOFC cells and stacks respectively.

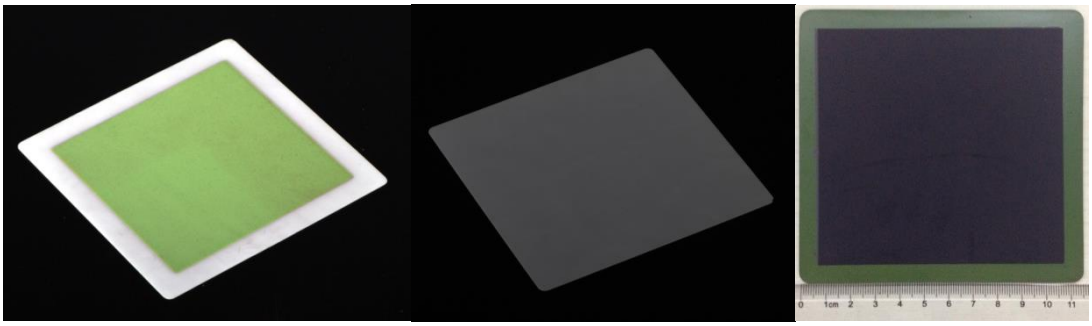

Figure 3.47 Huatsing New Energy SOFC cells. Right: Electrolyte Supported Cell, centre Anode Supported Cell, left Tri-layer YSZ-based cell [48].

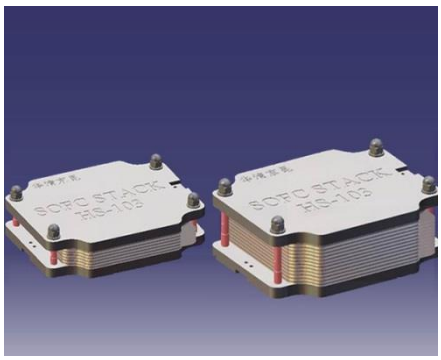

Figure 3.48. HS-103 type power stack 2.5–5kW, provides a voltage of 16.8–34 V [48].

3.4.6. Mitsubishi-Hitachi Heavy Industries (MHI)

It was established in 1914 and is a multinational engineering, electrical equipment and electronics company headquartered in Tokyo, Japan. MHI has been involved in the field of high-temperature fuel cells since the 1990s. In 1998, in cooperation with Electric Power Development Co. they produced a pressurized SOFC module which operated for 7000 hours and had a maximum power output of 21 kW. In 2004 MHI succeeded in the first domestic operation of a combined-cycle system combining SOFC and a micro gas turbine, with a confirmed generation of 75 kW at Mitsubishi's Nagasaki Shipyard & Machinery Works. As a result of its performance, in 2007 they decided to scale up the system to 200 kW, with a maximum power output of 229 kW and an electric efficiency of 52%. In 2009, MHI achieved an operation time of 3000 hours with this system, the longest so far in Japan. From this point forward, MHI has continued to increase the reliability and to further reduce the unit size, tying these qualities to the practical development of utility-size generation systems. Indeed, MHI is demonstrating a 250 kW coupled SOFC-microturbine in a triple combined cycle system (see Figures 3.49 and 3.50) which also generates steam to power a steam turbine, and which is currently operational at Kyushu Ito University.

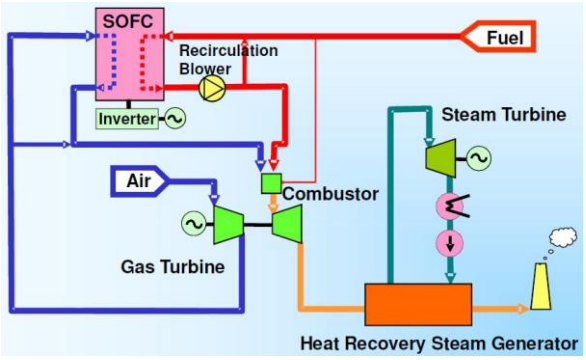

Figure 3.49. Mitsubishi's 250 kW coupled SOFC-microturbine system [49].

Figure 3.50. Mitsubishi is developing a SOFC-turbine triple combined cycle system [50].

Mitsubishi uses a mono-block layer built (MOLB) type of cell. This is a planar cell constructed of a ceramic substrate made up of anode, electrolyte and cathode (so-called generation membrane), dimpled in three dimensions and manufactured on an uneven surface and an interconnector that connects the generation membranes in series, and acts as a gas seal on the cell end.

MHI presented the first MOLB type SOFC (see Figure 3.51) cogeneration system in Japan at the World Fair held in Aichi in 2005, with a planar SOFC achieving a maximum output of 30 kilowatt through 100 percent internal reforming for the first time. Currently, the target is to further improve the fuel cell output, and research is proceeding.

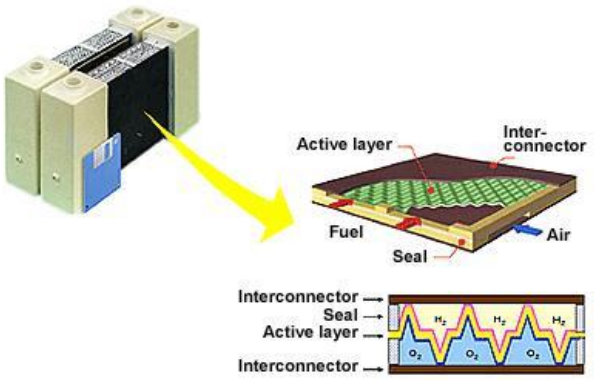

Figure 3.51. MOLB Type SOFC Structural Diagram [51].

3.4.7. MiCo

It was founded in 1996. It is associated with KoMico, MiCoBioMed. Core competences of MiCo has been manufacturing various ceramic parts with their core technologies achieved through continuous research & development on high-functional parts over the years. They produce SOFC materials, planar cells and micro-tubular cells (see Figure 3.52).

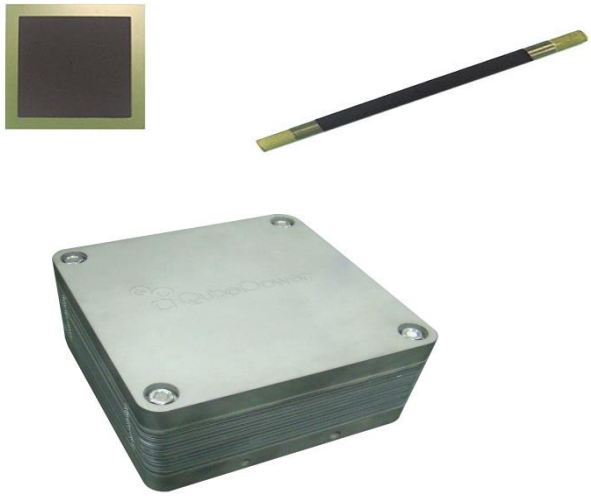

Figure 3.52. Anode Supported Cell, LSM (5 cm 5 cm), Anode Supported Micro-tubular Cell, LSM (3Φ×54 Φ) and the stack QubePower-200 [52]

3.4.8. POSCO Energy

It was founded in 1969 as Kyung-In Energy Company and having joined the POSCO FAMILY in 2005, is a comprehensive energy provider engaged in four key energy business areas: Power generation, Renewable energy, Fuel cell, and Resource development. Headquarters of POSCO

Energy is in Seoul City, South Korea. Fuel Cell Division of POSCO Energy is located at Pohang City. It produces also stationary application with MCFC and building applications with SOFC. POSCO ENERGY produces various fuel cell products ranging from 100 kW to 2.5MW to provide customers with a wide range of fuel cell products to suit their purposes. It currently supplies 100 kW, 300 kW, and 2.5 MW fuel cell products and is also developing other products applicable to various areas, as well as the next-generation SOFC technology. In Figure 3.53 there is a representation of Posco Energy's products.

Figure 3.53. Next-generation SOFC product of 300 kW [53].

3.4.9. SOFCMAN Energy Technology Co., Ltd.

It was founded in 2014 and is established in Ningbo, China. SOFCMAN are focused on the commercialization of proprietary SOFC technology into a growing international market. In Figures 3.54 and 3.55 there are examples of SOFCMAN's cells and stacks.

Figure 3.54. SOFC electrolyte supported cells and the SOFCMAN-ASC 60 Cell stack 601 with 10 cm x10 cm cells, maximum output power: 1600~2000W at 750℃, operation power :1400~1600W at 750℃, 0.70~0.75 V [54].

Figure 3.55. SOFCMAN-ASC 30-cell Stack-2 kW in this product the cell area is enlarged from 10cm x 10cm to 14cm x 14cm, SOFCMAN 30-cell stack (14cm x 14cm x 8cm) with double area showed a peak power of 2.6kW and current of 128A at 750℃. Under a self-sustained condition, the stack power reached 2.2 kW, at a current of 90A, average cell voltage of 0.8 V, fuel utilization of 68%, and electric efficiency of 44%. The volumetric power density is over 1.4kW/L [54].

4. MODELLING

In this chapter we provide a detailed state of the art of modelling approaches related to SOFC systems. This is very useful in order to make clear the importance of modelling tools in the work, where thanks to a numerical code we can analyze at two different length scales the performance, distribution of some chemical and physical parameters on the plane of the cell. Mathematical modelling can provide interesting information in limiting mechanisms, transport phenomena and electrochemistry on a local level throughout the cell. Also, numerical modelling can be useful to save costly experimental campaigns to carry out parametric studies. Regarding SOFCs systems, a further technological improvement is necessary to promote an extensive industrial commercialization. For this reason, synergy between experimentation and simulation is here proposed as the better approach to evaluate and optimise performance, providing solutions for diagnostic, predictive and development issues. In last years, a lot of scientists investigated in SOFC modelling to estimate physical, chemical and kinetic key performance indicators and attended the scale-up from the lab-scale to the industrial one. These models range from zero-dimensional (0-D) ones, which are lumped models using concentrated parameters and which can describe only cell global proprieties, to three dimensional (3-D) ones, which are detailed models using distributed parameters and which can describe cell local proprieties on the three spatial coordinates. The use of one of this type of model depends of the research aims: usually 3-D and 2-D models concern phenomena investigation, while 1-D and 0-D models are related to control purposes [55–60].

During SOFC system operation a lot of processes are taking place in a wide range of length and time scales. In table 4.1 are summarized typically phenomena occurring in SOFC with their corresponding length scales.

Table 4.1. Phenomena occurring in SOFCs at different length scales[61].

Scale [m]	Structure	Phenomena
10^{-8}-10^{-7}	Electrode material, Triple phase, Boundary electrode	Electrochemistry, diffusion trough the surface, chemical reaction
10^{-7}-10^{-5}	Porous media	Knudsen diffusion, flow through porous media, chemical reaction
10^{-5}-10^{-3}	Flow field	Diffusion, mass flow, heat exchange
10^{-3}-10^{-2}	Single cell	Transport of oxidant and fuel, thermal balancing
10^{-2}-10^{0}	Single cells/stack	Electrical circuit of the cell/stack, processes in the Electrical system, thermal balancing
10^{0}-10^{1}	System level	Control, automatics, regulation, safety systems, integration of the entire system

4.1. Modelling scales

A practical problem of fuel cells can be solved by 0D, 1D, 2D or 3D modelling [62–64]. A 2D grid in cell´s plane can be used to model planar SOFCs in co- or counter-flow gas feeding configurations [65,66]. A third coordinate is at times considered to take into account concentration and temperature gradients along perpendicular direction [67,68].

4.1.1. 0-D models

The simplest approach for SOFCs modelling is to consider system as a black-box, resulting in a 0-D model. Based on principles of thermodynamics and electrochemistry, the fuel cell is modeled into a group of algebra equations to solve for the cell output such as cell voltage, power output, and cell efficiency based on predefined operating conditions such as inlet gas composition, inlet temperature, fuel and air utilization ratio. Hence, the 0-D models are useful to evaluate the performance of the whole cell or stack, instead of local multiphysical phenomena inside the cell or stack. Examples of 0-D SOFCs modelling can be found in [69] where is developed a macroscopic model for control of SOFCs and gas turbine hybrid systems. Also in [70] we can find a 0D model of an SOFC with internal reforming for hybrid energy cycles.

4.1.2. 1-D models

In the 1-D model, the profiles of the chemico-physical properties are calculated only along the more significant coordinate, so that two of the geometrical dimensions are neglected [71–76]. Finally, 1-D models are based on groups of algebra equations to calculate for example cell voltage, power output and cell efficiency using a simplified macroscopic approach, effective for control purpose [77]. In literature we can find this type of model in [78] where there is a system ,with a SOFC stack, analysis performed by means of Aspen Plus software. Another example it is in [58] in which there is a dynamic analysis of direct internal reforming in a IT-SOFC stack with electrolyte-supported cell using a quasi-1-D model.

4.1.3. 2-D models

In 2-D model, the cell is represented as 2-D cross-sectional domain, and the changes of physics in the third coordinate are neglected. Examples of these types of model can be found in [79–81]. Based on this 2-D domain Jin and Xue [82] developed a transient 2D isothermal model, that could be operated in both SOFC and SOEC (solid oxide electrolyzer cell) mode to investigate complicated multi-physics processes during the transient process of mode switching. Verda et. al [83] applied their CFD model to an anode supported planar SOFC in 2D. Mahcene et. al [84] developed a 2-D single-cell model with co-flow pattern written in Fortran language to investigate distribution of the chemical species, temperature, current density and power density. This tool was based on mass, momentum and energy balances.

4.1.4. 3-D models

Compared with 2-D, 1-D and 0-D modelling, 3-D modelling can provide more detailed information of the SOFC behaviours [62]. Pasaogullari and Wang [85] proposed a 3-D model to describe the electrochemical kinetics, multi-dimensional gas dynamics, and multi-component transport of species in the SOFC. Wang et al.[86] used two 3-D Planar-SOFC single-cell models, with air and fuel channels in co-flow and counter-flow respectively, to predict the temperature distribution, molar concentration of gaseous species, current density, and over potential based on the fundamental conservation laws of mass, momentum, energy, and electrical charge. Detailed 3D fuel cell models are usually very computationally expensive due to the highly coupled and nonlinear nature of their mathematical formulation as well as many functional domains in the cell. In order to simplify the mathematical and computational complexity, the cell geometry is usually assumed to be 2-D [65,66,87], 1-D [71–73], or 0-D [88] instead of 3-D. However, these assumptions are likely to lower the fidelity of model predictions. In 3-D models the attention is focused on the local behavior providing temperature and reactants distribution along the three coordinates so as, for example in [89,90].

4.1.5. Grey and black box models

The mentioned models above can be defined “white” models, because based on explicit physical equations, or at least “grey” models, when based on a semi-empirical approach which integrates an a priori knowledge of the physical process and mathematical relations that describe the behavior of the system. In the latter case the model construction foresees at first the set-up of the basic model, then the conduction of experimental tests, finally the calibration and validation of the model on the basis of the experimental results. An example of this approach can be found in the work by Sorrentino and Pianese [91] for the diagnosis of a SOFC unit in a complex system. Nevertheless, in addition to these first principle models, also “black-box” models have been developed as behavioral models derived through statistical data-driven approach. Contrary to the physical models, they are not based on explicit physical equations, but on database of measured experimental values which are capable of reflecting the relationship between inputs and outputs, examples can be found in [92–97].

4.3. Governing equations

In this chapter it will be provided a full explanation of governing equation that are fundamental in SOFC modelling.

4.3.1. Reversible cell potential

As described above, in an SOFC there is a direct conversion of chemical energy into electrical energy [16]. In order to evaluate and express fuel energy the most useful approach is to use the Gibbs free energy because it represents the available energy to do work neglecting pressure and volume work. Gibbs free energy of formation for a reaction is written as:

$$\Delta G_f = G_f(\text{products}) - G_f(\text{reactants}) \tag{4.1}$$

For a fuel cell, the overall reaction is Equation 2.3 so:

$$\Delta G_f = (G_f)_{H_2O} - \left[(G_f)_{H_2} + \frac{1}{2}(G_f)_{O_2}\right] \tag{4.2}$$

In a fuel cell, along the external electrical circuit, for every mole of hydrogen used 2 electrons will migrate. The total charge flowing in the circuit will be -nF Coulombs, where n is the number of electrons involved in the electrochemical reaction.

The total work that have to be done in order to move -2F charge for ideal potential of fuel cell is given by:

$$W_{el} = -nFE \tag{4.3}$$

This work released Gibbs free energy (in ideal conditions):

$$\Delta G_f = -nFE \quad \Rightarrow \quad E = -\frac{\Delta G_f}{nF} \tag{4.4}$$

This is the electromotive force equation for a fuel cell, and E is the open circuit voltage of the cell.

For a generic reaction:

$$aA + bB \rightarrow cC + dD \tag{4.5}$$

Gibbs Free energy change is given by:

$$\Delta G_f = \Delta G_f^{\,0} + RT \ln\left(\frac{a_C{}^c a_D{}^d}{a_A{}^a a_B{}^b}\right) \tag{4.6}$$

Where $\Delta G_f{}^0$ is the free Gibbs energy change at pressure and temperature standard conditions, R is the gas constant and a_c, a_d, a_a, b_b are the activities of products and reactants of the reaction.

Substituting equation 4.4 in equation 4.6, we obtain the general form of the well-known Nernst equation:

$$E=E^0+\frac{RT}{nF}\ln\left(\frac{a_C{}^c a_D{}^d}{a_A{}^a a_B{}^b}\right) \tag{4.7}$$

It is clear from this, that if the concentration of reactants is increased the cell potential increases as well. The activity of an i^{th} ideal gas is defined as:

$$a_i = \frac{p_i}{p^0} \tag{4.8}$$

Where p^0 is the standard pressure equal to 0.1 MPa and p_i is the partial pressure of the $i^{th\ gas}$. If we consider the overall reaction of a fuel cell, Nernst equation will be:

$$E = E^0 + \frac{RT}{nF}\ln\left(\frac{p_{H_2} p_{O_2}{}^{\frac{1}{2}}}{p_{H_2O}}\right) \tag{4.9}$$

This equation expresses the theoretical ideal voltage, E, for an SOFC fed by hydrogen. The evaluation of Nernst equation and reversible cell potential can also be found in [3,16,98]

4.3.2. Polarization and cell losses

Actual performance of a SOFC is smaller than theoretical ideal voltage. In Figure 4.1 are depicted ideal and actual performance of cell.

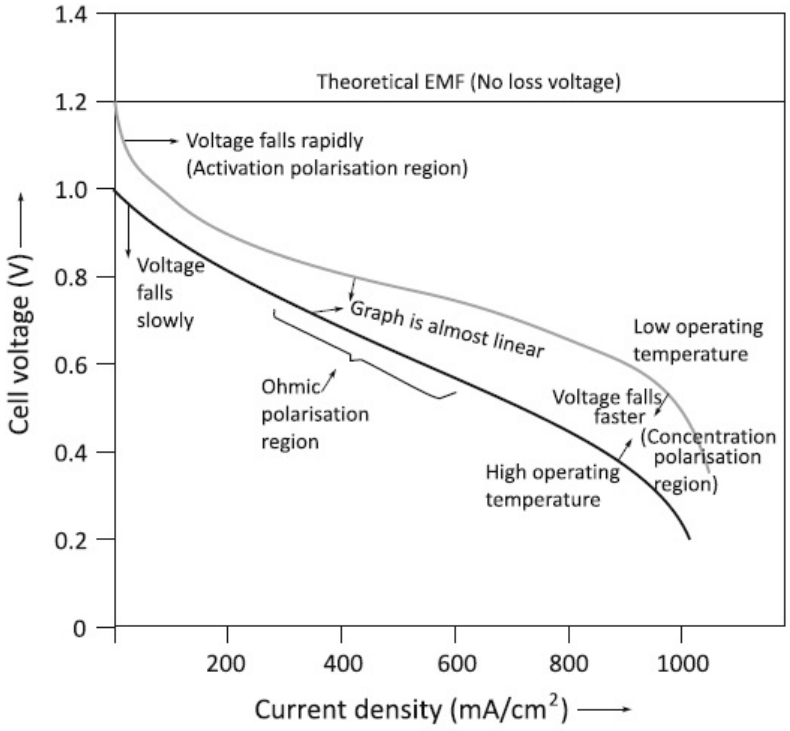

Figure 4.1. Representation of ideal and actual voltage[2]

Analyzing the figure, initial fall in voltage is small for cell operating at high temperature, instead is high for cell operating at low temperatures. In addition, cells operating at higher temperatures show more linear behavior. Actual voltage is penalized by irreversible losses in the system.

$$V = E - \eta \tag{4.10}$$

Primary sources of losses are three: activation polarization, Ohmic polarizations and concentration polarization.

- Activation losses are caused by the slow reaction kinetics on electrodes surface;
- Ohmic losses are due to the resistance offered to the electron´s flow and ions through electrodes and electrolytes, respectively;
- Concentration losses are due to the change in concentration of the reactants at the electrode surface.

4.3.3. Activation polarizations

A fraction of open circuit voltage is utilized to drive charge transfer reaction taking place at the three-phase boundary, e.g the region in which there is the contact between electrode, electrolyte and gas fuels, this fraction is activation polarization. Higher is activation polarization and higher will be the resistance for charge transfer reaction.

Butler-Volmer equation expresses the relationship between activation polarizations and current density:

$$i = i_0 \left[\exp\left(\frac{\alpha F \eta_{act}}{RT}\right) - \exp\left(\frac{(1-\alpha) F \eta_{act}}{RT}\right)\right] \quad (4.11)$$

where i_0 is the exchange current density, α is the number of electrons involved per reaction, R is the ideal gas constant, F is the faraday's constant, and T is the working temperature.

Exchange current density, i_0, is usually expressed as an Arrhenius-type equation [99] for both anode and cathode exchange current densities so:

$$i_{0,an} = i_{0,an}^{pre} \left(\frac{p_{H_2}}{P_{ref}}\right)^{\gamma^{H_2}} \left(\frac{p_{H_2O}}{P_{ref}}\right)^{\gamma^{H_2O}} \exp\left(-\frac{E_{act,an}}{RT}\right) \quad (4.12)$$

$$i_{0,cat} = i_{0,cat}^{pre} \left(\frac{p_{O_2}}{P_{ref}}\right)^{\gamma^{O_2}} \exp\left(-\frac{E_{act,cat}}{RT}\right) \quad (4.13)$$

where $i_{0,an}^{pre}$, $i_{0,cat}^{pre}$ are the exchange transfer current density pre-exponential factors in the anode and cathode respectively, $E_{act,\,anode}$ and $E_{act,\,cat}$ the activation energies for anode and cathode,

$P_{i,ref}$ the reference partial pressures which can all be equal to the ambient pressure, and γ_i is the reaction order of species i, *with* i =H_2, H_2O, O_2.

It is difficult to determine the reaction orders γ_k and in addition this value evaluated from exchange current density can differ considerably from those derived from elementary step kinetics. In its general form Butler-Volmer is difficult to use easily, so there are two simplifications useful in practical problems; at high activation polarizations first term of equation 4.11 becomes greater than the second one and so we can neglect the second one obtaining

$$\eta_{act} = \left(\frac{RT}{\alpha_a n_e F}\right) \ln i - \left(\frac{RT}{\alpha_a n_e F}\right) \ln i_0 \quad (4.14)$$

Or in more compact form

$$\eta_{act} = a + b \ln i \text{ [100]} \quad (4.15)$$

this equation is named Tafel equation. On the other hand, for low activation polarizations $\alpha_A \frac{n_e F \eta_{act}}{RT}$ becomes much less than unity and exponent can be expanded in terms of Taylor series and neglecting higher order terms we obtain the so called linear current-potential relation:

$$\eta_{act} = i\frac{RT}{n_e F i_0} \tag{4.16}$$

As these two last equations are simplifications, it is important to know their applicability range. Chan et. al [88] reported the lower limit of activation polarization for which Tafel equation is usable as η_{act} > 0.28 V and upper limit for linear current-potential relationship as η_{act}< 0.1 V.

4.3.4. Ohmic polarizations

In the state of the art anode supported cell Ohmic losses are very low because of the use of very thin electrolytes usually 5-10 μm thick. High temperature are not suitable because of damaging effects on fuel cell life time and cost of production of ceramic material required for high temperature operation [101]. Ohmic polarization can be evaluated as function of current density, i as:

$$\eta_{ohm} = iR_{ohm,tot} \text{ [102]} \tag{4.17}$$

Where $R_{ohm,\ tot}$ is the sum of all the contributions related to anode, cathode, electrolyte, interconnector and electrical contact to the overall ohmic resistance. However, in planar cells the main contribution to ohmic losses is related to the electrolyte. In order to have a relationship able to model Ohmic polarizations in a wide range of temperatures, for thermally activated charge transport mechanisms, such as the oxygen ion conduction in YSZ, in general the following relationship, derived from the Arrhenius equation, holds:

$$R_{ohm}(T) = \frac{T}{\sigma^0}\exp\left(\frac{E_{act,ohm}}{RT}\right) \text{ [103]} \tag{4.18}$$

Where T is the absolute temperature, σ^0 is constant in order to fit the experimental data and $E_{act,ohm}$ is the Ohmic activation energy.

4.3.5. Concentration polarizations

When a reactant is consumed by electrochemical reaction at electrode interface, it is often diluted by the products. The finite mass transport rates limit the supply of fresh reactant and the evacuation of products. So, a gradient of concentration is formed which drive the mass transport process. In a SOFC gas diffusion processes control mass transport. While at low current density and utilization factor concentration polarizations are negligible, under practical operating conditions (high current density and utilization factor) are very important in the study of cell performance. For SOFCs the rate of mass transport to electrode surface is described in many cases with first Fick´s law of diffusion:

$$i = \frac{n_e F D(c_B - c_S)}{\delta} \quad \text{[16]} \tag{4.19}$$

Where D is the coefficient of diffusion of reacting species, c_B and c_S are bulk and surface concentrations respectively and δ is the thickness of the diffusion layer. The limiting current density is a measure of the rate at which a reactant can be supplied to the electrode surface and it occurs when $c_S = 0$ so:

$$i_L = \frac{n_e F D(c_B)}{\delta} \tag{4.20}$$

Rearranging the last two expressions, we obtain:

$$\frac{c_S}{c_B} = 1 - \frac{i}{i_L} \tag{4.21}$$

At equilibrium condition Nernst equation is:

$$E = E^0 + \frac{RT}{n_e F} \ln c_B \tag{4.22}$$

When current flows through, surface concentrations become to be less than the bulk one so:

$$E_s = E^0 + \frac{RT}{n_e F} \ln c_S \tag{4.23}$$

The difference of potential produced by the change of concentration at electrode surface, will be:

$$E - E_s = \eta_{conc} = \frac{RT}{n_e F} \ln\left(\frac{c_s}{c_B}\right) \tag{4.24}$$

Or:

$$\eta_{conc} = \frac{RT}{n_e F} \ln\left(1 - \frac{i}{i_L}\right) \tag{4.25}$$

4.3.6. Mass transfer

Mass transfer of gaseous mixture in working fluid electrode is governed by continuity equation [104]:

$$\nabla \cdot (\rho \mathbf{v}) = S_{mass} \tag{4.26}$$

where ρ is the density of gas mixture, and **v** is the superficial velocity for the porous electrode.

Mass source terms, S_{mass}, can be evaluated by means of Faraday´s law [105]:

$$S_{mass} = -\sum_i \frac{\nu_i M_i |i|}{nF} \tag{4.27}$$

where ν_i is stoichiometric coefficient, and n is the number of electrons consumed or produced by cathode or anode half-cell reaction. Mass transport of uncharged species involves both convection and diffusion in the electrode and is dominated by the latter [106].

If we want to represent transport of gaseous species, we can write this equation in terms of mass flux:

$$\nabla \cdot (\rho\omega_i \mathbf{v} + \mathbf{J}_i) = S_i \tag{4.28}$$

$$s_i = \begin{cases} \frac{M_{O_2} i_c}{4F} \, (O_2, \text{cathode}) \\ \frac{M_{H_2O} i_a}{2F} (H_2O, \text{anode}) \\ -\frac{M_{H_2} i_a}{2F} (H_2, \text{anode}) \end{cases} \tag{4.29}$$

or in terms of molar flux

$$\nabla \cdot (c_i \mathbf{v} + \mathbf{J}_i) = S_i \tag{4.30}$$

$$s_i = \begin{cases} \frac{i_c}{4F} \, (O_2, \text{cathode}) \\ \frac{i_a}{2F} (H_2O, \text{anode}) \\ -\frac{i_a}{2F} (H_2, \text{anode}) \end{cases} \tag{4.31}$$

the first term on left-hand side of equation is related to convection, while the second is related to diffusion. In literature there are three diffusion models available to represent mass transfer of gaseous species in porous media, their names are Fick´s model, Stefan-Maxwell model, and Dusty-Gas model.

Fick´s model (FM) is the simplest diffusion model and it is used only for binary or dilute systems [65]. in FM mass diffusion flux of generical species i, is written as

$$\mathbf{J_i} = -\rho D_{ij} \nabla \omega_i \tag{4.32}$$

And in molar terms:

$$\mathbf{J}_i = -D_{ij} \nabla c_i = -c D_{ij} \nabla x_i \tag{4.33}$$

Where ω_i is mass fraction, x_i is molar fraction, c_i is molar concentration of species I, c is total molar concentration of gas mixture and D_{ij} is binary diffusivity for a binary mixture of component I and j.

To calculate diffusion in multicomponent systems is better to use Stefan-Maxwell equations written in this way:

$$-c \nabla x_i = \sum_{j=1, i \neq j}^{n} \frac{1}{D_{ij}} \left(x_j \mathbf{N_i} - x_i \mathbf{N_j} \right) \tag{4.34}$$

Where c is concentration of mixture, D_{ij} is the ordinary or binary diffusion coefficient of species I in j, x_i is the mole fraction of species I, and $\mathbf{N_i}$ is the diffusion flux of species i.

In Dusty gas model there is a combination of Stefan- Maxwell model with the Knudsen diffusion for small pore sizes. A diffusion model in which is considered both ordinary and Knudsen diffusion are expressed as

$$-c\nabla x_i = \sum_{j=1,i\neq j}^{n} \frac{1}{D_{ij}} \left(x_j \mathbf{N_i} - x_i \mathbf{N_j}\right) + \frac{\mathbf{N_i}}{D_{Kn,i}} \tag{4.35}$$

Rearranging the equation, we can write

$$-c\nabla x_i = \sum_{j=1,i\neq j}^{n} \frac{1}{\mathfrak{D}_{ij}} \left(x_j \mathbf{N_i} - x_i \mathbf{N_j}\right) \tag{4.36}$$

With $\mathfrak{D}_{ij}$ that is the combined diffusion coefficient

$$\mathfrak{D}_{ij} = \frac{D_{ij} D_{Kn,i}}{D_{ij} + D_{Kn,i}} \tag{4.37}$$

In order to take into account, the porosity of the electrodic structure diffusion coefficient has to be correct with some geometric factors like porosity and tortuosity so

$$D_{ij}^{eff} = \frac{\varepsilon}{\tau} \mathfrak{D}_{ij} \tag{4.38}$$

or in alternative we can use the Bruggeman correction

$$D_{ij}^{eff} = \varepsilon^{1.5} \mathfrak{D}_{ij} \tag{4.39}$$

where the exponent 1.5 is an empirical constant. At high temperature eq. is more accurate. Finally, with this formulation Dusty-gas model can be expressed as

$$-c\nabla x_i = \sum_{j=1,i\neq j}^{n} \frac{1}{D_{ij}^{eff}} \left(x_j \mathbf{N_i} - x_i \mathbf{N_j}\right) \tag{4.40}$$

In SOFC systems, both ordinary and Knudsen diffusion are important and should be considered together.

4.3.7. Energy transfer

Even if an isothermal state is often imposed on SOFC mathematical models, temperature could be not distributed uniformly throughout the cell or stack. Temperature distribution is related to the electrochemical kinetics of the cell: heat can be generated by the electrochemical reactions within the reaction zones and the current passing through the cell and be consumed by the endothermic internal reforming reactions at the anode side. Large temperature gradients can cause undesired large

thermal-mechanical stresses and thermal expansion mismatches, since the cell generally consists of ceramic components with different thermal expansion coefficients; this could cause degradation and/or structure failure of a SOFC. Above all material properties are strong influenced by temperature as well as reaction rates. So, it is very important to predict heat transfer and temperature distribution in order to design and optimize SOFC single cell and stack. In electrodes and solid component of cell heat transfer occurs mainly for conduction while convection is dominant mechanism in gas channel and pores. In the porous electrodes of SOFC usually heat transfer is modeled following two approaches: Local thermal equilibrium (LTE) and local thermal non-equilibrium (LTNE). LTE approach prescribes the same temperature, T, for gas and solid phase associated with effective transport properties.

So, heat flux is given by:

$$\mathbf{q} = -\nabla \cdot \left(\mathrm{k}^{\mathrm{eff}} \nabla \mathrm{T}\right) + \rho \mathrm{c}_{\mathrm{p,mix}} \mathbf{v} \cdot \nabla \mathrm{T} \tag{4.41}$$

where $\mathrm{c}_{\mathrm{p,mix}}$ is the specific heat of gas mixture, $\mathrm{k}^{\mathrm{eff}} = \varepsilon \mathrm{k}_{\mathrm{mix}} + (1-\varepsilon)\mathrm{k}_{\mathrm{s}}$ is the effective thermal conductivity depending on the porosity of the electrodes, ε, and thermal conductivities of gas mixture, $\mathrm{k}_{\mathrm{mix}}$, and solid phase, k_{s}.

LTNE approach, instead allows to predict the temperatures of the solid and gas phases, $\mathrm{T_s}$ and $\mathrm{T_g}$ in a separate way.

So, heat flux is, for the solid:

$$\mathbf{q}_{\mathrm{s}} = -\nabla \cdot \left(\mathrm{k}_{\mathrm{s}}^{\mathrm{eff}} \nabla \mathrm{T}_{\mathrm{s}}\right) \tag{4.42}$$

and for the gas mixture:

$$\mathbf{q}_{\boldsymbol{g}} = -\nabla \cdot \left(\mathrm{k}_{g}^{eff} \nabla \mathrm{T}_{g}\right) + \rho \mathrm{c}_{\mathrm{p,mix}} \mathbf{v} \cdot \nabla \mathrm{T}_{g} \tag{4.43}$$

in this case $\mathrm{k}_{\mathrm{s}}^{\mathrm{eff}} = (1-\varepsilon)\mathrm{k}_{\mathrm{s}}$ for solid phase and $\mathrm{k}_{\mathrm{g}}^{\mathrm{eff}} = \varepsilon \mathrm{k}_{\mathrm{mix}}$ for gas phase.

Usually when the difference between the temperatures of fluid and solid phase are small LTE approach is used. As provided by Zheng et. al [107] for SOFCs fed by hydrogen or hydrocarbon it is safe to use LTE approach. Usually radiation effect is neglected in SOFC model, even if some researches have been studied this [108].

4.3.8. Momentum transfer

The momentum transfer in the electrode of the SOFC can be described by the Darcy´s law, which is commonly applied with an assumption of a steady-state incompressible flow

$$\nabla \mathrm{p} = -\frac{\mu_{mix}}{\mathrm{k}} \mathbf{v} \tag{4.44}$$

Where p is the pressure, **v** is the superficial velocity, μ_{mix} is dynamic viscosity of the gas mixture and k is the permeability of porous media. In Darcy equation can not model a no-slip condition at the wall nor the resulting boundary layers, which means that it can only describe the flow within the porous structure well away from the walls and is problematic to define interfacial conditions at the interface between two domains.

4.4. Simulation of fuel cell tool

In order to study fuel cells, the process engineering research team (PERT) of University of Genoa developed an in-house code written in Fortran language, named Simulation of Fuel Cell (SIMFC). This code is able to predict performances and carry out parametric and optimization studies on these types of devices. This tool has been developed and successfully validated for Molten Carbonate Fuel Cells (MCFC) technology [1,109,110]. This modelling tool is a 2-D deterministic model based on local mass, energy, momentum and charge balances, allows the calculation of the maps on the cell plane of the main chemico-physical parameters (gas temperatures, electrical current density, Nernst voltage, polarization contributions, internal resistance, pressure drops, compositions and flow rates of the gaseous streams, etc.), can simulate steady state as well as transient conditions, runs quickly, is written in Fortran language and can be implemented in many commercial software for system simulation [111]. The general structure of the code, described quickly in the underlying diagrams, has been confirmed, but all the balances have been modified taking account of the reactions occurring in IT-SOFCs. In addition, the data related to the cell configuration and materials have been updated for the new technology and the gas co-flow feeding system has been set-up, as the SIMFC code had been previously validated for crossflow configuration[112].The basic equations used are reported in table 7, with modifications in order to adapt the code to the new technology. In order to solve the differential equation system shown in the table, finite difference method is used with relaxation method for the energy balance of the solid, which is a Fourier problem. In particular, the cell plane is divided into an optimised number of sub-cells where balances are applied and where thermodynamic and kinetic proprieties are calculated directly at the local operating conditions. In this way, for example, Nernst losses [1] due to the varying reactant and product concentration are directly considered thanks to the local approach and so the inaccuracy of combining equilibrium and non-equilibrium statements are avoided [113]. SIMFC needs the following main inputs: average current density (galvanostatic working condition), electro-kinetics parameters, thermodynamic and transport proprieties, composition and total flow rate of the feeding streams, cell geometrical characteristics, and convergence parameters (e.g., number of sub-cells and tolerance values).The resulting main outputs are: Cell voltage; fuel and oxidant utilisation factors; maps on the cell plane of electrical current densities, Nernst voltage, polarization contributions, temperature (of the solid and gaseous streams), pressure drops, compositions, and flow rates of the gaseous streams.

Table 4.2. Basic equations of SIMFC code.

Mass Balances	Anodic gas	$\frac{\partial n_i}{\partial x} = \frac{j}{2F}$
	Cathodic gas	$\frac{\partial n_i}{\partial y} = \frac{j}{4F}$
Energy Balances	Anodic gas	$\sum_i n_i c_{pi} \frac{\partial T_{an}}{\partial x} = \sum_i \frac{\partial n_i}{\partial x} \int_{T_{an}}^{T_{sol}} c_{pi} dT_{an} + Sh(T_{sol} - T_{an})$
	Cathodic gas	$\sum_i n_i c_{pi} \frac{\partial T_{cat}}{\partial x} = \sum_i \frac{\partial n_i}{\partial x} \int_{T_{cat}}^{T_{sol}} c_{pi} dT_{an} + Sh(T_{sol} - T_{cat})$
	Solid	$S_{an} h_{an}(T_{sol} - T_{an}) + S_{cat} h_{cat}(T_{sol} - T_{cat}) = Q_{cond} + Q_{reac}$ Where $Q_{cond} = \sum_n (\lambda_n s_n) \left(\frac{\partial^2 T_{sol}}{\partial x^2} + \frac{\partial^2 T_{sol}}{\partial y^2} \right)$
Momentum Balances	Anodic gas	$\frac{\partial p_{an}}{\partial x} = K_{an} \frac{\mu_{an} v_{an}}{d^2}$
	Cathodic gas	$\frac{\partial p_{cat}}{\partial y} = K_{cat} \frac{\mu_{cat} v_{cat}}{d^2}$
Local kinetics	Nernst voltage	$\Delta E = E_{an} - E_{cat} = E_0 + \frac{RT}{2F} \ln \frac{p_{H_2} p_{O_2}^{1/2}}{p_{H_2O}}$
	Resistance	$R_{tot} = P_1 \, T \exp\left(\frac{P_2}{T}\right) + \frac{T \exp\left(\frac{P_4}{T}\right)}{P_3 {p_{H_2}}^{P_5}} + \frac{T \exp\left(\frac{P_7}{T}\right)}{P_6 {p_{O_2}}^{P_8}}$
	Cell voltage	$\Delta V = \Delta E - R_{tot} j$

5. EXPERIMENTATION

5.1. Analysis tools and techniques

In this Chapter, a description of the basics of the principal and most renowned electrochemical characterization techniques employed in the study of SOFC cells, namely Polarization Curves (or i-V curves), Electrochemical Impedance Spectroscopy (EIS) and gas chromatography (GC) is provided.

5.1.1. Polarization curves

The polarization curve (or i-V curve) is the most employed diagnostic technique used to characterize the overall immediate performance of IT-SOFCs cells [16,98]. It consists in the measurement of the cell voltage with varying of the current generated and extracted from an external load. It provides information about the genera electrical response of the cell over the range of currents investigated, and hence it is a valuable instrument to assess the dependency of the cell performances to the operating conditions, but it can also suggest hints about the effect of the different polarization losses by examining the different portions of the plot. First, the Open Circuit Voltage (OCV), measured at i =0 A cm^2, can be compared to the theoretical voltage calculated from Nernst equation and the difference between them is a good estimation of losses related to gas leakages, since the Nernst voltage is the maximum voltage obtainable under ideal conditions. The rapid drop of the cell voltage at low current densities is the reflection of the polarization losses related to the overcoming of the activation energies for the electrochemical reactions at the electrodes. Hence, it weights the impact of the activation overpotential h_{act} of the both the anode and cathode reactions. The linear trend that covers most of the plot is caused by the ohmic polarization due to the internal resistance of the cell, which is constant with respect to a change in the current density (Ohm's law). From the slope of this central region of the i-V curve the physical quantity, known as Area Specific Resistance (ASR), measured in Ω cm^2, is generally estimated in order to compare the overall performance of different cells. Finally, when high current densities are required from the cell, an undersupply of reactants in the active regions of the cell occurs, which is caused by the mass transport limitations of gases through the electrolyte layers or by simple fuel starvation. The fast drop of the cell voltage is related to the concentration overpotential conc, and it represents the maximum current that can be supplied from the cell without incurring into severe material degradation.

5.1.2. Electrochemical Impedance Spectroscopy

Electrochemical Impedance Spectroscopy (EIS) is a very sensitive technique that maps an electrochemical cell's response to the application of a periodic small AC signal carried out at

different frequencies. In contrast to polarization curves, EIS measurements can shed light on the diverse physicochemical processes occurring in the active layers of the cell, as each process has associated a unique time-constant (relaxation time) and therefore each one of is exhibited at different frequencies[114].If the studied system satisfies contemporaneously the conditions of causality, linearity and time-invariance, the response to a sinusoidal voltage (or current) excitation signal is a sinusoidal current (or voltage) signal, sharing the same frequency [115]. For a generic sinusoidal voltage input signal e(t)=E cos (ωt + ϑ) the response is a current signal which can be expressed as: $i(t) = I * cos(\omega t + \theta)$ where ω=2πf, f being the signal's frequency, E and I are the amplitude of the voltage and current signals respectively, whilst θ and ϑ are their initial phases. Both sinusoidal expressions can be rewritten as complex-form functions, namely [116]:

$$e^*(t) = E * \exp[j(\omega t + \theta)] \quad (5.1)$$

$$i^*(t) = I * \exp[j(\omega t + \varphi)] \quad (5.2)$$

The impedance value measured at different frequencies is given by:

$$Z^*(\omega) = \frac{e^*(t)}{i^*(t)} = \frac{E}{I}\exp[j(\theta - \varphi)] + jsin(\theta - \varphi) \quad (5.3)$$

Which can be expressed as a complex number having its real and imaginary components expressed as follows:

$$Re[Z^*(\omega)] = Z'(\omega) = \frac{E}{I}cos(\theta - \varphi) \quad (5.4)$$

$$Im[Z^*(\omega)] = Z''(\omega) = \frac{E}{I}\sin(\theta - \varphi) \quad (5.5)$$

EIS measurements were carried out to analyze the the frequency response of the cells tested in this work, within the frequency range 10 kHz - 0.01 Hz, using a frequency response analyzer (FRA 1255B, Solartron Co.) coupled with an electrochemical dielectric interface (EI, 1287 Solartron Co.).

5.1.3. Gas Chromatography (GC)

Gas Chromatography is an analytical technique of great importance for the analysis of the compositions of gas mixtures. It is based on the different times of retention that different gas species possess when they pass through the stationary phase and reach a specific detector placed at the end of the column at different times, called elution (or retention) times.

The result of this analysis is a gas chromatograph which reports the intensity of the different peaks related to the gas species detected as a function of the elution time. From a gas chromatograph, qualitative information can be obtained based on literature data about elution time of single species

(most often employed in databases within the analysis software provided with the instrument). Quantitative analysis can be further performed comparing the areas of the peaks, on a percentage basis: the ratio between the areas of two peaks will be equal to the ratio of their concentration in the gas mixture. In particular, the gas chromatographic system of the High Temperature Fuel Cell laboratory in ENEA consists of two gas chromatographers CLARUS 680 (PerkinElmer, Waltham, MA, U.S.A.) customized by ARNEL.

This system is used for the analysis of specific compounds present in the fuel supplied to the fuel cells (e.g. hydrogen, methane, carbon monoxide, carbon dioxide, water, nitrogen, oxygen and different kind of contaminants such as Sulphur compounds, hydrocarbons and siloxanes). The configuration adopted to both instruments consists of five different and specific columns linked to 4 different kinds of detectors: two universals (Thermal Conductivity Detectors-TCD with a sensibility: 100 ppb), one specific for hydrocarbons (Flame Ionization detector-FID with a sensibility: 1 ppb) and one for Sulphur compounds (Flame Photometric Detector-FPD with a sensibility of 0.001 ppb); in order to allow even so particular analysis. Table 5.1 indicates the compounds that can be detected on the basis of the detectors and columns:

Table 5.1. Characteristics of the gas chromatographic system adopted

Thermal Conductivity Detectors-TCD	I: Column: HayeSep Q and Molecular Sieve 5A. Compounds: It is specific for the analysis of matrix compounds (H_2, CO_2, N_2, CO, CH_4, O_2) II: Column: HayeSep P. Compounds: is specific for the analysis of NH_3 and H_2O
Flame Ionization detector- FID	Column: Elite-5 Capillary Column 0.53 mm Compounds: it is specific for the analysis of Hydrocarbons (CH_4, Benzene, Toluene and Naphtalene etc.). and Siloxanes: (D4-D5-L2).
Flame Photometric Detector-FPD	Column: Silica Bond Plot Capillarity column 0.32 mm Compounds: it is specific for the analysis of Sulphur compounds (H_2S, COS, DMS, SO_2, CH_3SH, EtSH,THT)

This configuration let to perform in-operando gas analysis composition of the anodic surface, allowing the qualitative and quantitative analysis, showing on this way the evolution of the chemical and electrochemical reactions during the process.

5.2. ENEA test station and equipment

5.2.1. Single cell test station

In the framework of the European project NELLHI (New all European high-performance stack: design for mass production, grant agreement no. 621227) an innovative experimental setup for in-depth characterizations of Solid Oxide Fuel Cells has been developed. In this section, the design, the realization, and the assembly of a novel, in-house designed, multisampling housing will be described.

5.2.2. Multi sampling cell housing

The idea behind this project is to realize a setup enabling the sampling of temperature and gas compositions localized on the anode surface, to collect data on the evolution of anodic reactions along the surface. Thus, chemical and temperature gradients will be available and can be recorded during selected modes of operation of the cell, thereby increasing and deepening the level of characterization of the cells. This is particularly important for the direct fueling of IT-SOFC cells with syngas, where the dynamic processes of internal reforming and water gas shift reactions can create severe local gradients of temperature and gas compositions, inducing stresses and possible carbon deposition. Moreover, the novel housing has to allow electrochemical characterization, such as polarization curves and electrochemical impedance spectroscopy (EIS), not affecting (or at least with minor contributions) the cell response during the characterization. The design was realized in the ENEA Casaccia HOTLAB and is depicted in Figure 5.1. It consists of a number of levels separated by frame-shaped layers of gaskets, made of Thermiculite 866LS or CL87 manufactured by Flexitallic, a partner of the project. This multi-layer configuration is meant to provide both gas tightness and electrical insulation of the SOFC cell from the housing. This setup has been realized in order to allocate the 12 cm^2 (active area 121 cm^2) single cell manufactured by Elcogen AS (Tallin, Estony).

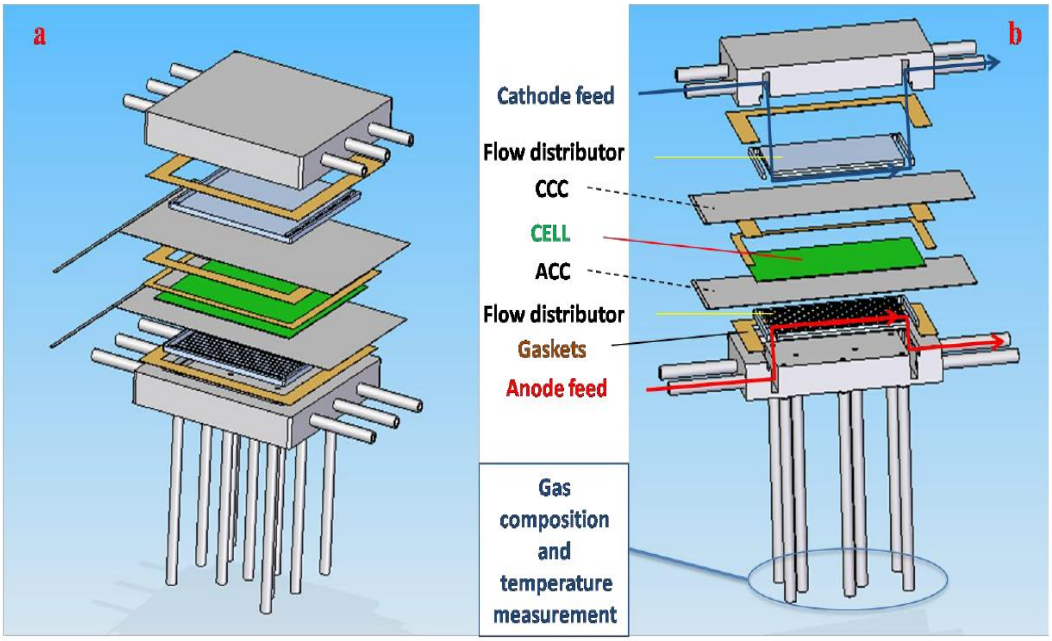

Figure 5.1 Exploded view (a) and cross section (b) drawings of the multisampling housing.

5.2.3. Materials and Manufacturing

5.2.4. Steel housing

Anodic and cathodic cases are made of AISI 310 stainless steel. Gas inlet and outlet tubes are made of Inconel, which is a material supposed to form a thick and stable passivating oxide layer on its surface, avoiding the chromium evaporation and, thus, the

cell contamination. Three short tubes are welded on the two-opposite side of the case, providing a better gas supply, and, on the other extremity, they are joined together to a longer and larger tube, which comes out from the furnace. The anodic case has been drilled on the surface for gas sampling, which is performed by means of capillary tubes, made of AISI 310 stainless steel, welded in correspondence to the holes. On the surface of both anodic and cathodic cases, a square shaped seat has been designed for the accommodation of the gas distribution plate. All the cases and tubes, together with the welding of the latter, were manufactured by RMP s.r.l. (Italy), based on the supplied designs.

5.2.5. Gas distribution plates

Gas distribution plates are made of AISI 310 stainless steel. Both anodic and cathodic plates have a set of parallel gas distribution channels, that connects the gas inlet and outlet, placed on the two

opposite sides. The anodic plate possesses also a set of holes in correspondence of those placed on the anodic case. To avoid electrical contact with current collectors and chromium evaporation, a layer of insulating Al_2O_3 has been deposited on the surface of the whole plate.

5.2.6. Current collectors

Anodic current collectors consist of a Crofer 22H stainless steel calendered mesh on which a series of Pt wires are welded on one side, very close to each other, and rolled together to form a bundle for the collection of the current. A single Pt wire is welded on the opposite side of the mesh, for the measurement of the cell potential. Cathodic current collectors consist of a gold (or Crofer 22H) calendered mesh, on which Pt wires are welded similarly to those on the anode mesh. Current collectors were manufactured by Fiaxell (Switzerland).

5.2.7. Gaskets

Gaskets consists of Thermiculite 866LS or Thermiculite CL87, provided by Flexitallic Ltd. (UK), hand-cut into frames according to the case dimensions. Two gaskets are placed between the current collectors and the respective steel case, avoiding, at the same time, gas leakages from the housing, and electrical contact between current collectors and the housing. Other two of them are placed at the cell level, in order to avoid short-circuiting between the electrodes. These gaskets provide gas tightness at the cell level and avoid the contact between the two current collectors.

5.2.8. Test bench

In Figure 5.2 the piping and instrumentation diagram of the single cell test station is reported.

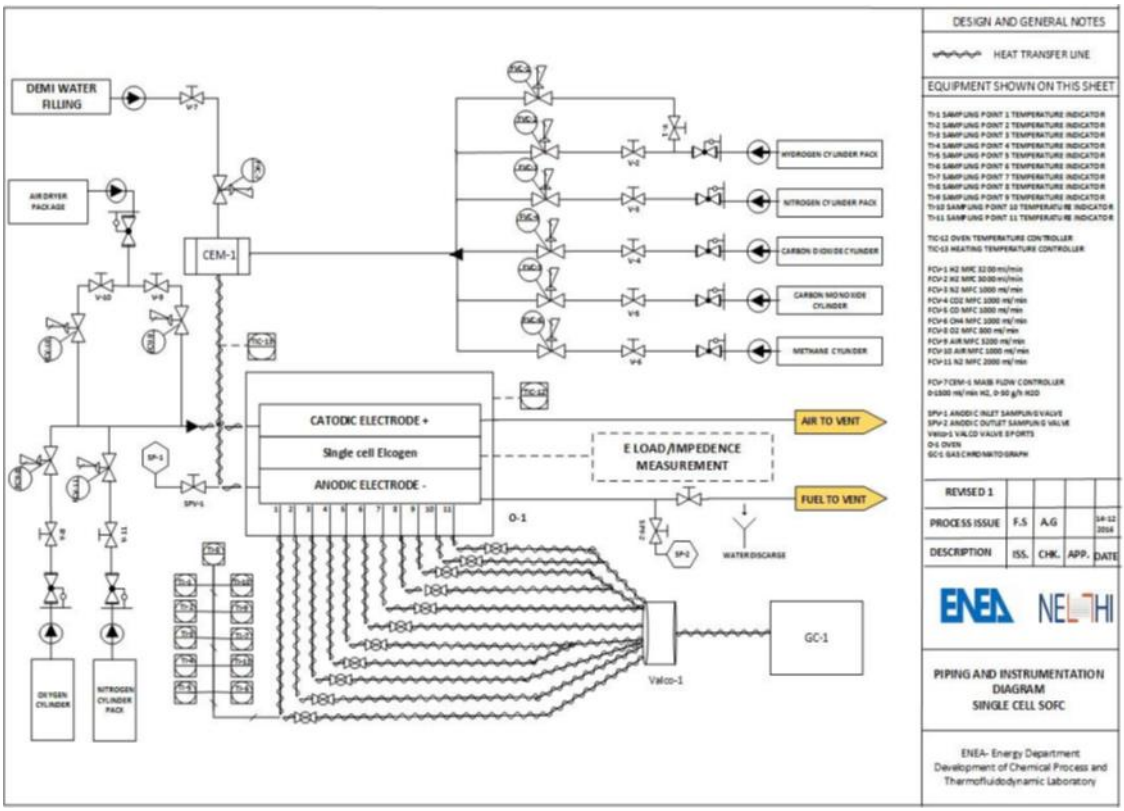

Figure 5.2. Piping and instrumentation diagram of the single cell test bench.

The single cell test bench is equipped with a temperature programmed oven, in which the single cell housing is inserted. The eleven sampling capillary tubes merge from the bottom of the furnace and converge to a multi-stage Valco valve, which selectively drives the gas coming from a single sampling spot to a Perkin-Elmer Clarus 680 GC gas-chromatograph (Waltham, Massachusetts, U.S.A.). In order to reduce the pressure, drop on the cell, and to avoid the mixing of the gas of different sampling spots, each capillary is also equipped with a single valve. A thermocouple (Type K) is inserted inside each capillary tube, ending in the immediate proximity of the corresponding holes. A set of mass flow controllers are employed to allow the cell to be fed with H_2, CO, CO_2, CH_4 and N_2; the fuel gas can be humidified by means of a controlled evaporator mixer and a liquid flow meter. On the cathode side, air is provided by a mass flow controller, and it can be further enriched or depleted in its oxygen content by means of dedicated mass flow controllers for N_2 and O_2. Anode exhaust is driven to a hermetic glass container for the water condensation, and the exhaust gas is then led to the vent. The cathode exhaust is driven to the vent too. The anode and cathode inlets and the capillary tubes are all trace heated in order to avoid water condensation. The test bench is equipped with a Kikusui 44 PLZ664W (Japan) electronic load connected in series with a Delta Elektronika SM-30-100D (Netherlands) power supply to record the polarization curves, measuring the cell potential by means of an TTi 1604 digital multimeter, and with a Solartron 1260 Impedance

Gain/Phase Analyzer module (UK) coupled with a Solartron 1287 (UK) Electrochemical Interface for the electrochemical impedance spectroscopy measurements.

5.3. Experimental validation of ENEA's single cell test rig

The innovative set up was tested on 10 x 10 cm^2 and 12 x 12 cm^2 IT-SOFCs operating in dry H_2 for the validations of cell performance, and in a mixture of dry H_2/N_2 for the temperature and gas sampling analysis [117]; air was provided at the cathode side. The active area, e.g. where reactions actually occur, for both the cells was of 91 cm^2 and 121 cm^2 respectively. The characteristics of the cells provided by Elcogen (Tallin, Estony) are summarized in table 5.1. The operative temperature of these type of devices is 650 °C

Table 5.1. Characteristics of IT-SOFC tested

Single cell	Material	Thickness (μm)
Anode	Ni-YSZ	350
Electrolyte	YSZ	5
Cathode	LSC	30

In Tables 5.2 and 5.3 the flows provided to the 10x10 cm^2 and 12x12 cm^2 cells during the performance evaluation are reported. Table 5.4 contains the details about the flows employed for the gas and temperature sampling.

Table 5.2. Performance evaluation: 10x10 cm^2 cell.

Anode	Flows [ml/min]	Percentage [%]
Hydrogen	660	100
Nitrogen	0	0
Cathode		
Air	1470	100

Table 5.3. Performance evaluation: 12x12 cm^2 cell.

Anode	Flows [ml/min]	Percentage [%]
Hydrogen	986	100
Nitrogen	0	0
Cathode		
Air	2196	100

Table 5.4. Test 1 composition reference hydrogen.

Anode	Flows [ml/min]	Percentage [%]
Hydrogen	520	50
Nitrogen	520	50
Cathode		
Air	2240	100

In both cases, the gas composition and temperature in each sampling point were measured under different conditions: at open circuit voltages (OCVs) and under a constant current density corresponding to a fuel utilization of 40%. For each composition, temperature analysis was carried out during the first hour of stabilization:

- 1st Equilibrium condition at OCV;
- 2nd Equilibrium condition under a constant current.

To evaluate the performance of this new set up has been decided to compare the polarization curve obtained from two cells of different size (10x10 cm^2 and 12x12 cm^2), with those obtained from an Elcogen 15-cell stack, tested by a NELLHI partner, CUTEC, using the same operating condition, scaled for the testing of a single cell. In Figure 5.3, it is shown the comparison between the polarization curves of the 10x10 cm^2 single cell with the average i-V response obtained from the cells within the Elcogen's stack.

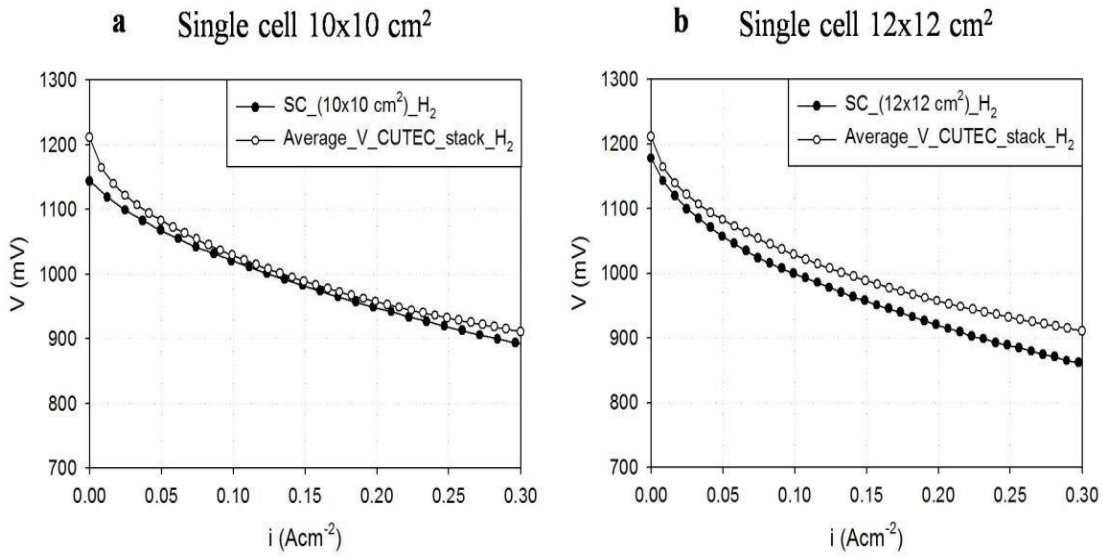

Figure 5.3. Performance comparison between tested single cells and 15-cell stack.

It is evident from the plot that the curves are broadly similar, presenting very similar values of the voltage for most of the current densities applied. Only a slight difference in OCV value is evident. This result validates to some extent this set up, proving that the obtainable performances are globally good. However, in the Figure 5.3, where the comparison with the 12 x 12 cm^2 single cell is shown, the difference between the obtained curve and the reference one results more pronounced than that obtained in the case of the 10 x 10 cm^2 cell. This evidence is imputable to the presence of more pronounced gas leakages, that highlights the need of an optimization of the set-up, in terms of mechanical load, to make the cell performances comparable to the performance of the Elcogen's stack. The composition and temperature distributions on the anodic surface are presented along 3 axes (see Figure 5.4): the central horizontal axis of the cell, namely X axis, the vertical axis close to the anodic inlet and the vertical axis close to the anodic outlet, namely Y axis and Y' axis respectively.

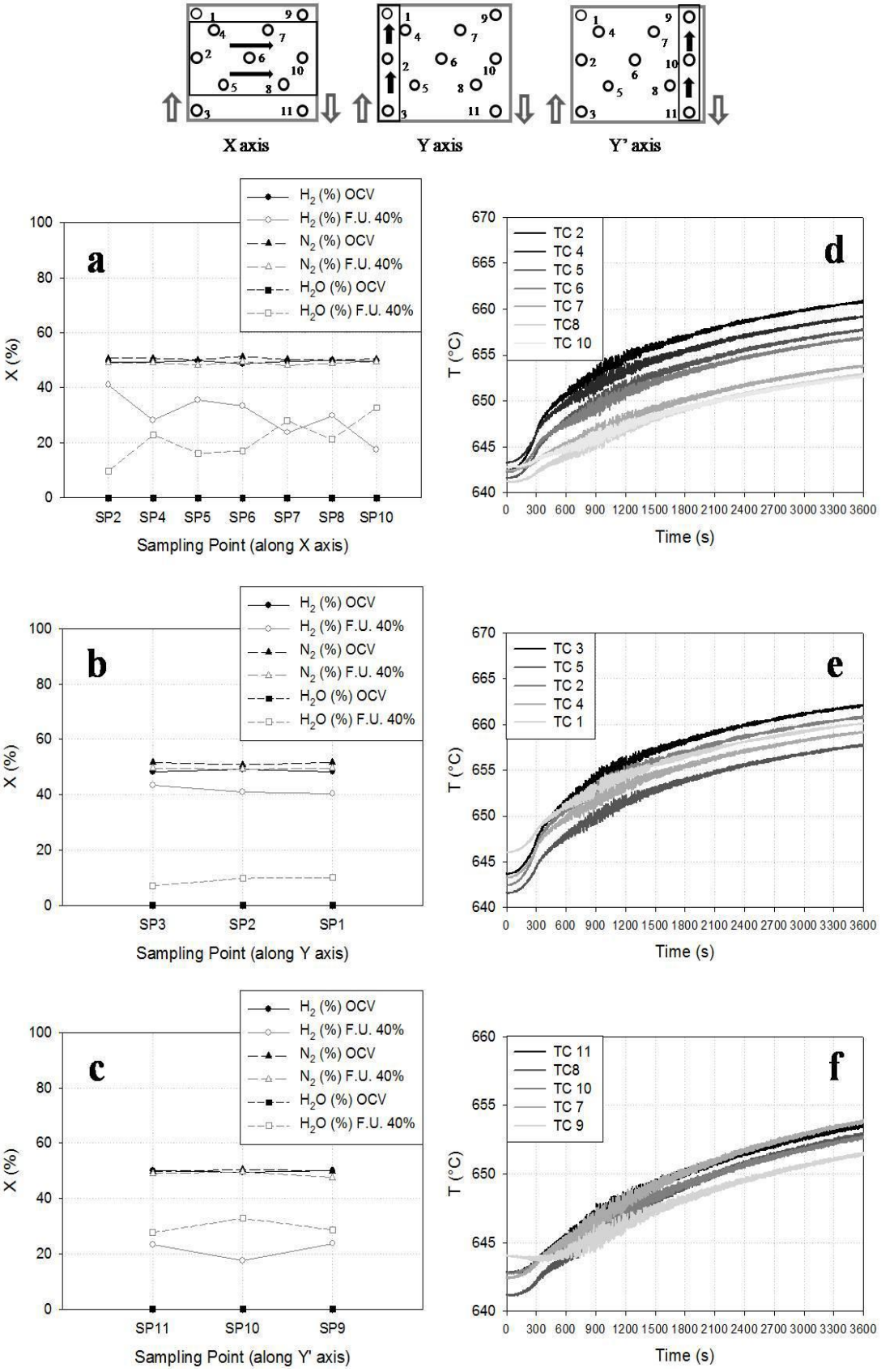

Figure 5.4. Composition (a,b,c) and temperature (d,e,f) analysis along the axes.

Every graph shown has a sampling point map on the top to show the position of the sampling point

to which the graph itself is referred. Figures 5.4 a, 5.4 b and 5.4 c represent the gas composition analysis, in OCV and under a current load of 30 A, obtained from the spots along the X, Y, and Y' axis respectively. Figures 5.4 d, 5.4 e and 5.4 f represent the values of the temperature obtained during the stabilization of cell conditions under a constant current load of 30 A. Since in OCV condition, for hydrogen operation, no reactions occur, the temperature profiles recorded showed no significant result, and are not presented. Comparing plots 5.4 a, 5.4 b and 5.4 c, it is evident that the chemical gradient variation is more significant along the X axis compared to the vertical ones; for this reason, all the assessments are referred to X axis (Fig. 5.4 a). The only information that can be deduced from plots 5.4 b and 5.4 c is that along the Y and Y' axis the gas composition. results quite homogeneous, suggesting a regular distribution of the species perpendicularly to the flow direction.

In OCV condition, the composition is the same in all the sampling points, so the chemical gradient inside the cell can be considered negligible. Since the N_2 is an inert gas, its molar fraction remains unaltered under current respect to the OCV condition. Instead, when current flows through the cell, there is a gradual decrease of H_2 along the X axis, corresponding to the increase of the molar fraction of H_2O, due to the electrochemical oxidation reaction of the hydrogen.

The presence of this exothermic reaction is confirmed in the temperature analysis shown in the fig. 5.4 d, where it is possible to observe a general increase of temperature going from the inlet to the outlet of the cell. In the first 300 seconds, in which the current was increased from OCV up to 30 A, the increment is more pronounced and rapid for the thermocouples located close to the inlet, as evident from the steepness of the inflection located at approximately 300 s. Moreover, during the regimen time, it is possible to observe that the increment of temperature in the sampling point located close to the anodic inlet (Y axis) is greater than the increment of those located close to the anodic outlet (Y' axis). In this phenomenon plays an important role the depletion of H_2 in the part close to the anodic outlet, due to the evolution of the electrochemical oxidation reaction. In fact, in the zones close to the outlet of the cell, the increase of the reaction product (H_2O) causes a decrease of the Nernst potential and, considering the cell voltage as the difference between the Nernst potential and the voltage drop caused by the whole resistance of the cell, the local current density results lower respect to that distributed closest to the inlet.

This decrease of the current density in the anodic outlet part is probably the cause of the decrease of the temperature measured. This non-homogeneous distribution of the current density inside the cell has also been verified in another work from DLR (*Deutsches Für Luftund Raumfahrt*) with a different experimental apparatus. In their work the local behavior of current and voltage in a segmented cell was studied, highlighting a considerable variation of current density for different cell segments. In particular, for the segment located close to the fuel outlet, the current density

results lower than the current density of segment located at the fuel inlet [118].

After the preliminary validation of the test-up, we used the new test rig in order to study a syngas simulating a mixture obtained from the natural gas reforming process using Nickel as catalyst at 873 K and is shown in Table 5.5 where the flows and compositions used are reported [119]. The gas composition and temperature in each sampling point were measured under different conditions, i.e. in open circuit voltage (OCV) and under two current density values: 165 mA cm $^{-2}$ and 330 mAcm^{-2} corresponding to 27% and 54% fuel utilization, respectively. In order to follow the thermal equilibrium progress, and so the chemical equilibrium, the temperature analyses were carried out for three hours each and under the following conditions:

- 1st equilibrium condition: achieved changing the composition from a mixture of H_2 and N_2, considered as the reference composition, to the syngas composition in OCV;
- 2nd equilibrium condition: from OCV to 20 A of current, using a current ramp of 0.1 A s^{-1};
- 3rd equilibrium condition: from OCV to 40 A of current, using a current ramp of 0.1 A s^{-1}.
-

Table 5.5. Syngas composition tested.

Gas composition	Flow rate [ml/min]	Molar fraction
Anode		
H_2	140	0.25
CO	23	0.04
CO_2	133	0.24
CH_4	90	0.16
H_2O	174	0.31
Cathode		
Air	2240	-

The composition and temperature distributions over the anodic surface are analyzed over five different coordinates across and seven coordinates along the flow direction, as shown in Figure 5.5, resulting in an efficient mapping of the anode surface. 11 thermo-couples are introduced through the sampling tubes to allow the temperature measurements inside the anode GDP channels. Considering the disposition of each sampling point, the results are presented by Cartesian coordinates: X axis

(along the flow direction), and two vertical axes (across the flow direction, one close to the inlet and the other close to the outlet), named Y axes. Every graph shown in this work has a map on the top to highlight the position of the sampling points to which the graph itself refers.

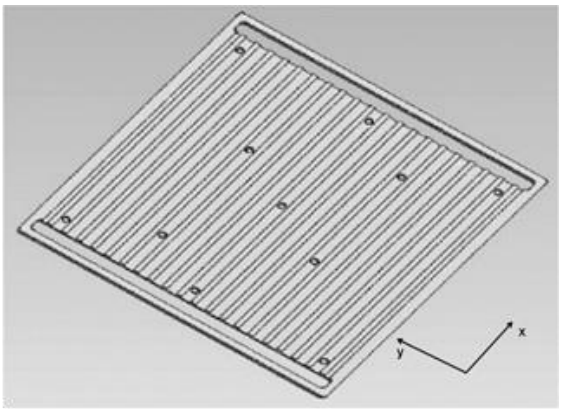

Figure 5.5. Top view of the anodic gas distribution plate with sampling points.

The results obtained from the gas composition analysis along the two Y axes are reported in Fig. 5.6, showing that the composition profiles are uniform across the flow direction from the inlet to the outlet of the cell, indicating a plug-flow pattern. Analogous results along these directions were achieved running the cell under 20 A, and 40 A confirming that the chemical gradient can be considered negligible along the vertical axes. This is consistent with the result presented in our previous work [117].

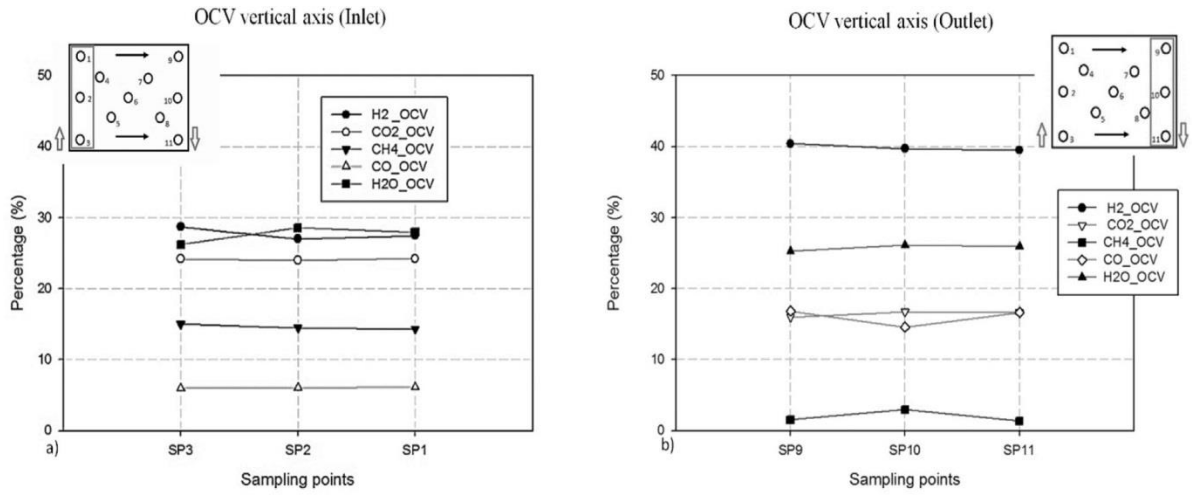

Figure5.6. Co-axial distribution of the gas composition (a) in the inlet and (b) in the outlet, both in OCV condition and showing a uniform profile

Thus, all following assessments about the composition analysis are referred only to the X axis (see Figure 5.6). Fig. 5.6 (a) presents the composition trends along the anode surface under OCV conditions. It shows that the CO_2, H_2O and CH_4 chemical gradients decrease along the flow direction, revealing the internal reforming phenomenon. There is the possibility that carbon dioxide and water compete in methane reforming leading to the presence of two different types of methane reforming: steam reforming and dry reforming, as explained in detail in the first section of the work (equations (2.4) and (2.6)). In both cases, H_2 and CO are generated as the reaction products. The simultaneous presence of the two reforming reactions is due to the similar CO_2/CH_4 and H_2O/CH_4 mole ratios, as also have been reported in the work of Choudhary [120]. In Figure 5.7 it is represented the evolution of the gas composition at different electric load conditions.

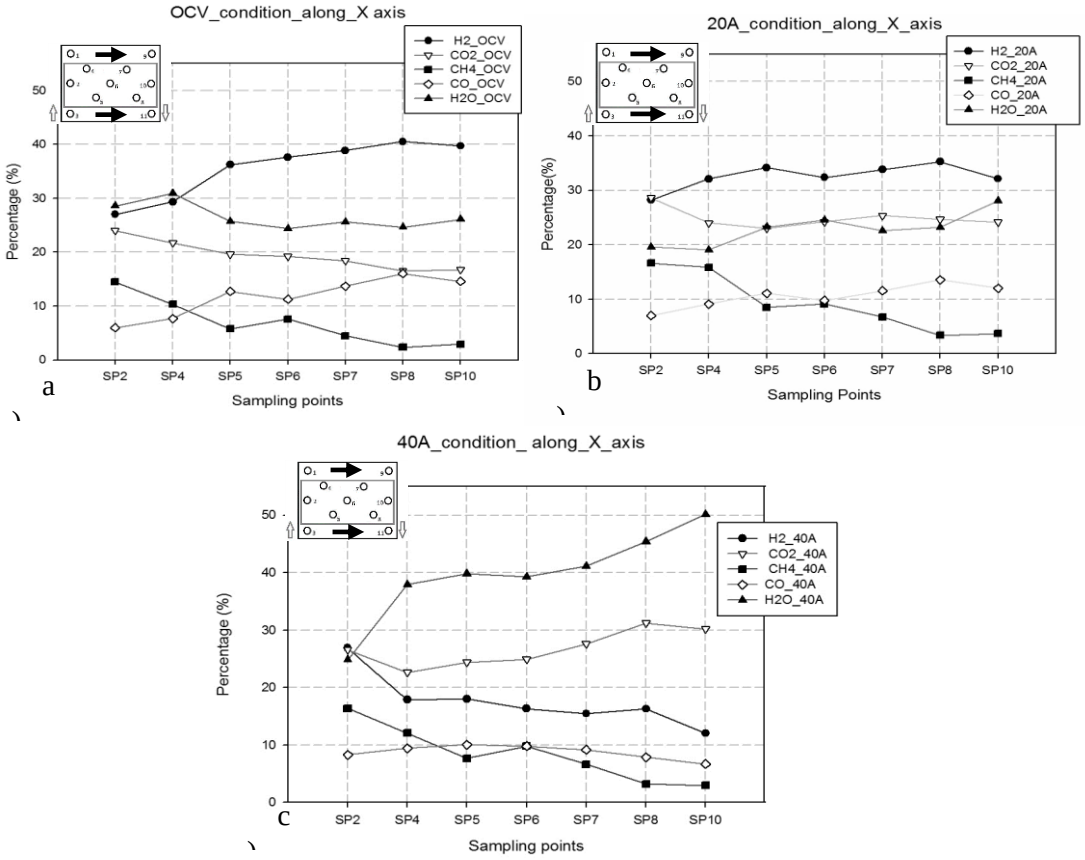

Figure 5.7. Evolution of the gas compositions through the cell in (a) OCV, (b) 20 A and, (c) 40A.

Recent studies suggest that steam reforming of CH_4 (equation 2.4) and dry reforming of CH_4 (equation 2.6) are mechanistically equivalent to the decomposition reaction of CH_4. It was postulated and confirmed via experiments that the catalytic sequence, intrinsic kinetics and even the mechanisms are equivalent for reactions (equation 2.4) and (equation 2.6) [121,122]. Another reaction named reverse water gas shift can occur:

$$CO_2 + H_2 \leftrightarrows CO + H_2O \qquad \Delta H^0_{298} = 41\ kJ/mol \tag{5.1}$$

The possible role of the reverse water gas shift (rWGS) in the reduction of CO_2 has been excluded on the base of the increase of H_2 and the decrease of H_2O shown along the anode surface. In Figure 5.8. (a), is reported the local temperature analysis along X axis in OCV condition. The temperature behaviors confirm the results obtained with the gas composition analysis. In fact, a slight temperature decrement trend is evident along the anode surface, caused by the endothermic nature of the internal reforming reactions, demonstrating their dominance respect to the others. The thermal equilibrium in this condition is achieved after 2.5 hours at stable conditions. The distribution of temperature at the thermal equilibrium on the anode surface is shown using a Contour graph in Figure 5.8 (b). The lower temperature is localized close to the inlet zone of the cell, in accordance with the faster kinetics of the steam and dry reforming. Beside the thermocouples localized close to outlet present a slight increase of temperature probably due to the presence of the water gas shift reaction (WGS). As 20 A of current is drawn (Figure 5.8 (b)), corresponding to 165 mA cm^{-2} of current density, some changes appear in the axial gas concentration distributions: CO increases (less markedly than in OCV), and at the same time, the CO_2 shows a particular behavior decreasing in the first half of the anode surface (from SP2 to SP5) and increasing in the second half (from SP 6 to SP 10). The initial decrement may be due to the fast kinetics of the dry and methane steam reforming reactions while in the second half of the anode surface other reactions become dominant, such as water gas shift (equation 2.5), that produces CO_2, causing the increase shown in its curve. The behavior of H_2O changes with respect to the OCV condition, increasing as an effect of the hydrogen electrochemical oxidation (equation 2.2). H_2 presents a slight increment despite the electro-chemical oxidation that should lead to its decrement, demonstrating that reforming reactions are still predominant compared to the electrochemical oxidation. Regarding to CH_4 behavior, it shows the same trend as in OCV condition.

H_2 trend with this fuel composition and under low values of fuel utilization shows the availability of the SOFC system to coproduce hydrogen fuel, along with generating electricity. The coproduction concept is based upon a symbiotic relationship between hydrocarbon reforming processes and fuel cell electrochemical processes. Several advantages are reported in literature for this type of approach such as the energy conversion efficiency is theoretically higher [121] ,and less air is needed for cooling, so the air flow rate can be decreased resulting in fewer parasitic losses [123]. However, there are also potential disadvantages concerning to the anode fuel reformation process, such as the possibility of large temperature gradients in the fuel cell as well as the possibility of carbon coking [124,125]. The problem relative to internal reformation leading to large temperature gradients on the anode surface obtains some answers in this work, whereas the problem of coking is left as a topic of future research. Under low value of fuel utilization, the thermo-dynamical equilibrium, represented by the curve plateau in Figure 5.8 (c), is achieved faster

respect the other two conditions studied. In fact, the plateau has been reached after one hour over the entire anode surface, showing a slight exothermic trend. At the thermal equilibrium, represented in the contour plot in Figure 5.8 (d), the temperature distribution is homogeneous reporting a maximum difference in temperature across the anode surface of This prove that when the equilibrium condition is achieved, the contributions of the exothermic and endothermic reactions are almost similar, suggesting that the problem of large temperature gradient caused by internal reforming is avoided under these conditions. Comparing the equilibrium contour plot in OCV and under the low value of fuel utilization (Figure 5.8 (b) and (d)) the same phenomena are evident, even if in OCV the maximum difference in temperature across the anode surface is higher respect to the low current density condition. The benefit to use low values of fuel utilization for the coproduction is also reported in the modeling work presented by

Shaffer and Hansuck [126]. They developed a quasi-3-D dynamic model of an internally reforming planar SOFC for the study of the impacts of varying fuel for electricity and hydrogen co-production. The model shows the steady-state SOFC performance for various operating conditions and the dynamic response of the cell during fuel utilization transients, concluding that the maximum of H_2 production, electrochemical efficiency and the minimum parasitic losses occur for conditions of low value of fuel utilization. The chemical trend changes completely when 40 A of current is drawn, with the exception of the CH_4 that shows the same trend as in OCV and under 20 A of current, suggesting that the reforming the reforming reaction is unaffected by the current load. The effective consumption of H2 from the inlet to the outlet coupled with the increment of H2O, confirms the strong relevance of the electro-chemical oxidation reaction in this condition. It is possible to note also a net decrement of CO coupled with an increase of CO_2, pointing to a greater contribution of the WGS reaction. The electrochemical oxidation of CO could be possible, however since the WGS process, globally, is faster compared to the electrochemical oxidation [127,128] it is more likely that, for fuels as syngas, the CO oxidation proceeds largely through water gas shift, not by direct electrochemical oxidation. The temperature evolution over time on the anode surface under 40 A of current (Figure 5.8 (c)) shows a more marked exothermic trend compared to 20 A, highlighting the predominant contribution of exothermic reactions with respect to the endothermic ones. Moreover, when the thermal equilibrium is achieved is evident that the temperature increment in the sampling points located close to the anodic inlet is greater than the increment of those located close to the anodic outlet (ΔT = 13 K).

This non-homogeneous temperature rise inside the cell was also verified in a previous work [117], feeding the cell with a mixture of dry H_2/N_2 under a current load of 30 A. Also, in this case, the reason should be sought in the depletion of H_2 due to the evolution of the electrochemical oxidation, causing a non-uniform current generation (and therefore heat generation) over the anodic surface, decreasing from the inlet (rich in H_2) to the outlet (poor in H_2).

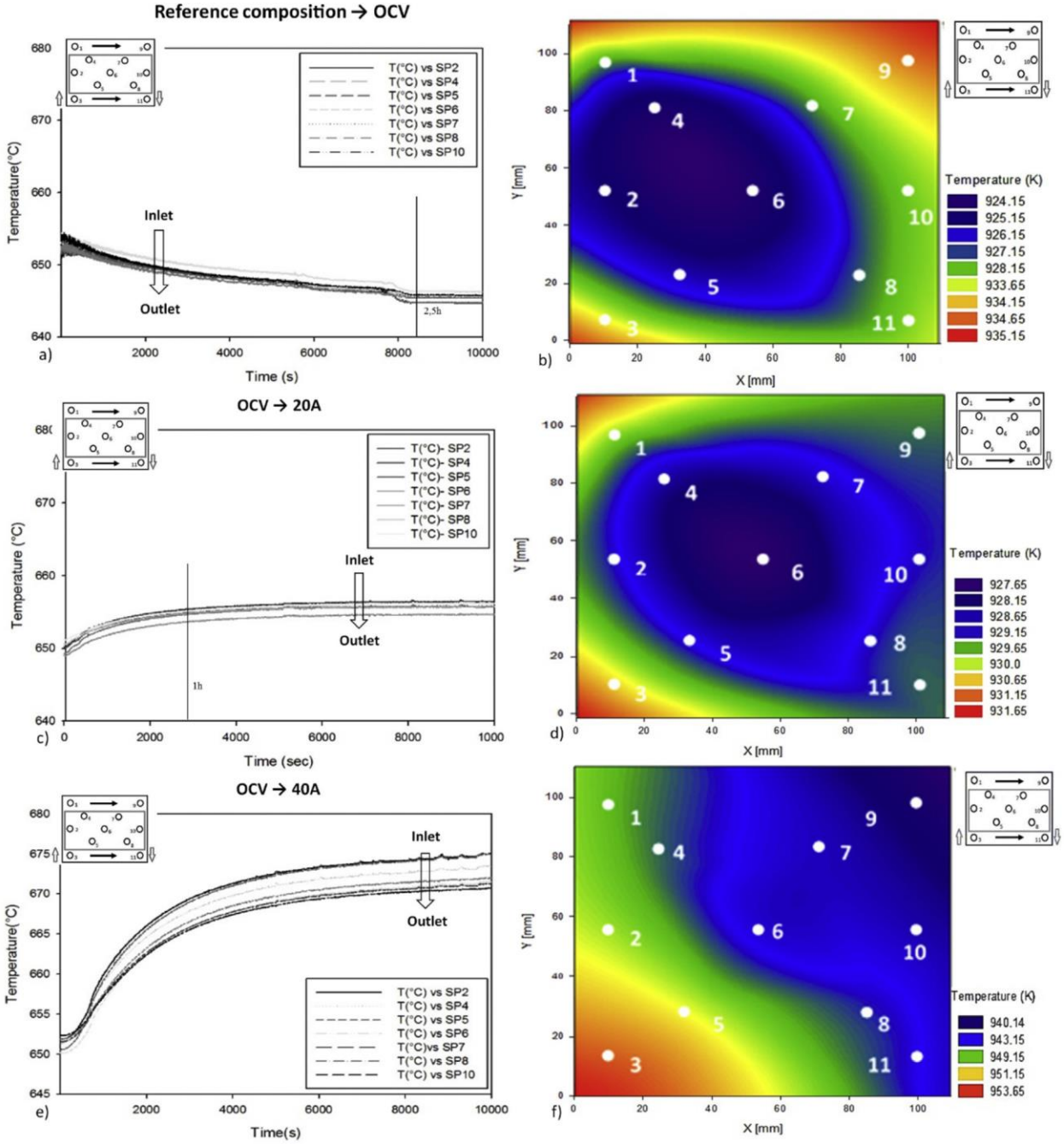

Figure 5.8. Temperature analysis: in the graphs (a, b, c) are reported the temperature profiles along the X axis through the anode surface under OCV, 20 A and 40 A, whereas in the contour plots (b, d, f) are reported the temperature distributions at the thermal equilibrium in the same conditions.

5.4. VTT single cell test station

In order to collect another set of experimental data, the performance commercial anode-supported solid oxide fuel cell (Elcogen AS,Tallinn, Estony) were investigated with H_2/N_2 mixtures by measuring the characteristic curves and electrochemical impedance spectra at different operative conditions. Experiments were performed in Fuel cell and Hydrogen lab of VTT Technical Research Centre of Finland Ltd. The cell is circular-shaped with a diameter of diameter of 60 mm and an active surface of ~ 16 cm^2. The anode of the cells consists of Ni/YSZ porous layer that provides support for the 8YSZ thin electrolyte (6 mm dense layer) and the cathode, which is a porous layer made by LSC. Experiments were performed in a temperature-controlled oven. The cells were placed in an unsealed alumina test-fixture providing radial gas distribution from the cell center, where the gas inlet is located, to the border. Metallic grids of nickel (anode) and platinum (cathode) were used for current collection, while the electrodes' voltage was measured with two separate sensing wires contacting the cathodic and anodic grids. A thermocouple is located in the cell center near to the anode surface, providing the temperature of the experiment. The schematic representation of experimental setup is shown in Figure 5.9.

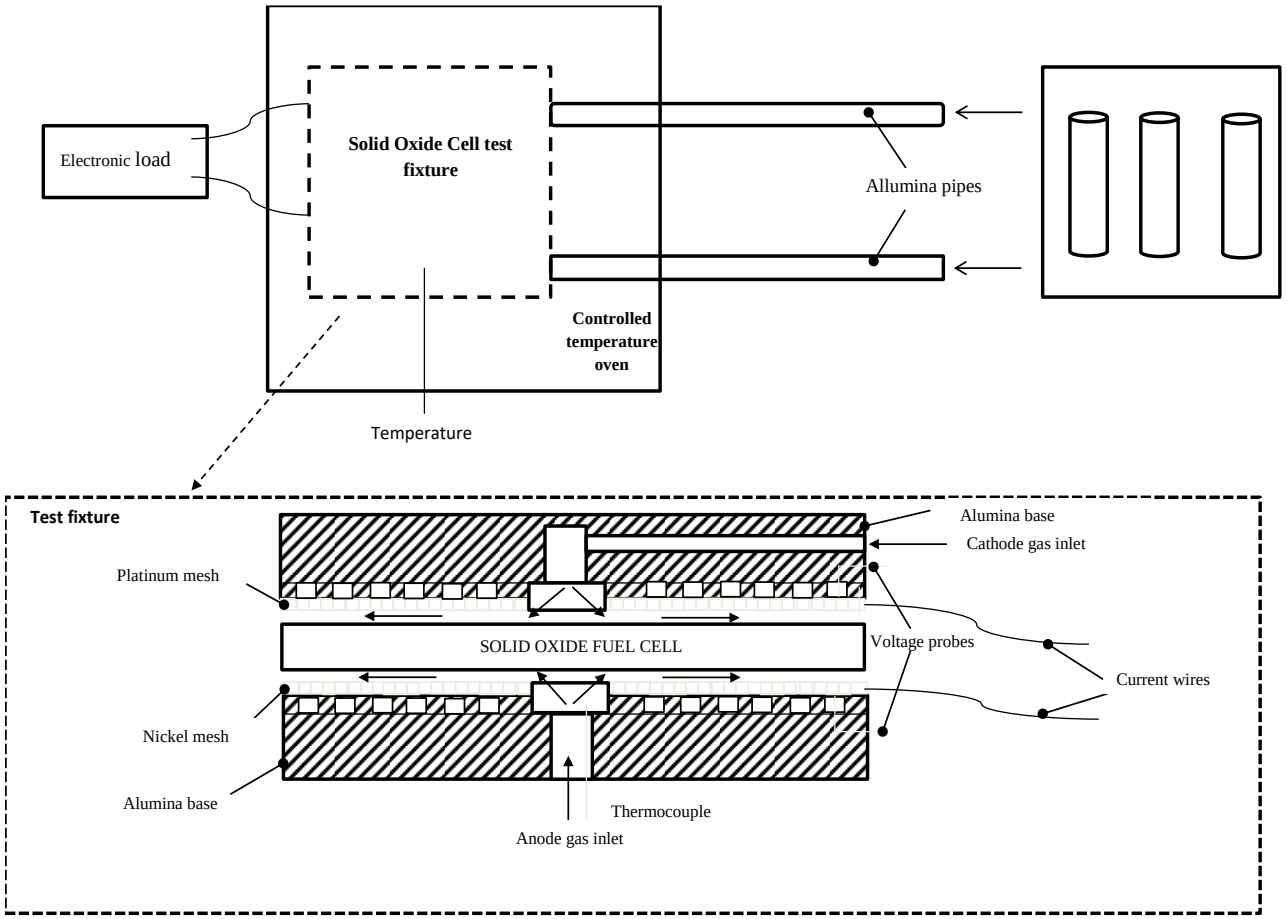

Figure 5.9. Schematic representation of the VTT's test apparatus.

5.4.1. Experimental tests at VTT

In this section we can show experimental data collected at VTT Technical Research Centre of Finland Ltd. using experimental test rig explained in the previous section. In table we can see the test conditions used. In particular the experiments have been performed to measure characteristic curves by varying the electric load, guaranteeing a low reactant utilization factor to avoid diffusion limits.

The temperature and reactant composition have been changed one at a time (with N_2 balancing) in order to isolate their effect on the electrochemical model.

All experiments were carried out at atmospheric pressure. We also carry out EIS measurement with a value of current of 0.24 A cm^2 provided by the manufacturer in order to see the behaviour of spectra changing temperature and reactant composition. The test conditions are summarized in table 5.6.

Table 5.6. Test conditions.

Conditions	T K	Anode						Cathode			
		Flow Rate (Nml min^{-1})			% mol			Flow Rate (Nml min^{-1})		% mol	
		H_2	N_2	H_2O	H_2	N_2	H_2O	O_2	N_2	O_2	N_2
H_2 50 %	923	171	171	0	50	50	0	92.8	349.1	21	79
H_2 30 %	923	93	225	0	30	70	0	92.8	349.1	21	79
H_2 21 %	923	70	258	0	21	79	0	92.8	349.1	21	79
H_2 17 %	923	56	272	0	17		0	92.8	349.1	21	79
O_2 5 %	923	171	171	0	50		50	92.8	1607.2	5	95
O_2 10 %	923	171	171	0	50		50	92.8	801.8	10	90
O_2 13 %	923	171	171	0	50		50	92.8	803.2	13	87
O_2 15 %	923	171	171	0	50		50	92.8	516.8	15	85
T 898	898	171	171	0	50		50	92.8	349.1	21	79
T 923	923	171	171	0	50		50	92.8	349.1	21	79
T 948	948	171	171	0	50		50	92.8	349.1	21	79
T 973	973	171	171	0	50		50	92.8	349.1	21	79
T 998	998	171	171	0	50		50	92.8	349.1	21	79
T 1023	1023	171	171	0	50		50	92.8	349.1	21	79

In Figures 5.10, 5.11 and 5.12 have been showed the results of tests.

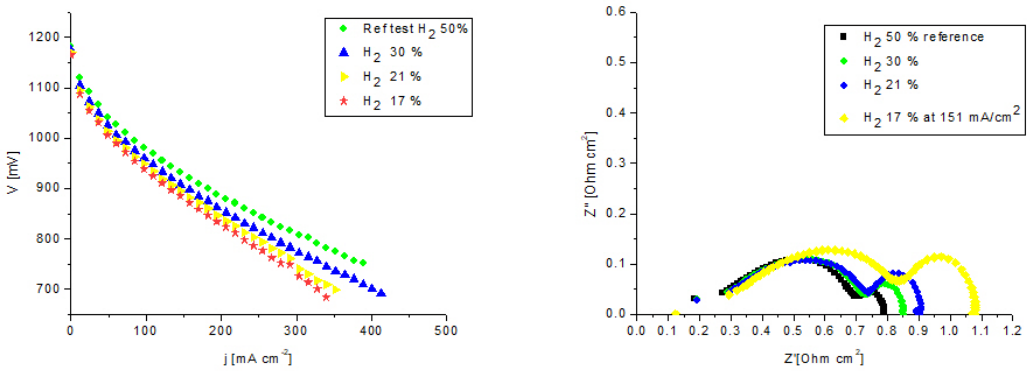

(a) **(b)**

Figure 5.10. (**a**) Characteristic curves and (**b**) EIS at reference temperature (923 K) and cathodic composition (21% O_2), varying the anodic composition.

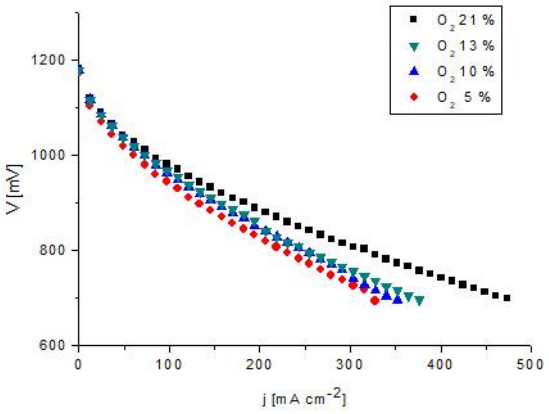

Figure 5.11. Characteristic curves at reference temperature (923 K) and anodic composition (50% H_2), varying the cathodic composition.

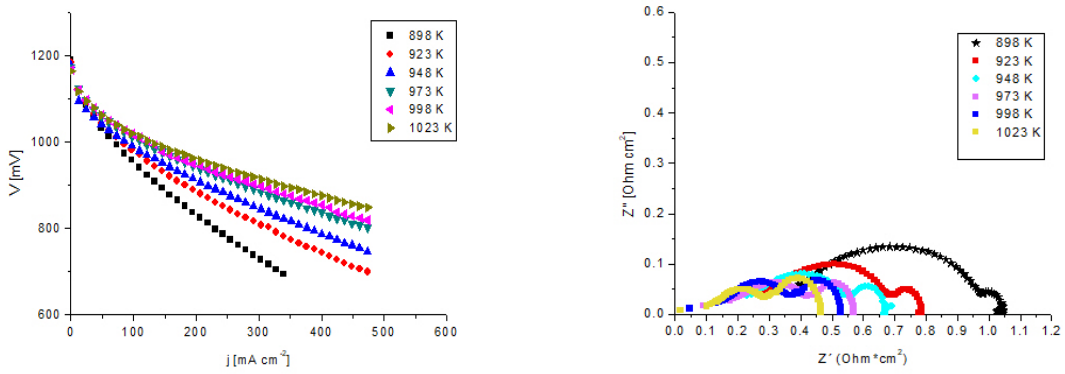

(a) **(b)**

Figure 5.12. **(a)** Characteristic curves and **(b)** EIS at reference composition (50 % H_2, 21 % O_2) and varying the operating temperature.

We decided to show these experimental tests, only for a qualitative analysis, surely this data can be very useful for future works. From a preliminary analysis of experimental data, we can note as with the increase of content of fuel in anodic mixture and oxidant in cathodic flux, the performance of fuel cell increases, this is confirmed both from polarization curves and EIS spectra (see Figures 5.10 and Figure 5.11). Finally, in Figure 5.12 it is shown the effect of temperature, as temperature increase performances of fuel cell increase. We chose to make more clearly EIS spectra to see more detail on the arcs. The EIS spectra show two main points: these two intercepts with the x-axis of the Nyquist plot. The first one identifies the Ohmic resistance and it is seem not affected by the composition change, but it is difficult to see properly this point, because of some problems in test equipment. The second intercept, related to the amplitude of the curve, gives a measure of the decreasing of the sum of Ohmic and polarization resistances when a richer anodic flow rate is fed in (see Figure 5.10). Finally, in Figure 5.12 there is the representation of the effect of temperature, and in this case both of the two main point of EIS spectra change; the improving performances at a higher temperature confirm how the total resistance decreases when temperature increases. In this case, the Ohmic resistance also varies, assuming high values at high temperatures. The experimental data are not so good, because these tests have the objectives to optimize the test rig in VTT laboratories in order to make better tests in future,

5.5. Quality assurance and standardization

To introduce innovative technologies into industrial and consumer environments it is necessary that they respect essential requirements in regulations and the associated technical specifications in regulations, codes and standards (RCS). In the case of IT-SOFCs and hydrogen technologies, these have centered around two main themes:

- Safety standards, that are essential safety requirements imposed by normative bodies to reduce the risk of hazards during operation;
- Technical specifications, that define specifications and procurement of testing samples, the overall test matrix and test procedures, and which can also include validation of the cell/stack assembly unit in solid oxide operation [129,130].

The successful market launch requires also reliable assessment, testing and prediction of performance and durability. Also, the complexity of IT-SOFC units and the appendant test systems increases the need of detailed test schemes, procedures and protocols. In Figure 5.13 there is a schematic representation of the complex correlations which should be considered to get reliable object test results.

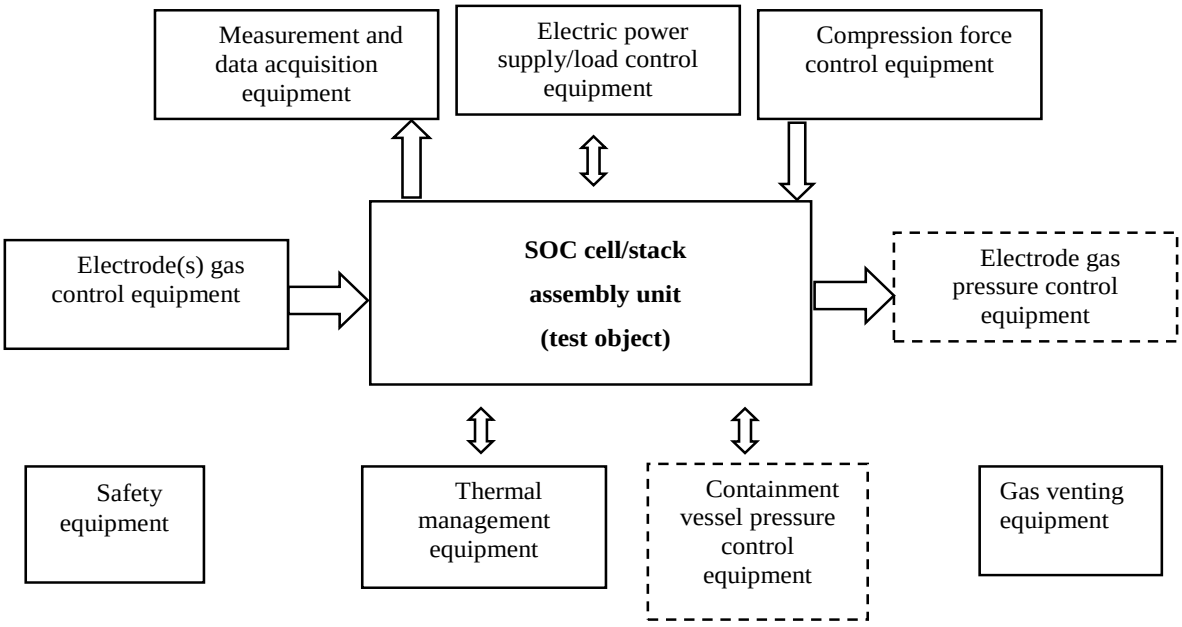

Figure 5.13. Schematic graph of a test system for high temperature solid oxide assembly unit.

Nowadays, nine active standardization platforms have published several standards for fuel cell/stack system and hydrogen fuel specifications. For fuel cell/stack systems and components, The International Electrotechnical Commission (IEC) is a non-profit International Standards developing organization that

develops and publishes International Standards for all fields of electrotechnics and electronic device. Technical committee 105 deals with the design manufacturing, operation and utilization of fuel cell power systems. In 2017, the TC/IEC Technical Committee on Fuel Cell technologies (TC105) has developed and published 16 International Standards of the IEC 62282 serie covering a wide range of topics related to standardization of fuel cell power systems. The list of IEC standards is presented in Table 5.7.

Table 5.7. IEC standards related to fuel cell technologies.

No.	International Standards
1	IEC/TS 62282-1 (2013-11) Ed.3.0: Terminology
2	IEC/TS 62282-2 (2012-03) Ed.2.0: Fuel Cell Modules
3	IEC/TS 62282-3-100 (2012-02): Stationary Fuel Cell Power Systems – Safety
4	IEC/TS 62282-3-200 (2011-10): Stationary Fuel Cell Power Systems – Performance Test Methods
5	IEC 62282-3-201: Small stationary polymer electrolyte fuel cell power system – Performance test methods
6	IEC 62282-3-300 (2012-06): Stationary Fuel Cell Power systems – Installation
7	IEC 62282-4-101: Fuel cell power systems for industrial electrical forklift trucks – Safety
8	IEC 62282-4-102: Fuel cell power systems for forklift applications – Performance requirements and test procedure
9	IEC 62282-5-1 (2012-09): Portable Fuel Cell Appliances - Safety
10	IEC 62282-6-100 (2012-10): Micro Fuel Cell Power Stems – Safety
11	IEC/PAS 62282-6-150: Micro Fuel Cells – Safety - Water reactive (UN Division 4.3) compounds in indirect PEM fuel cells
12	IEC 62282-6-200 (2012-07): Micro Fuel Cell Power Systems – Performance
13	IEC 62282-6-300 (2012-12): Micro Fuel Cell Power Systems – Fuel Cartridge Interchangeability
14	IEC 62282-7-1-: Single Cell Test Method for Polymer Electrolyte Fuel Cells
15	IEC 62282-7-2: Single Cell and Stack – Performance Test Methods for Solid Oxide Fuel Cells
16	IEC-62282-3-400: Stationary fuel cell power systems – Small stationary fuel cell power system with combined heat and power output

The intent is to cover the market demand of:

- Component, sub-system and fuel cell supplier;
- Fuel cell and system installers;
- Fuel cell and system manufacturers;
- Testing and certification bodies;
- Regulators, authorities, approval organizations;
- Original equipment manufacturers.

In a truly worldwide playing field, International Standards are one way of overcoming technical barriers in international commerce caused by differences among technical regulations and standards developed independently and separately by each nation, national standards organization, or company. IEC provides a platform to companies, industries and governments for meeting, discussing and developing the International Standards they require. International standards are used for data exchanges in commercial transactions between cell/stack manufacturers and system developers or for acquiring data on a cell or stack in order to estimate the performance of a system based on it. Users of this International standard may selectively execute test items suitable for their purposes from those described in such an International Standard. The aim of the European project *Solid Oxide Cell and Stack Testing, Safety and Quality Assurance* (SOCTESQA) is to develop uniform and industry wide test procedures and protocols for Solid Oxide Cell/stack assembly.

6. MODEL VALIDATION ON ENEA EXPERIMENTAL DATA

6.1. Semi-empirical kinetics

In this section we develop a semi-empirical relationship for IT-SOFCs starting from equation 4.9 with E_0 that is the reversible cell voltage, which can be expressed as a function of temperature using this relationship [16]:

$$E_0=1.253 - 2.4516\ 10^{-4}T \tag{6.1}$$

Analysing the problem from a kinetic point of view as explained in detail in the previous sections of the work, under load the operating cell voltage ΔV is penalized by polarizations which can be considered as follows:

$$\Delta V=\Delta E- \eta_{Ohm}- \eta_{an}- \eta_{cat} \tag{6.2}$$

where η_{Ohm} is the voltage loss due to the purely Ohmic internal resistance as well as the contact resistance, η_{anode} and $\eta_{cathode}$ are the polarizations at the electrode scale due to activation and reactant diffusion phenomena.

Working at sufficiently low fuel utilization factors, that is ratios between reacted hydrogen and fed hydrogen lower than 30 %, the characteristic curves result quite linear and the equation 4.11 has been simplified assuming:

$$\Delta V=\Delta E- R_{tot}\, j \tag{6.3}$$

where

$$R_{tot} = R_{Ohm}+R_{an}+R_{cat} \tag{6.4}$$

Ohmic resistance R_{Ohm} can be evaluated by means of a temperature dependent relationship

$$R_{ohm}=P_0 + P_1 T \exp\left(\frac{P_2}{T}\right) \tag{6.5}$$

where P_0 represents the contact resistance, usually negligible [103,131,132], while P_1 and P_2 are phenomenological coefficients evaluated by fitting experimental data.

The electrode polarizations have been derived from the Butler-Volmer equation [1]

$$j=j_0\left[\exp^{(2F\eta/RT)}\prod_i \frac{c_{isur}^{\alpha_i'}}{c_i^{\alpha_i'}} - \exp^{(2F\eta/RT)}\prod_i \frac{c_{isur}^{\alpha_i''}}{c_i^{\alpha_i''}}\right] \tag{6.6}$$

when the reverse reaction, diffusion phenomena and non-linear terms are neglected.

In terms of electrode resistances R_{an} and R_{cat}, it can be obtained:

$$R_{an\ (or\ cat)} \cong \frac{RT}{2Fj_{0,an\ (or\ cat)}} \tag{6.7}$$

where j_0 is the exchange current density which can be expressed as follows [133]:

$$j_{0,an} = A\left(\frac{p_{H_2}}{p_{ref}}\right)^B \left(\frac{p_{H_2O}}{p_{ref}}\right)^C \exp\left(-\frac{D}{T}\right) \tag{6.8}$$

$$j_{0,cat} = L\left(\frac{p_{O_2}}{p_{ref}}\right)^M \exp\left(-\frac{N}{T}\right) \tag{6.9}$$

where A, B, C, D, L, M and N are phenomenological coefficients based on experimental data and/or evaluated by physical equations.

As the reference operating pressure is equal to 1 atm and in the studied operating conditions it is possible to neglect the dependence on water thanks to the low ratio $\frac{p_{H_2O}}{p_{H_2}}$ [134], it is possible to write:

$$R_{an,H_2} = \frac{R\,T\exp\left(\frac{P_4}{T}\right)}{P_3 2F\left(x_{H_2}\right)^{P_5}} \tag{6.10}$$

$$R_{cat,O_2} = \frac{R\,T\exp\left(\frac{P_7}{T}\right)}{P_6\,2F\left(x_{O_2}\right)^{P_8}} \tag{6.11}$$

Finally, the semi-empirical kinetic formulation for IT-SOFCs is obtained:

$$\Delta V = \Delta E - R_{tot}\,j = \Delta E - \left(P_1 T\exp\left(\frac{P_2}{T}\right) + \frac{R\,T\exp\left(\frac{P_4}{T}\right)}{P_3 2F\left(x_{H_2}\right)^{P_5}} + \frac{R\,T\exp\left(\frac{P_7}{T}\right)}{P_6 2F\left(x_{O_2}\right)^{P_8}}\right) j \tag{6.12}$$

where the empirical coefficients P_1, P_2, P_3, P_4, P_5, P_6, P_7 and P_8 must be identified with experimental tests. The physical meanings of the phenomenological parameters cited before, is the following:

- P_1 and P_2 are related to the calculation of the fuel cell conductivity;
- P_3, P_4 and P_5 are related to the pre-exponential factor, activation energy and order of anodic reaction of the expression of the linear part of the resistance respectively;
- P_6, P_7 and P_8 are related to the pre-exponential factor, activation energy and order of cathodic reaction of the expression of the linear part of the resistance respectively.

6.2. Validation tests

In order to identify the kinetic parameters (P_1-P_8) previously discussed and subsequently validate the local results of the model, a number of experimental tests was carried out as summarized in Table 6.1.

The experiments have been performed to measure characteristic curves by varying the electric load, maintaining the input constant molar flow rates, and guaranteeing a low reactant utilization factor to avoid diffusion limits.

The temperature and reactant composition have been changed one at a time (with N_2 balancing) in order to isolate their effect on the electrochemical model.

All experiments were carried out at atmospheric pressure.

Table 6.1. Test operating conditions.

Conditions	T K	Anode						Cathode			
		Flow Rate (10^{-4} mol s^{-1})			% mol			Flow Rate (10^{-4}mol s^{-1})		% mol	
		H_2	N_2	H_2O	H_2	N_2	H_2O	O_2	N_2	O_2	N_2
H_2 96%	923	11.2	0	0.4	96	0	4	3.8	14.5	21	79
H_2 80% (Reference condition)	923	9.3	1.9	0.4	80	16	4	3.8	14.5	21	79
H_2 60%	923	7.0	4.2	0.4	60	36	4	3.8	14.5	21	79
H_2 40%	923	4.7	6.5	0.4	40	56	4	3.8	14.5	21	79
O_2 9%	923	9.3	1.9	0.4	80	16	4	2.1	21.4	9	91
O_2 11%	923	9.3	1.9	0.4	80	16	4	2.6	20.9	11	89
O_2 13%	923	9.3	1.9	0.4	80	16	4	3.1	20.5	13	87
O_2 15%	923	9.3	1.9	0.4	80	16	4	3.5	20.0	15	85
T 948	948	9.3	1.9	0.4	80	16	4	3.8	14.5	21	79
T 973	973	9.3	1.9	0.4	80	16	4	3.8	14.5	21	79
T 998	998	9.3	1.9	0.4	80	16	4	3.8	14.5	21	79

6.3. Experimental data

In Figure 6.1 the data obtained at the operating conditions named H_2 96%, H_2 80%, H_2 60%, and H_2 40% (see Table 6.1) are reported: as expected the performance improves when the content of hydrogen in the anodic flow rate increases. From the characteristic curves, the voltage trend can be evaluated, while the Electrochemical Impedance Spectra (EIS) spectra show two main points: these two intercepts with the x-axis of the Nyquist plot. The first one identifies the Ohmic resistance and it is not affected by the composition change. Due to the measurement procedure used, this evaluation does not take into account the contact resistance, nevertheless it has been assumed to be negligible as was previously mentioned [103,131,135]. The second intercept, related to the amplitude of the curve, gives a measure of the decreasing of the sum of Ohmic and polarization resistances when a richer anodic flow rate is fed in.

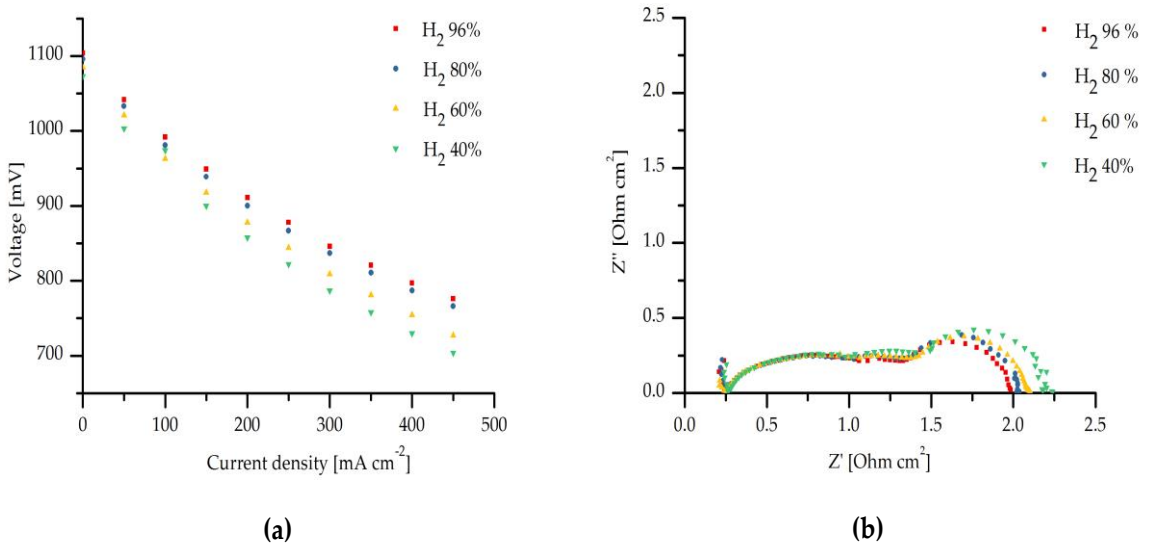

Figure 6.1. **(a)** Characteristic curves and **(b)** EIS at reference temperature (923 K) and cathodic composition (21% O_2), varying the anodic composition.

Similar considerations can be made observing the data obtained varying the feeding concentration of the cathodic reactant (see Figure 6.2).

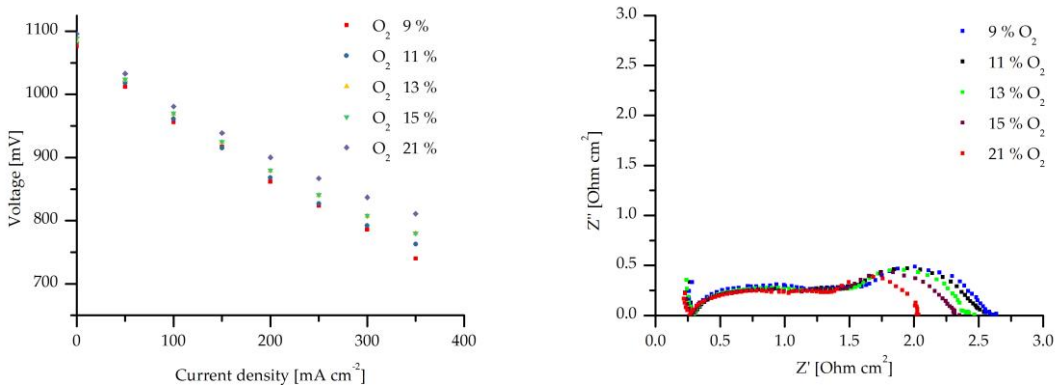

(a) **(b)**

Figure 6.2. **(a)** Characteristic curves and **(b)** EIS at reference temperature (923 K) and anodic composition (80% H_2), varying the cathodic composition.

Finally, Figure 6.3 shows the results obtained varying the operating temperature. The improving performances at a higher temperature confirm how the total resistance decreases when temperature increases. The same trend is clearly shown by the EIS spectra. In this case, the Ohmic resistance also varies, assuming high values at high temperatures.

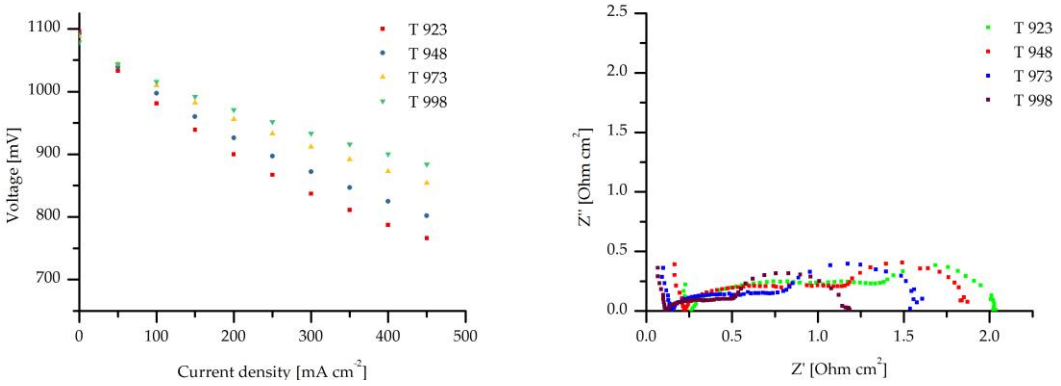

(a) **(b)**

Figure 6.3. **(a)** Characteristic curves and **(b)** EIS at reference composition (80% H_2, 21% O_2) and varying the operating temperature.

6.4. Parameter identification

The above discussed experimental data have been used to identify the parameters necessary to calculate the local total resistance R_{tot} according to the kinetic formulation of equation 6.12.
Considering the Ohmic contribution, neglecting the contac losses P_0, the parameters P_1 and P_2 were identified by means of the OriginLab© software (version 8, OriginLab Corporation, Northampton, MA (USA)), and the experimental data collected thanks to the EIS analyses at different operating conditions. Table 6.2 compares the obtained results and some literature values: The orders of magnitude are the same.

Table 6.2. Values of P_1 and P_2 ((equation 6.5) of Ohmic resistance) from data fitting and literature.

Parameter	Data Fitting	Ref. [136]	Ref. [131]
P_1 [Ohm cm^2 K^{-1}]	2×10^{-9}	6.34×10^{-7}	1.72×10^{-9}
P_2 [K]	10986	5210	11024

Regarding the other terms of the equation 6.12, namely R_{an,H_2}, and R_{cat,O_2}, the parameters have been identified thanks to the above discussed characteristic curves. In particular, this procedure has been followed:

1. The slope of the curves has been calculated and interpreted as a global resistance;
2. The Nernst loss due to the reactant consumption under different loads has been calculated assuming a linear dependence on current density [1];
3. The local total resistance R_{tot} has been calculated subtracting the Nernst loss from the global resistance;
4. The sum of the contributions R_{an,H_2} and R_{cat,O_2} have been obtained by subtracting the Ohmic contribution from the local total resistance;
5. P_3 and P_6 have been obtained by using the resulting values of $R_{an,H_2} + R_{cat,O_2}$.

Table 6.3. Values of P_3 and P_6 (equation 6.12 of total resistance) from data fitting and literature.

Parameter	Data Fitting	Ref. [137]	Ref. [131]	Ref. [138]	Ref. [139]
P_3 [A cm^{-2}]	3.65×10^9	1.34×10^{10}	1.68×10^9	5×10^9	1.4×10^{10}
P_6 [A cm^{-2}]	1.49×10^{10}	2.05×10^9	4.76×10^{10}	2×10^9	-

It can be noted that, referring to similar kinetic formulation in the literature, the equivalent parameters, which can be found present in the same orders of magnitude (Table 6.3). Regarding P_4 and P_7 we chose to use 13230 K [140] and 14433 K [139], respectively, taking them from literature as related to the activation energies of the occurring reactions.

Finally, both P_5 and P_8, have been assumed equal to 0.5, as provided in References [134,141].

The characteristic curves presented above, have been simulated with the SIMFC code using the identified kinetic parameters. As a systematic error of about 0.018 V has been observed in the open circuit comparing the experimental voltage and the theoretical one calculated with the Nernst equation, this correction has been forced in the SIMFC code (subtracting 0.018 V to the theoretical value).

In Figures 6.4, 6.5 and 6.6, the obtained results concerning the comparison between experimental and calculated polarisation curves are reported. These figures refer to different operating conditions and, in each case, show a good agreement, with an average error of 1.7 % on the voltages. The error does not show a particular trend and it is calculated in every graph as the average of the deviation between experimental and simulated data at the different current densities. In detail, Figures 6.5 and 6.5 show how performance increases when the reactant concentration increases. A wider range of hydrogen concentrations has been tested to hypothesise different fuel types, while the oxygen concentration has been maintained around the typical value of industrial applications. In Figure 6.6, characteristic curves at different temperatures are reported and show the expected positive effect of the temperature increase on the performance due to the reduction of the resistances, despite the Nernst potential penalisation.

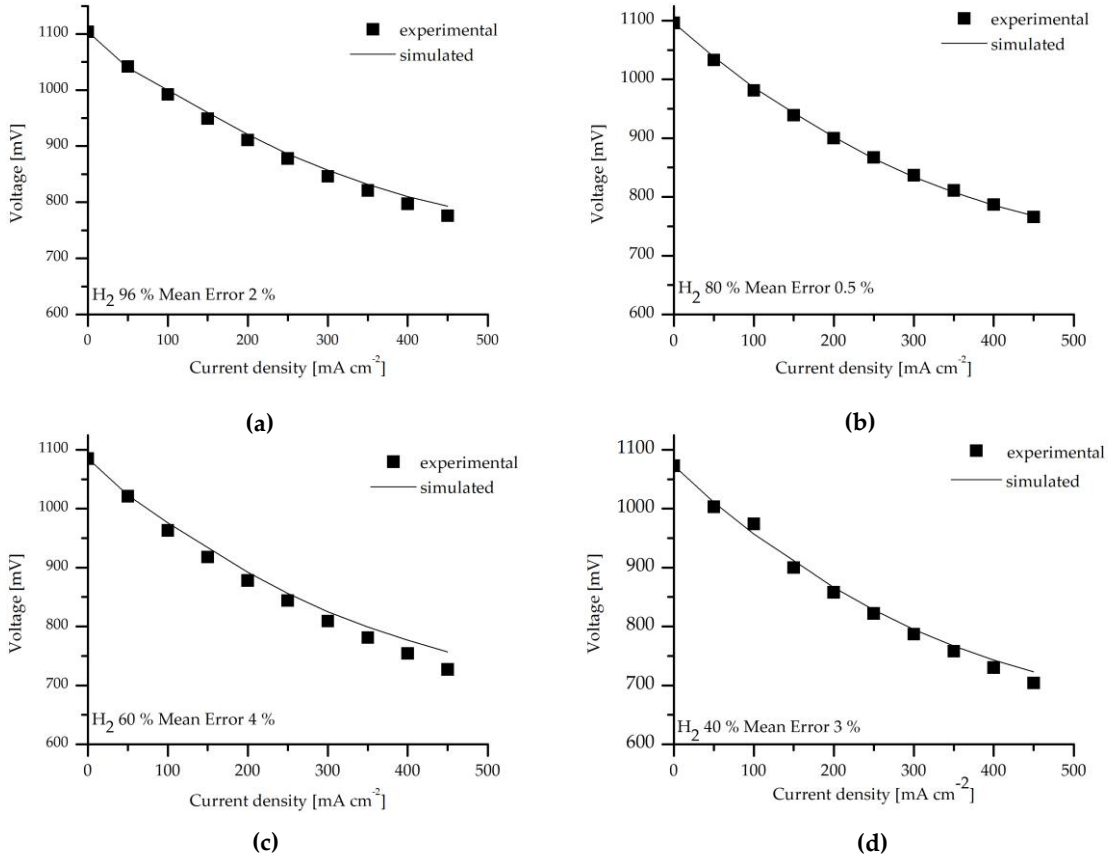

Figure 6.4. Simulation of the characteristics curves using SIMFC: different anodic compositions (a) H_2 96%, (b) H_2 80%, (c) H_2 60%, and (d) H_2 40%, with cathodic composition 21% O_2.

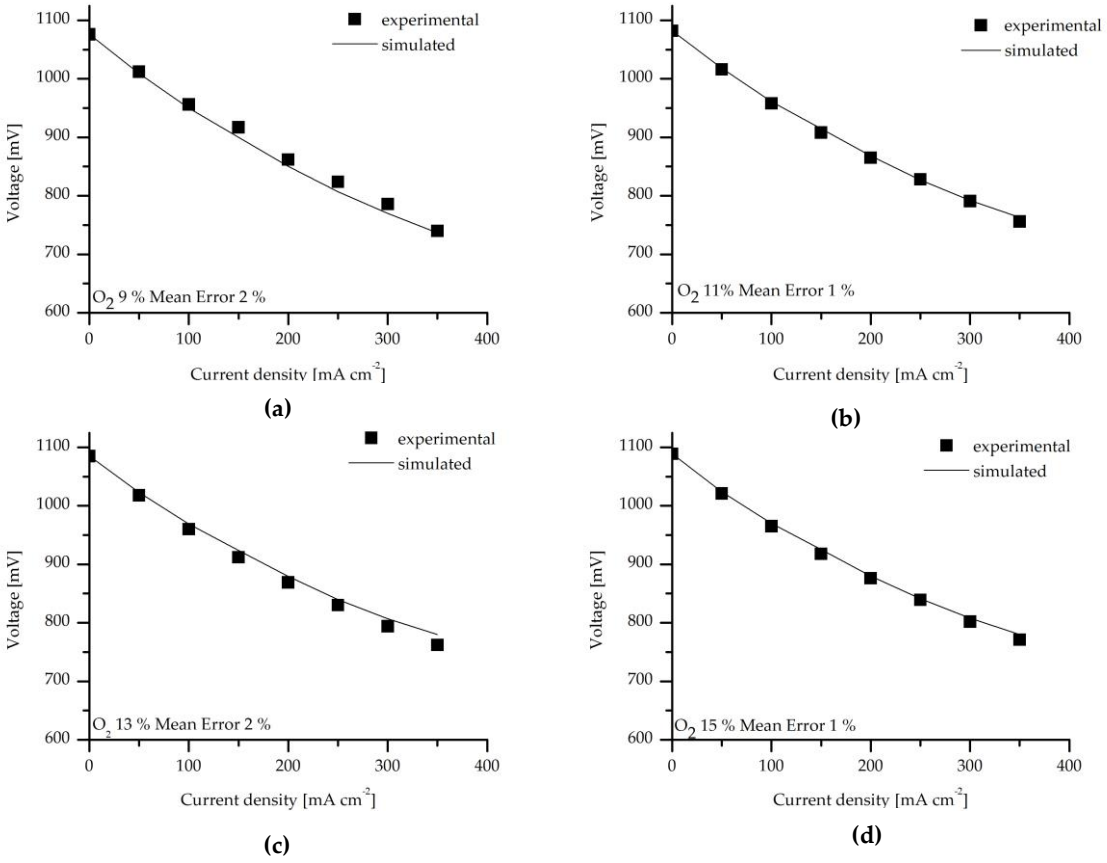

Figure 6.5. Simulation of the characteristics curves using SIMFC: different cathodic compositions (a) O_2 9%, (b) O_2 11%, (c) O_2 13%, (d) O_2 15%, with anodic composition 80% H_2.

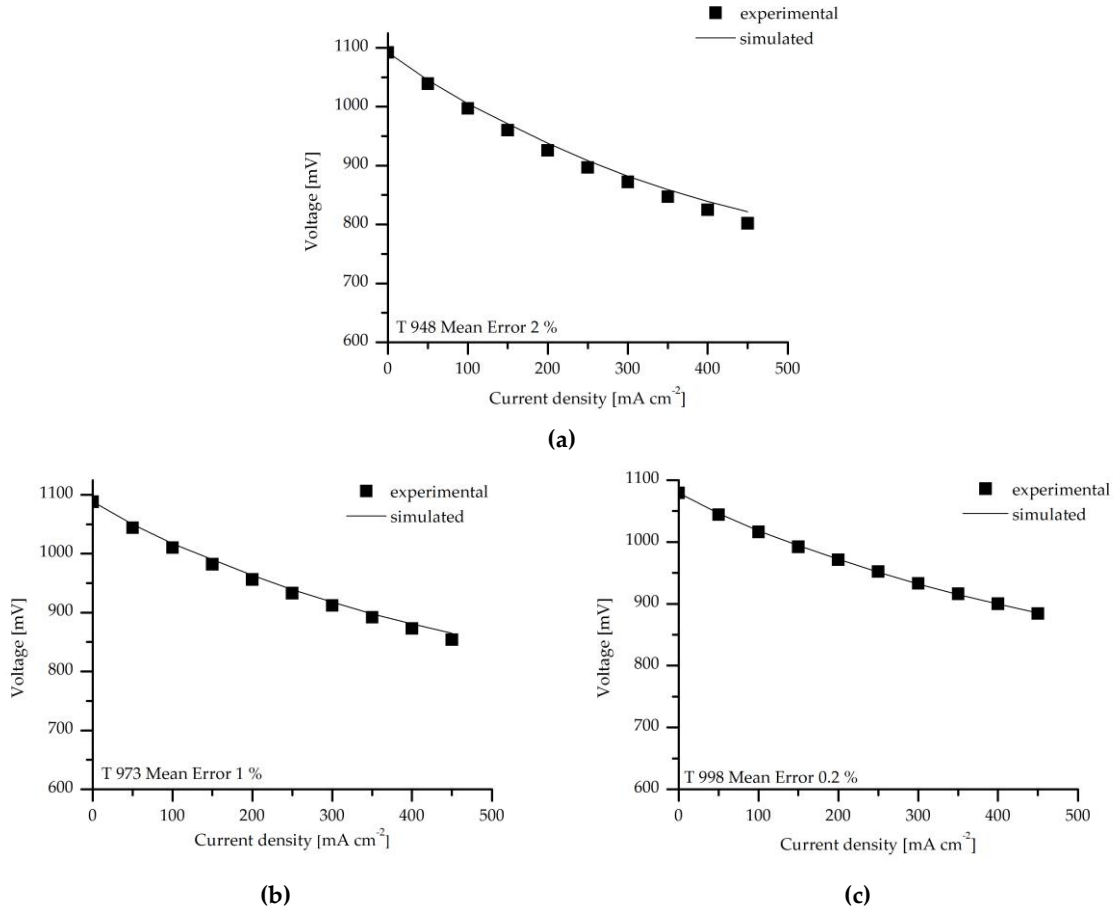

Figure 6.6. Simulation of the characteristic curves using SIMFC: different temperatures (a) T 948, (b) T 973, and (c) T 998 with anodic composition 80% H2 and cathodic composition 21 % O_2.

6.5. Local validation

As above mentioned, by means of SIMFC it is possible to calculate the maps of the main chemical-physical variables on the cell plane, while the innovative test rig in the ENEA lab allows an evaluation of in-operando local values of temperature and hydrogen molar percentage at the anode side. In this way, simulated maps can be validated thanks to the available experimental local values.

The results of the 2-D simulation are reported in Figure 6.7 in terms of hydrogen content and referring to the reference operating conditions at two electrical loads (123 mA cm^{-2} and 248 mA cm^{-2}).

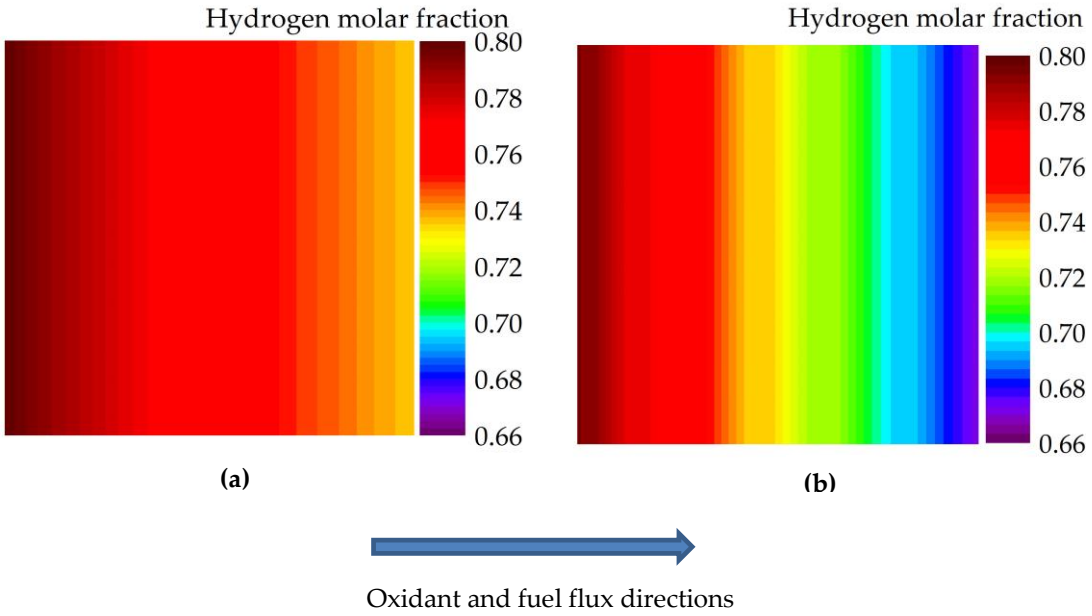

Figure 6.7. Simulated maps of hydrogen molar fraction for the reference conditions (21% O_2, 80% H_2, 923 K) at (a) 123 mA cm^{-2} and (b) 248 mA cm^{-2}.

As expected, from the inlet to the outlet in co-flow gas feeding configuration, the hydrogen content decreases due to the electrochemical reaction occurring in the fuel cell. The decrement is more evident at 248 mA cm^{-2}, where the fuel utilization factor is higher with respect to the electrical load condition at 123 mA cm^{-2}.

In Figure 6.8 there is a schematic representation of the position of the sampling points on the cell plane. The results of simulation are compared with the experimental values in Table 6.4.

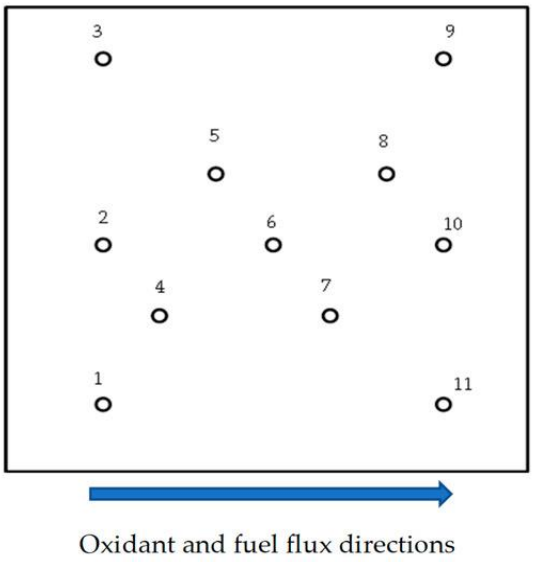

Figure 6.8. Position of the sampling points on the cell plane.

Table 6.4. Comparison of experimental and simulated local H_2 molar fraction (x_{H_2}) under different loads on the cell plane.

Current Density	123 mA cm^{-2}			248 mA cm^{-2}		
Sample point	Experimental (x_{H_2})	Simulated (x_{H_2})	Error (%)	Experimental (x_{H_2})	Simulated (x_{H_2})	Error (%)
1	0.8	0.78	2	0.79	0.77	2
2	0.80	0.78	2	0.78	0.77	1
3	0.80	0.78	2	0.78	0.77	1
4	0.76	0.78	2	0.79	0.76	4
5	0.78	0.77	1	0.78	0.74	5
6	0.77	0.76	1	0.78	0.72	8
7	0.78	0.75	3	0.77	0.72	6
8	0.76	0.75	1	0.77	0.7	9
9	0.68	0.74	9	0.68	0.69	1
10	0.69	0.74	7	0.67	0.69	3
11	0.69	0.74	7	0.66	0.69	4

The validation shows a satisfactory agreement between simulated and experimental results with an average error of 4 %.

From a thermal point of view, Figure 6.9 shows the maps of the anodic gas temperature on the cell plane at the two studied current densities. Heat exchange through the top and bottom surfaces of the cell with the surrounding atmosphere of the test facility was predicted.

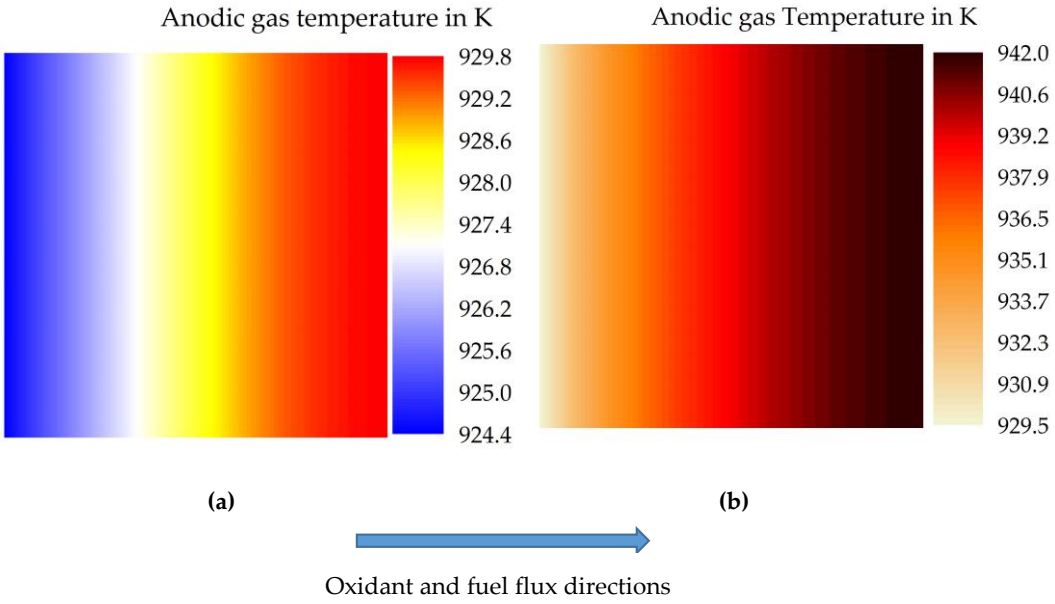

Figure 6.9. Simulated maps of the anodic gas temperature for the reference conditions at (a) 123 mA cm^{-2} and (b) 248 mA cm^{-2}.

The temperature of the anodic gas, as expected, increases from the inlet to the outlet in both load conditions because of the co-flow feeding configuration of the test facility.

Similarly, in the case of the molar composition maps, in Table 6.5 it is possible to compare simulated and experimental temperature values of the sampling points reported in Figure 6.8.

Table 6.5. Comparison of experimental and simulated anodic gas temperature under different loads on the cell plane.

Current Density	123 mA cm^{-2}			248 mA cm^{-2}		
Sample point	Experimental Temperature [K]	Simulated Temperature [K]	Error (%)	Experimental Temperature [K]	Simulated Temperature [K]	Error (%)
1	929.3	925.5	0.4	932.8	933.6	0.1
2	931.2	925.5	0.6	933	933.6	0.1
3	928.8	925.5	0.4	932.4	933.6	0.1
4	930.2	926.2	0.4	932.5	935.4	0.3
5	929.8	927	0.3	932.3	936.9	0.5
6	929.7	928.1	0.2	932.9	938.8	0.6
7	931.5	928.6	0.3	938.7	939.8	0.1
8	933.4	929.2	0.4	938.9	940.5	0.2
9	931.1	929.6	0.2	937.7	941.6	0.4
10	934.9	929.6	0.6	936.2	941.6	0.6
11	934.9	929.6	0.6	938.2	941.6	0.4

The agreement obtained is very good, with an average error of 0.3 % referring to all the available data.

7. CONCLUSIONS

An IT-SOFC (11x11 cm^2 of active area) fed with reformate natural gas was tested using an innovative set up for in-depth and in-operando characterization of the anode processes. The innovative test bench enable simultaneous measurement of temperature and gas compositions by means of gas chromatography through eleven sampling points allowing to detect the variation of thermodynamic and chemical conditions across the anode surface in steady state and in real time. Tests show that a flow uniformity across its direction, allowing on this way a clear assessment of the axial evolution of the chemical reactions taking place in OCV and under current.

The results obtained for this composition under OCV condition and low current density values show a possible competition between carbon dioxide and water in methane internal reforming leading to the presence of two different types of methane reforming: Steam Reforming and Dry Reforming. The CH_4 chemical gradient along the surface of the cell is the same in three different conditions (OCV, 20 A and 40 A), demonstrating that it is not at all affected by the current.

The contribution of the Water Gas Shift reaction in OCV is shown only in the anodic portion close to the outlet of the cell. This is probably due to the strong presence of the endothermic reforming reaction that hide the exothermic contribution of the Water Gas Shift reaction along the surface.

Whereas, under current its contribution seems to be greater, leading to an increase of water and CO_2

Moreover under low values of fuel utilization the H_2 trend shows the availability of the SOFC system to co-produce hydrogen fuel, along with generating electricity.

The temperature analyses are consistent with the composition ones, showing in OCV a net cooling effect owed to the endothermal reforming reaction on the cell. Under current, the exothermic reaction became dominant leading to a slightly temperature increment under 20A and a net increment under 40 A.

The possibility to locally investigate the electrochemical and chemical reactions during operation, correlating them with the temperature in each point, allows the generation of data that have not been previously published in scientific literature in order to validate models that provide the main electrical, chemical and physical parameters on the cell plane as simulation results.

A new version of the SIMFC code has been set-up to allow the simulation of planar co-flow IT-SOFCs fed by H_2 as an ideal case study. The resulting 2-D code has been demonstrated to be a potential interesting tool, which can be useful for diagnostic and predictive issues.

The kinetic core of the model is a simplified semi-empirical formulation, which considers only the linear part of the polarization terms because of the low utilization factors used in the reference experimental tests. The challenges of adapting the code, previously written for Molten Carbonate Fuel Cells, to SOFC application have been mainly the modification of the kinetic formulation, the

identification of new kinetic parameters, the updating of the local mass balances, the adjustment of the material properties.

IT-SOFCs fed by H_2 as an ideal case study. The resulting 2-D code has been demonstrated to be a potential interesting tool, which can be useful for diagnostic and predictive issues.

The kinetic core of the model is a simplified semi-empirical formulation, which considers only the linear part of the polarization terms because of the low utilization factors used in the reference experimental tests. The challenges of translating the code from MCFC to SOFC have been mainly the modifications of kinetic parameters to express electrochemical performance of these type of different fuel cells. The differences between the two technology in terms of numerical code can be express in term of different equation for mass, energy balances and material properties.

The preliminary comparison between experimental and calculated results showed a good agreement, with average errors equal to 1.4%, 4%, and 0.3% in terms of cell voltage, local H_2 molar fraction and local anodic gas temperature, respectively. The obtained results encourage further studies which allow the model validation on a greater quantity of data and under a wider range of operating conditions.

Some of the expected outputs have been achieved, as the new release of SIMFC code for SOFC technology and the validation of it on the basis of local values thanks to the innovative setup of ENEA laboratories. Some points have to be taken into consideration in future works, mainly the validation of the model on a greater quantity of data under a wider range of operation conditions. Other related point that have to be implemented, is the integration of reforming reaction in the numerical code and its validation on local value. Another point that need future developments is the integration of 3-D approaches into SIMFC code for SOFC, in order to simulate performance and predict several parameters as well in stationary and transient conditions for stacks. Finally, strong challenges are the development of different flow arrangements, such as counter flow and cross flow gas feeding configurations and the update of other geometrical configuration such as tubular design.

Nomenclature

a_i Activity of ith component

A, B, C, D, L, M and N Phenomenological coefficients used in equation 74 and 75

c_i Concentration of the i^{th} chemical component, mol m^{-3}

c_{isur} Surface concentration of i^{th} chemical component, mol m^{-3}

c_{pi} Specific heat of the i^{th} chemical component, J mol^{-1} K^{-1}

d Channel height, m

E Nernst potential, V

E^0 Reversible potential of the cell, V

F Faraday constant, C mol^{-1}

h Heat transfer coefficient, W m^{-2} K^{-1}

j Current density, A m^{-2}

j_0 Exchange current density, A m^{-2}

$n_{i\ Linear}$ flow rate of i^{th} chemical component, mol m^{-1} s^{-1}

n Number of electrons

K Constant in Momentum Balances

P_0, P_1, P_2, P_3, P_4, P_5, P_6, P_7 and P_8 Empirical coefficients used in equations (76), (77) and (78)

$P_{H_2}, P_{H_2O}, P_{O_2}$ Partial pressure of hydrogen, steam and oxygen, Pa

R_{tot} Total Polarization resistance, Ω cm^2

R Universal gas constant, J mol^{-1} K

r Reaction rate, mol m^{-2} s^{-1}

s Cell component thickness, m

S Specific gas/solid interface area, m^2 m^{-2}

T Temperature, K

x,y Cell coordinate, m

W_{el} Total electrical work [J]

$x_{H_2}, x_{O_2}, x_{H_2O}$ Molar fraction of hydrogen, oxygen and steam

Greek letters

$\alpha'_{i,}\alpha''_{i,}$ Reaction rate orders related to the i^{th} chemical component

$\Delta G_{f,i}$ Variation of Gibbs free energy of i^{th} component, j mol^{-1}

ΔH_j Formation enthalpy of j^{esim} component, J mol^{-1}

η Polarization, V

λ Heat conductivity, W m^{-1} K^{-1}

μ Gas viscosity, Pa s

ν Stochiometric coefficient

Subscript

an Anode

cat Cathode

sol Solid

Ohm Ohmic

cond Conduction

react Reactant

Publication

Graziadio, M., Conti, B., Giannini, A., Munoz, C.B., McPhail, S.J., Carlini, M., An nalysis of the effects of test bench architecture on solid oxide fuel cell and electrolysis characterization and the role of international standards, ECS transactions, 75, Issue 37, 2016, Pages 15-22, DOI: 10.1149/07537.0015ecst;

Pumiglia, D.; Santoni, F.; Viceconti, E.; Conti, B.; Boigues Muñoz, C.; Bosio, B.; Carlini, M.; McPhail,S.J. SOFC anode process characterization by means of a spot-sampling set-up for in-operando gas analysis. In *ECS Transactions*; 2016; Vol. 75.

Santoni, F.; Silva Mosqueda, D.M.; Pumiglia, D.; Viceconti, E.; Conti, B.; Boigues Muñoz, C.; Bosio, B.; Ulgiati, S.; McPhail, S.J. In-situ study of the gas-phase composition and temperature of an intermediate-temperature solid oxide fuel cell anode surface fed by reformate natural gas. *J. Power Sources* **2017**, *370*, doi:10.1016/j.jpowsour.2017.09.078.

McPhail, S.J.; Conti, B.; Kiviaho, J. The Yellow Pages of SOFC Technology - International Status of SOFC deployment 2017; ENEA.; VTT, Technical Research Centre of Finland Ltd.: Espoo (Finland), **2017**; ISBN 978-88-8286-290-9.

Conti, B.; Bosio, B.; McPhail, S.J.; Santoni, F.; Pumiglia, D.; Arato, E. 2-D model for Intermediate Temperature Solid Oxide Fuel Cells Preliminarily Validated on Local Values;Catalysts 2019, 9(1),36, doi:10.3390/catal9010036

References

1. Bosio, B.; Di Giulio, N.; Nam, S.W.; Moreno, A. An effective semi-empiric model for MCFC kinetics: Theoretical development and experimental parameters identification. *Int. J. Hydrogen Energy* **2014**, *39*, 12273–12284, doi:10.1016/j.ijhydene.2014.04.119.
2. Larminie, A.; Dicks, J. *Fuel Cell Systems Explained*; 2003; ISBN 047084857X.
3. Irvine, J.T.S.; Connor, P. *Solid oxide fuels cells: Facts and figures: Past, present and future perspectives for SOFC Technologies*; 2013; Vol. 55; ISBN 9781447144557.
4. Cleveland, C.J.; Morris, C. *Fuel Cells*; 2014; ISBN 9780124170131.
5. Zhao, Y.; Xia, C.; Jia, L.; Wang, Z.; Li, H.; Yu, J.; Li, Y. Recent progress on solid oxide fuel cell: Lowering temperature and utilizing non-hydrogen fuels. *Int. J. Hydrogen Energy* **2013**, *38*, 16498–16517, doi:10.1016/j.ijhydene.2013.07.077.
6. Bocci, E.; Carlo, A. Di; McPhail, S.J.; Gallucci, K.; Foscolo, P.U.; Moneti, M.; Villarini, M.; Carlini, M. Biomass to fuel cells state of the art: A review of the most innovative technology solutions. *Int. J. Hydrogen Energy* **2014**, *39*, 21876–21895, doi:10.1016/j.ijhydene.2014.09.022.
7. W. Nernst Uber die elektrolytische Leitung fester K• orper bei sehr hohen Temperaturen. *Z. Elektrochem., VI. Hauptversammlung der Dtsch. Elektrochemischen Gesellschaft vom 25. bis 27. Mai 1899 G• ottingen.* **1899**, *6*, 41–43, doi:10.1002/bbpc.18990060205.
8. Steele, B.C.H. Material science and engineering: The enabling technology for the commercialisation of fuel cell systems. *J. Mater. Sci.* **2001**, *36*, 1053–1068, doi:10.1023/A:1004853019349.
9. Steele, B. Appraisal of Ce1−yGdyO2−y/2 electrolytes for IT-SOFC operation at 500°C. *Solid State Ionics* **2000**, *129*, 95–110, doi:10.1016/S0167-2738(99)00319-7.
10. Marina, O.A.; Bagger, C.; Primdahl, S.; Mogensen, M. A solid oxide fuel cell with a gadolinia-doped ceria anode: preparation and performance. *Solid State Ionics* **1999**, *123*, 199–208, doi:10.1016/S0167-2738(99)00111-3.
11. Mogensen, M.; Lindegaard, T.; Hansen, U.R.; Mogensen, G. Physical properties of mixed conductor solid oxide fuel cell anodes of doped CeO2. *J. Electrochem. Soc.* **1994**, *141*, 2122–2128, doi:10.1149/1.2055072.
12. Haanappel, V.A.C.; Shemet, V.; Vinke, I.C.; Gross, S.M.; Koppitz, T.; Menzler, N.H.; Zahid, M.; Quadakkers, W.J. Evaluation of the suitability of various glass sealant - Alloy combinations under SOFC stack conditions. *J. Mater. Sci.* **2005**, *40*, 1583–1592, doi:10.1007/s10853-005-0657-0.
13. Froitzheim, J.; Meier, G.H.; Niewolak, L.; Ennis, P.J.; Hattendorf, H.; Singheiser, L.; Quadakkers, W.J. Development of high strength ferritic steel for interconnect application in SOFCs. *J. Power Sources* **2008**, *178*, 163–173, doi:10.1016/j.jpowsour.2007.12.028.
14. Chou, Y.S.; Stevenson, J.W.; Chick, L.A. Ultra-low leak rate of hybrid compressive mica seals for solid oxide fuel cells. *J. Power Sources* **2002**, *112*, 130–136, doi:10.1016/S0378-7753(02)00356-7.
15. Singhal, S.C. *Solid Oxide Fuel Cells : Past , Present and Future*; ISBN 9781447144564.
16. *Fuel Cell Handbook*; 7th ed.; EG&G Technical Services, Inc, U.S.A.: Morgantown, West Virginia, 2004; ISBN 0442319266.
17. Larminie, J.; Dicks, A. *Fuel cell systems explained*; Wiley, 2000; ISBN 0471490261.

18. TLP library Available online: https://www.doitpoms.ac.uk/tlplib/fuel-cells/high_temp_sofc.php.
19. Proceeding of Fuel Cell Seminar and Exposition. In; 2011.
20. BMW, courtesy of Forschungs Zentrum Jülich Available online: http://www.fz-juelich.de/portal/DE/Home/home_node.html.
21. Hexis Available online: http://www.hexis.com/.
22. International Energy Agency *IEA, advanced fuel cells implementing agreement e annual report*; Didcot, 2011;
23. Bloomenergy Available online: https://www.bloomenergy.com/.
24. Ceramatec Available online: https://www.bloomberg.com/profiles/companies/7580716Z:US-ceramatec-inc.
25. Delphi Available online: http://hfcnexus.com/organizations/delphi-corporation/.
26. National Energy Technology Laboratories Available online: https://www.netl.doe.gov/.
27. Ghezel-Ayagh, H. 12th Annual SECA Workshop. In; 2011.
28. Materials and Systems Research, Inc.
29. Protonex Available online: https://protonex.com/.
30. ULTRA-USSI Available online: https://www.ultra-ussi.com/.
31. adelan Available online: https://adelan.co.uk/.
32. BOSCH Thermotechnology Available online: https://www.bosch-climate.us/.
33. Cerespower Available online: http://www.cerespower.com/.
34. Convion Available online: http://convion.fi/.
35. Elcogen Available online: https://elcogen.com/.
36. Erlingklinger Available online: https://www.elringklinger.de/de.
37. topsoe Available online: https://www.topsoe.com/.
38. Kerafol Available online: https://www.kerafol.com/.
39. m power Available online: http://mpowergmbh.de/.
40. new enerday Available online: https://www.sunfire.de/en/company/news/detail/sunfire-concentrates-fuel-cell-activities-in-neubrandenburg?utm_source=newenerday.
41. Plansee Available online: https://www.plansee.com/en/index.html.
42. SOLIDpower Available online: https://www.solidpower.com/it/.
43. Sunfire Available online: https://www.sunfire.de/en/.
44. ZEGpower Available online: http://www.zegpower.no/?lang=en.
45. Aisin Available online: www.aisingroup.com.
46. cctt Available online: http://cctt.com/.
47. G cell Available online: https://gcell.com/.

48. huatsing power Available online: http://en.huatsing-power.com/.

49. NEDO Available online: https://www.nedo.go.jp/english/.

50. MHI, Proceedings of Fuel Cell Seminar 2011. In.

51. Mitsubishi heavy industries Available online: https://www.mhi.com/.

52. MiCo Available online: http://www.mico.kr/eng/business_09.html.

53. POSCO Energy Available online: http://eng.poscoenergy.com/_service/main.asp.

54. SOFCMAN Available online: http://www.sofcman.com/index.html.

55. D'Andrea, G.; Gandiglio, M.; Lanzini, A.; Santarelli, M. Dynamic model with experimental validation of a biogas-fed SOFC plant. *Energy Convers. Manag.* **2017**, *135*, 21–34, doi:10.1016/j.enconman.2016.12.063.

56. Brunaccini, G.; Sergi, F.; Aloisio, D.; Ferraro, M.; Blesznowski, M.; Kupecki, J.; Motylinski, K.; Antonucci, V. Modeling of a SOFC-HT battery hybrid system for optimal design of off-grid base transceiver station. *Int. J. Hydrogen Energy* **2017**, *42*, 27962–27978, doi:10.1016/j.ijhydene.2017.09.062.

57. Safari, A.; Shahsavari, H.; Salehi, J. A mathematical model of SOFC power plant for dynamic simulation of multi-machine power systems. *Energy* **2018**, *149*, 397–413, doi:10.1016/j.energy.2018.02.068.

58. Kupecki, J.; Motylinski, K.; Milewski, J. Dynamic analysis of direct internal reforming in a SOFC stack with electrolyte-supported cells using a quasi-1D model. *Appl. Energy* **2017**, 1–8, doi:10.1016/j.apenergy.2017.07.122.

59. Cheddie, D.F. Integration of a solid oxide fuel cell into a 10 MW gas turbine power plant. *Energies* **2010**, *3*, 754–769, doi:10.3390/en3040754.

60. Rabbani, A.; Rokni, M. Modeling and analysis of transport processes and efficiency of combined SOFC and PEMFC systems. *Energies* **2014**, *7*, 5502–5522, doi:10.3390/en7095502.

61. Smoothing, S. *Reduced Modelling of Planar Fuel Cells*; 2017; ISBN 9783319426457.

62. Bove, R.; Ubertini, S. *Modeling solid oxide fuel cells: methods, procedures and techniques*; NP, B., Ed.; Fuel Cells and Hydrogen energy.Springer, 2008; ISBN 9781402069949.

63. Kakaç, S.; Pramuanjaroenkij, A.; Zhou, X.Y. A review of numerical modeling of solid oxide fuel cells. *Int. J. Hydrogen Energy* **2007**, *32*, 761–786, doi:10.1016/j.ijhydene.2006.11.028.

64. Ozgur Colpan, C.; Ibrahim, D.; Feridun, H. A review on macro-level modeling of planar solid oxide fuel cells C. *Int. J. energy Res.* **2008**, *32*, 336–355, doi:10.1002/er.

65. Pramuanjaroenkij, A.; Kakaç, S.; Yang Zhou, X. Mathematical analysis of planar solid oxide fuel cells. *Int. J. Hydrogen Energy* **2008**, *33*, 2547–2565, doi:10.1016/j.ijhydene.2008.02.043.

66. Jeon, D.H. A comprehensive CFD model of anode-supported solid oxide fuel cells. *Electrochim. Acta* **2009**, *54*, 2727–2736, doi:10.1016/j.electacta.2008.11.048.

67. Cheng, C.H.; Chang, Y.W.; Hong, C.W. Multiscale Parametric Studies on the Transport Phenomenon of a Solid Oxide Fuel Cell. *J. Fuel Cell Sci. Technol.* **2005**, *2*, 219, doi:10.1115/1.2039950.

68. Recknagle, K.P.; Williford, R.E.; Chick, L.A.; Rector, D.R.; Khaleel, M.A. Three-dimensional thermo-fluid electrochemical modeling of planar SOFC stacks. *J. Power Sources*

2003, *113*, 109–114, doi:10.1016/S0378-7753(02)00487-1.

69. Badur, C.; Wang, Y.; Feng, D.; Jiang, Z.; Zhang, X. Macroscopic modeling of solid oxide fuel cell (SOFC) and model-based control of SOFC and gas turbine hybrid system. *Prog. Energy Combust. Sci.* **2018**, *66*, 83–140, doi:10.1016/j.pecs.2017.12.002.

70. Kowalczyk, T. Zero-dimensional robust model of an SOFC with internal reforming for hybrid energy cycles. **2018**, *158*, 128–138, doi:10.1016/j.energy.2018.05.203.

71. Iora, P.; Aguiar, P.; Adjiman, C.S.; Brandon, N.P. Comparison of two IT DIR-SOFC models: Impact of variable thermodynamic, physical, and flow properties. Steady-state and dynamic analysis. *Chem. Eng. Sci.* **2005**, *60*, 2963–2975, doi:10.1016/j.ces.2005.01.007.

72. Cheddie, D.F.; Munroe, N.D.H. A dynamic 1D model of a solid oxide fuel cell for real time simulation. *J. Power Sources* **2007**, *171*, 634–643, doi:10.1016/j.jpowsour.2007.06.170.

73. KANG, Y.; LI, J.; CAO, G.; TU, H.; LI, J.; YANG, J. One-dimensional Dynamic Modeling and Simulation of a Planar Direct Internal Reforming Solid Oxide Fuel Cell. *Chinese J. Chem. Eng.* **2009**, *17*, 304–317, doi:10.1016/S1004-9541(08)60209-8.

74. Wang, C.; Nehrir, M.H. A physically based dynamic model for solid oxide fuel cells. *IEEE Trans. Energy Convers.* **2007**, *22*, 887–897, doi:10.1109/TEC.2007.895468.

75. Wang, C.; Nehrir, M.H.; Shaw, S.R. Dynamic models and model validation for PEM fuel cells using electrical circuits. *IEEE Trans. Energy Convers.* **2005**, *20*, 442–451, doi:10.1109/TEC.2004.842357.

76. Chan, S..; Khor, K..; Xia, Z.. A complete polarization model of a solid oxide fuel cell and its sensitivity to the change of cell component thickness. *J. Power Sources* **2001**, *93*, 130–140, doi:10.1016/S0378-7753(00)00556-5.

77. Sorrentino, M.; Pianese, C. Grey-Box Modeling of SOFC Unit for Design , Control and Diagnostics Applications Grey-Box Modeling of SOFC Unit for Design , Control and Diagnostics Applications. In *European Fuel Cell Forum*; Lucerne, Switzerland.

78. Amiri, A.; Vijay, P.; Tadé, M.O.; Ahmed, K.; Ingram, G.D.; Pareek, V.; Utikar, R. Planar SOFC system modelling and simulation including a 3D stack module. *Int. J. Hydrogen Energy* **2016**, *41*, 2919–2930, doi:10.1016/j.ijhydene.2015.12.076.

79. Shen, S.; Kuang, Y.; Zheng, K.; Gao, Q. A 2D model for solid oxide fuel cell with a mixed ionic and electronic conducting electrolyte. *Solid State Ionics* **2018**, *315*, 44–51, doi:10.1016/j.ssi.2017.11.028.

80. Luo, X.J.; Fong, K.F. Development of 2D dynamic model for hydrogen-fed and methane-fed solid oxide fuel cells. *J. Power Sources* **2016**, *328*, 91–104, doi:10.1016/j.jpowsour.2016.08.005.

81. Aydın, Ö.; Nakajima, H.; Kitahara, T. Reliability of the numerical SOFC models for estimating the spatial current and temperature variations. *Int. J. Hydrogen Energy* **2016**, *41*, 15311–15324, doi:10.1016/j.ijhydene.2016.06.194.

82. Jin, X.; Xue, X. Mathematical modeling analysis of regenerative solid oxide fuel cells in switching mode conditions. *J. Power Sources* **2010**, *195*, 6652–6658, doi:10.1016/j.jpowsour.2010.04.018.

83. Verda, V.; Von Spakovsky, M.R. Development of a detailed planar solid oxide fuel cell computational fluid dynamics model for analyzing cell performance degradation. *J. Fuel Cell Sci. Technol.* **2009**, *6*, 0110051–0110059, doi:10.1115/1.2971046.

84. Mahcene, H.; Moussa, H. Ben; Bouguettaia, H.; Bechki, D.; Babay, S.; Meftah, M.S. Study

of species, temperature distributions and the solid oxide fuel cells performance in a 2-D model. *Int. J. Hydrogen Energy* **2011**, *36*, 4244–4252, doi:10.1016/j.ijhydene.2010.07.075.

85. Pasaogullari, U.; Wang, C. Computational Fluid Dynamics Modeling of Solid Oxide Fuel Cells. *Proc. SOFC-VIII* **2003**, 1403–1412, doi:10.1243/095765005X7583.

86. Wang, G.; Yang, Y.; Zhang, H.; Xia, W. 3-D model of thermo-fluid and electrochemical for planar SOFC. *J. Power Sources* **2007**, *167*, 398–405, doi:10.1016/j.jpowsour.2007.02.019.

87. Yuan, K.; Ji, Y.; Chung, J.N. Physics-based modeling of a low-temperature solid oxide fuel cell with consideration of microstructure and interfacial effects. *J. Power Sources* **2009**, *194*, 908–919, doi:10.1016/j.jpowsour.2009.05.045.

88. Chan, S..; Khor, K..; Xia, Z.. A complete polarization model of a solid oxide fuel cell and its sensitivity to the change of cell component thickness. *J. Power Sources* **2001**, *93*, 130–140, doi:10.1016/S0378-7753(00)00556-5.

89. Tang, S.; Amiri, A.; Vijay, P.; Tadé, M.O. Development and validation of a computationally efficient pseudo 3D model for planar SOFC integrated with a heating furnace. *Chem. Eng. J.* **2016**, doi:10.1016/j.cej.2016.01.040.

90. Ghorbani, B.; Vijayaraghavan, K. 3D and simplified pseudo-2D modeling of single cell of a high temperature solid oxide fuel cell to be used for online control strategies. *Int. J. Hydrogen Energy* **2018**, *43*, 9733–9748, doi:10.1016/j.ijhydene.2018.03.211.

91. Sorrentino, M.; Pianese, C.; Guezennec, Y.G. A hierarchical modeling approach to the simulation and control of planar solid oxide fuel cells. *J. Power Sources* **2008**, *180*, 380–392, doi:10.1016/j.jpowsour.2008.02.021.

92. Razbani, O.; Assadi, M. Artificial neural network model of a short stack solid oxide fuel cell based on experimental data. *J. Power Sources* **2014**, *246*, 581–586, doi:10.1016/j.jpowsour.2013.08.018.

93. Bicer, Y.; Dincer, I.; Aydin, M. Maximizing performance of fuel cell using artificial neural network approach for smart grid applications. *Energy* **2016**, *116*, 1205–1217, doi:10.1016/j.energy.2016.10.050.

94. Polverino, P.; Sorrentino, M.; Pianese, C. Improved Fault Isolability for Solid Oxide Fuel Cell Diagnosis Through Sub-system Analysis. *Energy Procedia* **2017**, *105*, 1918–1923, doi:10.1016/j.egypro.2017.03.560.

95. Koeppel, B.J.; Lai, C.; Iyengar, A.K.S.; Xu, Z.; Wang, C.; Hackett, G.A. Use of a Reduced Order Model (ROM) to Simulate SOFC Performance in System Models. *ECS Trans.* **2017**, *78*, 2595–2605, doi:10.1149/07801.2595ecst.

96. Chakraborty, U.K.; Abbott, T.E.; Das, S.K. PEM fuel cell modeling using differential evolution. *Energy* **2012**, *40*, 387–399, doi:10.1016/j.energy.2012.01.039.

97. Chakraborty, U.K. Static and dynamic modeling of solid oxide fuel cell using genetic programming. *Energy* **2009**, *34*, 740–751, doi:10.1016/j.energy.2009.02.012.

98. Larminie, James; Dicks, A. *Fuel Cell Systems Explained*; 2003; ISBN 047084857X.

99. Janardhanan, V.M.; Deutschmann, O. CFD analysis of a solid oxide fuel cell with internal reforming: Coupled interactions of transport, heterogeneous catalysis and electrochemical processes. *J. Power Sources* **2006**, *162*, 1192–1202, doi:10.1016/j.jpowsour.2006.08.017.

100. Kaur, G. *Solid oxide fuel cell components: Interfacial compatibility of SOFC glass seals*; 2015; ISBN 9783319255989.

101. Nguyen, T.L.; Honda, T.; Kato, T.; Iimura, Y.; Kato, K.; Negishi, A.; Nozaki, K.; Shiono,

M.; Kobayashi, A.; Hosoda, K.; Cai, Z.; Dokiya, M. Fabrication and Characterization of Anode-Supported Tubular SOFCs with Zirconia-Based Electrolyte for Reduced Temperature Operation. *J. Electrochem. Soc.* **2004**, *151*, A1230, doi:10.1149/1.1768131.

102. Bove, R.; Ubertini, S. Modeling solid oxide fuel cell operation: Approaches, techniques and results. *J. Power Sources* **2006**, *159*, 543–559, doi:10.1016/j.jpowsour.2005.11.045.

103. Boigues-Muñoz, C.; Pumiglia, D.; McPhail, S.J.; Santori, G.; Montinaro, D.; Comodi, G.; Carlini, M.; Polonara, F. More accurate macro-models of solid oxide fuel cells through electrochemical and microstructural parameter estimation - Part II: Parameter estimation. *J. Power Sources* **2015**, *286*, 321–329, doi:10.1016/j.jpowsour.2015.03.129.

104. Byron Bird, R.; Stewart E., W.; Lightfoot N., E. *Transport Phenomena*; second edi.; Wiley: New York, 2007; ISBN 978-0-470-11539-8.

105. Newman, J.; Thomas, K.E. *Electrochemical Systems*; 2004; Vol. 3; ISBN 9788578110796.

106. Nam, J.H.; Jeon, D.H. A comprehensive micro-scale model for transport and reaction in intermediate temperature solid oxide fuel cells. *Electrochim. Acta* **2006**, *51*, 3446–3460, doi:10.1016/j.electacta.2005.09.041.

107. Zheng, K.; Sun, Q.; Ni, M. Local Non-Equilibrium Thermal Effects in Solid Oxide Fuel Cells with Various Fuels. *Energy Technol.* **2013**, *1*, 35–41, doi:10.1002/ente.201200014.

108. Damm, D.L.; Fedorov, A.G. Radiation heat transfer in SOFC materials and components. *J. Power Sources* **2005**, *143*, 158–165, doi:10.1016/j.jpowsour.2004.11.063.

109. Arato, E.; Audasso, E.; Barelli, L.; Bosio, B.; Discepoli, G. Kinetic modelling of molten carbonate fuel cells: Effects of cathode water and electrode materials. *J. Power Sources* **2016**, *330*, 18–27, doi:10.1016/j.jpowsour.2016.08.123.

110. Audasso, E.; Barelli, L.; Bidini, G.; Bosio, B.; Discepoli, G. Molten Carbonate Fuel Cell performance analysis varying cathode operating conditions for carbon capture applications. *J. Power Sources* **2017**, *348*, doi:10.1016/j.jpowsour.2017.02.081.

111. Marra, D.; Bosio, B. Process analysis of 1 MW MCFC plant. *Int. J. Hydrogen Energy* **2007**, *32*, 809–818, doi:10.1016/j.ijhydene.2006.11.016.

112. Bosio, B.; Marra, D.; Arato, E. Thermal management of the molten carbonate fuel cell plane. *J. Power Sources* **2010**, *195*, 4826–4834, doi:10.1016/j.jpowsour.2010.02.031.

113. Chakraborty, U.K. Reversible and irreversible potentials and an inaccuracy in popularmodels in the fuel cell literature. *Energies* **2018**, *11*, doi:10.3390/en11071851.

114. Minh, N.Q.; T., T. *Science and Technology of Ceramic Fuel Cells*; Science, E., Ed.; 1995;

115. Barsoukov, E.; Macdonald, J.R. *Theory , Experiment , and applications*; John Wiley & Sons, Inc., 2005; Vol. 177; ISBN 9786468600.

116. Gabrielli, C. Identification of electrochemical processes by frequency response analysis. **1998**, 130.

117. Pumiglia, D.; Santoni, F.; Viceconti, E.; Conti, B.; Boigues Muñoz, C.; Bosio, B.; Carlini, M.; McPhail, S.J. SOFC anode process characterization by means of a spot-sampling set-up for in-operando gas analysis. In *ECS Transactions*; 2016; Vol. 75.

118. Bessler, W.G.; Gewies, S.; Willich, C.; Schiller, G.; Friedrich, K.A. Spatial distribution of electrochemical performance in a segmented SOFC: A combined modeling and experimental study. *Fuel Cells* **2010**, *10*, 411–418, doi:10.1002/fuce.200900083.

119. Santoni, F.; Silva Mosqueda, D.M.; Pumiglia, D.; Viceconti, E.; Conti, B.; Boigues Muñoz,

C.; Bosio, B.; Ulgiati, S.; McPhail, S.J. In-situ study of the gas-phase composition and temperature of an intermediate-temperature solid oxide fuel cell anode surface fed by reformate natural gas. *J. Power Sources* **2017**, *370*, doi:10.1016/j.jpowsour.2017.09.078.

120. Choudhary, V.R.; Rajput, A.M. Simultaneous carbon dioxide and steam reforming of methane to syngas over NiO-CaO catalyst. *Ind. Eng. Chem. Res.* **1996**, *35*, 3934–3939, doi:10.1021/ie960002l.

121. Yuan, J.L.; Sunden, B. Analysis of chemically reacting transport phenomena in an anode duct of intermediate temperature SOFCs. *J. Fuel Cell Sci. Technol.* **2006**, *3*, 89–98, doi:10.1115/1.2173662.

122. Wei, J.; Iglesia, E. Isotopic and kinetic assessment of the mechanism of reactions of CH4with CO2or H2O to form synthesis gas and carbon on nickel catalysts. *J. Catal.* **2004**, *224*, 370–383, doi:10.1016/j.jcat.2004.02.032.

123. Dicks, A.L. Hydrogen generation from natural gas for the fuel cell systems of tomorrow. *J. Power Sources* **1996**, *61*, 113–124, doi:10.1016/S0378-7753(96)02347-6.

124. Palm, C.; Stolten, D.; Peters, R.; Dahl, R.; Klu, U. Internal reforming of methane in solid oxide fuel cell systems. *J. Power Sources* **2002**, *106*, 238–244, doi:10.1016/S0378-7753(01)01039-4.

125. Finnerty, C.M.; Coe, N.J.; Cunningham, R.H.; Ormerod, R.M. Carbon formation on and deactivation of nickel-based/zirconia anodes in solid oxide fuel cells running on methane. *Catal. Today* **1998**, *46*, 137–145, doi:10.1016/S0920-5861(98)00335-6.

126. Shaffer, B.; Hunsuck, M.; Brouwer, J. FUELCELL08-65193. **2017**, 1–15.

127. Moyer, C.J.; Sullivan, N.P.; Zhu, H.; Kee, R.J. Polarization Characteristics and Chemistry in Reversible Tubular Solid-Oxide Cells Operating on Mixtures of H[sub 2], CO, H[sub 2]O, and CO[sub 2]. *J. Electrochem. Soc.* **2011**, *158*, B117, doi:10.1149/1.3518413.

128. Matsuzaki, Y.; Yasuda, I. Electrochemical Oxidation of H[sub 2] and CO in a H[sub 2]-H[sub 2]O-CO-CO[sub 2] System at the Interface of a Ni-YSZ Cermet Electrode and YSZ Electrolyte. *J. Electrochem. Soc.* **2000**, *147*, 1630, doi:10.1149/1.1393409.

129. Transactions, E.C.S.; Society, T.E. Solid Oxide Cell and Stack Testing, Safety and Quality Assurance (SOCTESQA) C. Auer. **2015**, *68*, 1897–1905.

130. Sharaf, O.Z.; Orhan, M.F. An overview of fuel cell technology: Fundamentals and applications. *Renew. Sustain. Energy Rev.* 2014, *32*.

131. Leonide, a.; Apel, Y.; Ivers-Tiffée, E. SOFC modeling and parameter identification by means of impedance spectroscopy. *ECS Trans.* **2009**, *19*, 81–109, doi:10.1149/1.3247567.

132. Costamagna, P.; Selimovic, A.; Del Borghi, M.; Agnew, G. Electrochemical model of the integrated planar solid oxide fuel cell (IP-SOFC). *Chem. Eng. J.* **2004**, *102*, 61–69, doi:10.1016/j.cej.2004.02.005.

133. Ni, M.; Leung, M.K.H.; Leung, D.Y.C. Parametric study of solid oxide fuel cell performance. *Energy Convers. Manag.* **2007**, *48*, 1525–1535, doi:10.1016/j.enconman.2006.11.016.

134. Mizusaki, J.; Tagawa, H.; Saito, T.; Yamamura, T.; Kamitani, K.; Hirano, K.; Ehara, S.; Takagi, T.; Hikita, T.; Ippommatsu, M.; Nakagawa, S.; Hashimoto, K. Kinetic studies of the reaction at the nickel pattern electrode on YSZ in H2H2O atmospheres. *Solid State Ionics* **1994**, *70–71*, 52–58, doi:10.1016/0167-2738(94)90286-0.

135. Costamagna, P.; Selimovic, A.; Del Borghi, M.; Agnew, G.; Grosso, S.; Travis, R.; Magistri, L. Electrochemical model of the integrated planar solid oxide fuel cell (IP-SOFC). *Chem.*

Eng. J. **2004**, *102*, 61–69, doi:10.1016/j.cej.2004.02.005.

136. Boigues Muñoz, C.; Pumiglia, D.; McPhail, S.J.; Montinaro, D.; Comodi, G.; Santori, G.; Carlini, M.; Polonara, F. More accurate macro-models of solid oxide fuel cells through electrochemical and microstructural parameter estimation - Part I: Experimentation. *J. Power Sources* **2015**, *294*, 658–668, doi:10.1016/j.jpowsour.2015.06.118.

137. Ni, M.; Leung, M.K.H.; Leung, D.Y.C. Parametric study of solid oxide fuel cell performance. *Energy Convers. Manag.* **2007**, *48*, 1525–1535, doi:10.1016/j.enconman.2006.11.016.

138. Greene, E.S.; Chiu, W.K.S.; Burke, A.A.; Medeiros, M.G.; Carreiro, L.G. Modeling and Verification of Steady State Operational Changes on the Performance of a Solid Oxide Fuel Cell. *J. Fuel Cell Sci. Technol.* **2009**, *6*, 041001, doi:10.1115/1.3080811.

139. Achenbach, E. Three-dimensional and time-dependent simulation of a planar solid oxide fuel cell stack. **1994**, *49*, 333–348, doi:10.1016/0378-7753(93)01833-4.

140. Yahya, A.; Ferrero, D.; Dhahri, H.; Leone, P.; Slimi, K.; Santarelli, M. Electrochemical performance of solid oxide fuel cell: Experimental study and calibrated model. *Energy* **2018**, *142*, 932–943, doi:10.1016/j.energy.2017.10.088.

141. Nagata, S.; Momma, A.; Kato, T.; Kasuga, Y. Numerical analysis of output characteristics of tubular SOFC with internal reformer. *J. Power Sources* **2001**, *101*, 60–71, doi:10.1016/S0378-7753(01)00547-X.